1989

Continuous precipitation of yttrium hydroxycarbonate spheres of narrow size distribution

Harold Ray Jouett II
Iowa State University

Order Number 9014913

Continuous precipitation of yttrium hydroxycarbonate spheres of narrow size distribution

Jouett, Harold Ray, II, Ph.D.

Iowa State University, 1989

U·M·I
300 N. Zeeb Rd.
Ann Arbor, MI 48106

Continuous precipitation of yttrium hydroxycarbonate spheres of narrow size distribution

by

Harold Ray Jouett II

A Dissertation Submitted to the
Graduate Faculty in Partial Fulfillment of the
Requirements for the Degree of
DOCTOR OF PHILOSOPHY

Major: Chemical Engineering

Approved:

Signature was redacted for privacy.

In Charge of Major Work

Signature was redacted for privacy.

For the Major Department

Signature was redacted for privacy.

For the Graduate College

Iowa State University
Ames, Iowa

1989

TABLE OF CONTENTS

INTRODUCTION

Over the years, few natural phenomena have stirred the interest and curiosity of scientists as much as large populations of very small particles of uniform size and shape. Natural opal, for example, has been shown to consist of close-packed arrangements of monosize silica spheres, less than one micrometer in diameter, cemented together by the chemical action of groundwater at the points where the spheres touch each other. We now know that the "opalescence" of this gemstone is a result of Bragg diffraction of visible light by close-packed spheres, in much the same way as x-rays are scattered by planes of atoms in crystals.

The natural origin of these monosize silica spheres raised questions about particle nucleation and growth. How they came to be arranged in regular close-packed geometry raised questions in colloid and surface science, because the behavior of such small particles in suspension is dominated by their surface properties. Indeed, attempts to explain the formation and behavior of such small monodisperse particles, and to produce them in the laboratory, coincides chronologically with the development of colloid and surface science as a separate branch of physical chemistry.

The story of monodisperse particles, which is outlined briefly in the following section of this report, begins at about the turn of the century. During the first forty years, a number of important but often

apparently unrelated papers appeared. Then, about 1950, many interrelations among the earlier papers became apparent, the early results of the DLVO theory of particle-particle interaction became available, and a larger number of people became interested in preparing monodisperse particles. Interestingly, the first issue of the Journal of Colloidal and Interface Science also appeared in 1950.

In the 1970's, "colloidal crystals" - which are suspensions of monodisperse particles spaced equidistant from each other - and their sedimentation into dense, ordered cakes were studied. Finally, in 1982, Barringer and Bowen (1), at the Massachusetts Institute of Technology adapted the science of the formation and packing of monodisperse particles to the preparation of ceramics as a means of eliminating or minimizing many of the problems associated with large-scale production of "high-performance" ceramics for electronic and structural applications.

To be commercially useful, electronic ceramics must be chemically homogeneous and also must not have physical flaws which can block, or short-circuit, the flow of current from the desired path. The major problem inherent in structural ceramics is their propensity for brittle failure. The material cannot deform, like a metal, to relieve stresses imposed by a load. As a result, ceramics maintain their shape under stress until the fracture threshold is exceeded; the material then fails catastrophically. Ceramic materials could be made much more crack resistant if miniscule defects such as voids and chemical impurities between the materials grains could be eliminated.

A ceramic's chemical composition and microstructure ultimately determine all of its macroscopic properties. These in turn are determined by the processing methods. The general fabrication scheme involves preparing the powder, forming the green compact, and sintering it to final form. Unlike powder metallurgy, where the sintered form can be subjected to some of the mechanical and heat treatments used to improve the properties of metals, little can be done to change the properties of a ceramic part after it has been sintered. Therefore, the early powder preparation steps, which typically involve precipitation, drying, and calcination, are considered to be crucial operations, since most flaws in the green cake are carried over into the final sintered product.

The main obstacle in the production of high technology ceramics is the inability to produce them reliably and reproducibly in large quantities (2). The performance of many ceramic components is not as good as one would predict based on data obtained from laboratory samples. This lack of reproducibility in properties lies in the inability to control the microstructure of the presintered component. The microstructure of the presintered body depends upon particle shape, size, size distribution, and state of agglomeration of the powder.

Depending on the ceramic component being manufactured, the cost of rejection of finished parts, which do not meet required specifications, is about 50% ($\pm$ 25%) of the total manufacturing cost (3). Because of the strong interrelationships between microstructure, properties, and processing, reliable and reproducible manufacturing continues to be a technological goal which is currently stimulating researchers to develop

a more fundamental understanding of the physics and chemistry of ceramic powder processing. It is at this point that the pioneering work of Barringer and Bowen bridges the gap between colloid science and ceramic science. Their rationale was that if one could produce a ceramic powder consisting of small, monodisperse spheres, and pack these spheres with a uniform distribution of void space, then the resulting component should sinter to a high density with very few flaws. The resulting ceramic part should have a very uniform fine-grained microstructure that should greatly increase the homogeneity and the fracture toughness of the ceramic part.

Typically, batch precipitation techniques are used to produce monosized particles. Batch processes are commercially undesirable because operating costs are high and there is usually a certain amount of batch-to-batch variation in the product. On the other hand, continuous stirred tank reactors, typically used for continuous precipitation, generate broad particle size distributions. For continuous precipitation of monosized particles, a reactor must have a narrow residence time distribution typical of plug flow.

The purpose of this research was to continuously produce spherical particles of the yttria precursor $Y(OH)CO_3 \cdot H_2O$ with a controlled size distribution and with as narrow a size distribution as feasible. The particles were produced by homogeneous precipitation in three types of reactors: mixed-suspension mixed-product removal (MSMPR), semi-batch, and packed bed. The thermal decomposition of urea was used to release carbonate ions uniformly throughout the volume of the reactors.

LITERATURE REVIEW

Early Work

The history of work on monodisperse particles is quite fascinating; portions of it are found in a variety of different fields, and in the work of many famous chemists and physicists.

A logical place to begin a review of the literature is the work of Perrin in 1909 (4). Perrin was attempting to prove the existence of molecules by studying the random motion of monodisperse colloidal particles as they moved in response to the thermal motion of the molecules of the suspending medium. Using Einstein's and von Smoluchowski's analysis of Brownian motion (5,6), which had just then been published, Perrin arrived at an experimental value for Avagadro's number which, according to the newly developed theory of Brownian motion, was related to the root-mean-square displacement of the colloidal particles.

To obtain a sufficient quantity of monodisperse particles, Perrin and his students started with a kilogram of polydisperse gamboge powder and, after several months of fractional separations by repeated centrifugal sedimentation, they finally accumulated several hundred milligrams of a monodisperse fraction. The effort was justly rewarded, however, for in 1926 Perrin received the Nobel prize in physics for "putting a definite end to the struggle regarding the real existence of

molecules".

In the same year (1926), Zsigmondy received the postponed 1925 Nobel prize in chemistry for work involving monodisperse colloids. Part of Zsigmondy's Nobel citation read, "for experimental methods used which have laid the foundation of modern colloidal chemistry." One of these methods was a seeding technique for the preparation of monodisperse gold sols (7). He first made a very fine gold sol (about 3 nm. particles) by reducing a dilute $HAuCl_4$ solution with phosphorous. This sol was then used to seed a second $HAuCl_4$ solution in which the gold was reduced slowly with formaldehyde, causing it to precipitate out on the small seed particles. An approximately monodisperse sol was formed.

Zsigmondy made three important observations about his gold particles. First, as the particles became larger, their size distribution became more narrow. Second, the size of the particles was determined by the amount of $HAuCl_4$ reduced. Third, the number of particles was strictly proportional to the amount of seed solution added added - thus proving that no new nuclei had been formed.

Svedberg (8), yet another Nobel prize winner, investigated the sedimentation of proteins from solution and showed convincingly, both in sedimentation velocity and in sedimentation equilibrium experiments, that proteins were truly monodisperse and that they were well-defined molecules rather than aggregates of smaller polypeptides.

Overbeek (9), reviewing the work of these early Nobel Laureates in his 1981 Alexander Memorial Lecture at the University of Sidney commented, "What a difference between the work of these three men. Perrin, painstakingly, practically hand picked his monodisperse

particles, Zsigmondy introduced a chemical method still much in use today for preparing monodisperse systems, and Svedberg turned to nature and found his monodisperse material nearly ready made."

Later, in 1943, LaMer and Barnes (10) prepared nearly monodisperse colloidal sulphur suspensions by rapid mixing of dilute solutions of sodium thiosulphate and hydrochloric acid. They observed, as did Zsigmondy with his gold sols, that the size distribution of the sulphur particles narrowed with time. A beam of white light passing through the suspension of growing particles was initially turbid, because the polydisperse particles scattered the light in random directions - a phenomenon known as the Tyndall effect. After a sufficient period of growth, bands of colored light called higher order Tyndall spectra (HOTS) began to appear, indicative of the presence of a monodisperse suspension. The uniformly sized particles caused the component colors of white light to be scattered preferentially at certain angles to the incident beam. A 360^{o} scan of the scattered light revealed a sequence of colored bands which are repeated at intervals. LaMer and his associates were the first to employ this effect, combined with calculations using Mie's theory of light scattering, published in 1908 (11) as a means of actually determining the size of the particles in a monodisperse suspension.

LaMer and Dinegar(12) explained the narrow size distribution of such sulphur sols with the aid of the diagram shown in Figure 1.

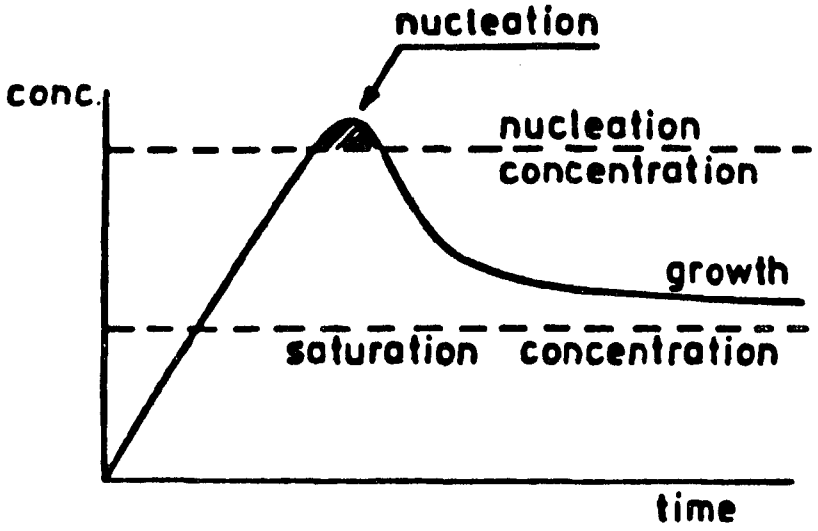

Figure 1. Schematic representation of the concentration of molecularly dissolved sulfur before and after nucleation as a function of time

Sulphur was formed slowly by the chemical reaction,

$$H^+ + S_2O_3^{=} \rightarrow HSO_3^- + S \qquad (1)$$

As the reaction proceeded, the sulphur concentration rose until a sufficiently high supersaturation was reached that a sudden nucleation shower occured, with a corresponding sudden decrease in the supersaturation. Thereafter, if the chemical reaction was slow enough, the increase in sulphur concentration was relieved by particle growth

and no further nucleation occurred.

LaMer's method was not greatly different than that used by Zsigmondy, who used small seed crystals to provide the initial nuclei. Thereafter, in both cases, the supersaturation was controlled so that particle growth occurred at a rate that just consumed all of the material generated by chemical reaction.

The reason for the narrowing of the size distribution as the particles grew remained a question. Reiss and LaMer (13) and Zaiser and LaMer (14) attributed the effect to diffusion-controlled growth, showing theoretically that under such conditions the particle radius should increase linearly with the square root of time ($dr/dt = k/r$, where k is a constant). In other words, in a polydisperse system undergoing diffusion-controlled growth, smaller particles should grow more rapidly than larger ones. Later, Bradford et al. (15) would show, by examining other types of particle growth, that as long as the radial growth rate was proportional to a power less than the positive first power of the radius, the distribution would become narrower with growth for particles that all begin growing at the same time. Thus, other growth mechanisms also could produce similar effects.

It was through the work of LaMer that scientists became aware of the usefulness of the controlled nucleation and growth method for preparing monodisperse systems.

Later Work

Monodisperse latexes

The use of monodisperse spherical particles became much more widespread in scientific work after the accidental discovery, in 1947, by scientists at the Dow Chemical Company, of a way to prepare almost perfectly spherical, monodisperse latex particles (14) by emulsion polymerization. The process proceeds by free radical formation, initiation of the polymerization reaction, propagation of the polymer chains, and termination of the chains. A 0.1 μm latex particle consists of about 1000 entangled polymer chains.

Since their discovery, Dow has prepared and marketed these monodisperse latexes as a scientific service. They have found use in the calibration of particle size measuring instruments and electron microscopes, in determining the pore sizes of filters and biological membranes, in medical diagnostic procedures, and in the study of the mechanisms and kinetics of emulsion polymerization processes. However, it is their unprecedented role as model systems in the study of the solid-liquid transition in molecular physics that gives them a position of unique importance in this review. This aspect of monodisperse latexes will be covered in detail later in a separate section because it involves ordering and packing of colloidal spheres - phenomena which led to the current interest of ceramists in monodisperse particles.

Aging of metal salt solutions

The voluminous amount of work by Matijevic and his students at Clarkson University, on the preparation of monodisperse colloidal suspensions of metal hydrous oxide particles, is of special interest because these compounds are useful in ceramics and in catalysis. In 1969, Demchak and Matijevic (17) described the preparation of monodisperse spherical chromium hydrous oxide sols - the first report of colloidal metal hydrous oxide particles with a very narrow size distribution. Since then, Matijevic and his co-workers have produced monodisperse metal hydrous oxide sols of aluminum, iron, titanium, and copper by aging metal salt solutions (18,19,20,21,22,23,24,25,26).

These sols were made by forced hydrolysis of metal ions in acidic solutions of metal salts. The solutions were aged at elevated temperatures (75 - 180^{o}C) for varying periods of time (20 minutes to several weeks). In some cases the particles were amorphous and in other cases they were crystalline. The reasons for the structural differences are still being discussed in the current literature. Matijevic (19) concluded that if the hydrolysis products consisted of discrete, well defined ionic complexes, then crystal growth ensued, yielding particles of fixed stoichiometry and most often well defined crystal habits. If, on the other hand, the hydrolysis resulted in the formation of polymeric metal complexes, spherical amorphous particles were produced, just as with organic polymers. The presence of certain anions, notably sulfate or phosphate, often had a profound effect on the morphology of the particles. They were thought to promote polymerization of the

hydrolyzed species, a reaction which would not occur in the presence of such ions as perchlorate, nitrate, or chloride, which do not readily coordinate to form polynuclear complexes.

Matijevic's precipitations by aging of metal salt solutions were done batchwise; the time required for the reactions, and the typical yields obtained were such that the technique is not generally useful for preparing metal hydrous oxides in any substantial quantity. His work has been summarized in a series of review articles that have appeared periodically (18,19,21,27).

Hydrolysis of metal alkoxides

In 1974, Catone and Matijevic (28) carried out the first successful synthesis of monodisperse hydrous metal oxide particles by metal alkoxide hydrolysis. They added aluminum secondary butoxide to an aqueous solution containing sulfate ions at room temperature, treated the mixture ultrasonically, and then stirred it for about an hour. This gave a slightly turbid suspension. After aging it at 99°C for two days, spherical particles of hydrous aluminum oxide, 0.45 μm in diameter, were obtained. As with many of the other processes for making monodisperse particles, monodispersivity was achieved over only a narrow range of the processing variables.

Catone and Matijevic also commented on another question which is still not completely resolved. Why are most of the monodisperse spherical particles, obtained by a variety of methods, nearly always limited in size to something less than about 1 μm? According to Catone

and Matijevic, in their work the final particle size was governed by the amount of sulfate present during sol preparation. As the sulfate concentration was increased, larger, less positively charged particles formed. The effect that surface charge had on the final particle size was further substantiated when sulfate was added as $MgSO_4$ instead of the monovalent Na_2SO_4. The result was smaller more positively charged particles than were produced by systems containing sulfates of monovalent cations. They concluded that the equilibrium, or final, size was determined by the surface potential, which in their case was a function of the pH and the surface sulfate complexing.

Alkoxide hydrolysis was used later, in a different form, by Barringer and Bowen (1) to make high-quality ceramic powders. They made monodisperse spherical TiO_2 particles by the controlled hydrolysis of dilute alcoholic solutions of titanium tetraethoxide, $Ti(OC_2H_5)_4$, to which a stoichiometric amount of water was added to react with the alkoxide. Precipitation occurred in 2 to 90 seconds, depending on the concentration of the reactants. The final particle size obtained was typically between 0.3 and 0.4 μm and the ratio of the standard deviation to the mean particle size of the distribution ($\sigma/\bar{L}$ x 100%), known as the coefficient of variation, C.V., was generally in the range of 30% to 40%.

Controlled hydrolysis of metal alkoxides has been used subsequently to prepare monodisperse powders of Al_2O_3, TiO_2, ZnO, ZrO_2, SiO_2 and ZrO_2 ZrO_2 - Al_2O_3 (29). The basic method of preparation is to hydrolyze a dilute solution (~ 0.2 to 0.4 M) of the respective metal alkoxide in an appropriate alcohol by adding an equal volume of the alcohol containing

the proper amount of deionized water. The second solution is poured into the first solution and the mixture is stirred. Water is an active reactant and the reaction must be carried out in a glove box under a dry nitrogen atmosphere, usually at room temperature. The hydrolysis reaction can be represented by the general equation.

$$M(OR)_x + x/2\ H_2O \rightarrow MO_{x/2} + x\ ROH \qquad (2)$$

where x is a function of the valence of the metal cation.

Pickles and Lilley (30) prepared colloidal TiO_2 spheres by alkoxide hydrolysis, embedded them in a resin, and then examined sections of the spheres, obtained by slicing the resin cake with an ultramicrotome. Their results suggested that the amorphous TiO_2 spheres were formed by the controlled coagulation of much smaller primary particles. A similar result was found by Heistand and Chia (31) whose spherical ZnO particles, approximately 0.2 μm in diameter, consisted of aggregated 150 Angstrom crystallites. Thus, there is increasing evidence that in some cases particle growth occurs by coagulation of small primary particles.

For large scale production of ceramic powders, alkoxide hydrolysis has several disadvantages. The moisture sensitivity of the reaction requires that it be carried out in a controlled atmosphere. The alkoxides are expensive, and not all ceramic materials of commercial interest can be made this way. On the other hand, the oxide rather than a hydroxide or a basic salt is produced. Thus, no calcination of the particles is necessary and dense cakes can be formed directly by sedimentation without ever having to remove them from a liquid

suspension.

A technique developed in 1968 by Stober et al. (32) also deserves special mention because of its extensive later use by ceramists in preparing monodisperse spherical particles of silica for the study of glass ceramics. They prepared their particles by the hydrolysis and subsequent condensation of silicic acid in an alcoholic solution. Ammonia was used as a morphological catalyst since its presence was found to be essential for making spherical particles. The geometric standard deviation, σ_g, of the particle size distribution was typically less than 1.1 (C.V. = $[\exp(\ln \sigma_g)^2 - 1]^{1/2} \times 100\%$). Occasionally, a bimodal particle size distribution was observed, a possible indication of two homogeneous nucleation events during the growth of the particles or perhaps evidence of both heterogeneous and homogeneous nucleation occurring at different times.

Homogeneous precipitation

One final way of preparing monodisperse particles is by precipitation from homogeneous solution, or simply homogeneous precipitation. The roots of this method can be traced back to the early work of Willard and Tang (33), in 1937, who used it as a means of precipitating cations so that a coarse, easily filterable precipitate could be obtained, thus avoiding the slimy, gelatinous precipitate that formed when many of the metal hydrous oxides were brought down by the simple addition of base. In homogeneous precipitation, the precipitant is generated in situ by decomposition in solution of an appropriate

precursor.

Willard and Tang found that to obtain a dense precipitate, the presence of an appropriate anion such as the sulfate ion was necessary. The need for an appropriate anion was, of course, a result which Matijevic discovered later in his preparation of monodisperse particles of hydrous oxides or basic salts by forced hydrolysis and aging of metal salt solutions.

Other observations made by Willard and his students during their work on homogeneous precipitation also pre-date results that are more commonly identified with the work of later investigators. Willard and Tang (33) observed that their aluminum basic sulfate particles "consisted of independent spherical granules of almost uniform size" and that "the precipitate either contained very little crystalline material or consisted of a crystalline mixture of such complexity that the net result was similar to that which would be obtained from amorphous material." In 1953, Willard and Gordon (34) observed dried films of basic stannic sulfate particles which were transparent and exhibited colored interference patterns.

Although the mechanism of nucleation and growth of the particles in the dense precipitates is not discussed in the early papers of Willard, it is apparent that the mechanism is the same as that described about fifteen years later by LaMer and Dinegar (12).

Since it was first described in 1937 by Willard and Tang, homogeneous precipitation has become widely used in analytical chemistry. Methods of precipitating a variety of different metal complexes (sulfates, sulfides, oxalates, phosphates, etc.) are described

by Gordon et al. (35) in a book published in 1959. However, the text gives little indication of the size distribution or of the morphology of the precipitate particles.

Much of the more recent work involving homogeneous precipitation has been done with the specific purpose of obtaining monodisperse spherical particles. Williams et al. (36) prepared uniform spherical particles of zinc sulfide by the thermal decomposition of thioacetamide in a zinc salt solution. Uniform spheres were obtained only over a pH range from 1.5 to 2.0. The particles were polycrystalline, with a mean diameter of 3 μm, a coefficient of variation of less than 10%, and an x-ray crystallite size of about 120 Angstroms. They grew at a rate proportional to the square root of time, which is consistent with a diffusion-controlled growth mechanism. By considering the concentration of various species in solution, they were able to determine that the diffusion of the HS^- ion to the growing particle was the rate limiting process.

Haruta et al. (37) prepared colloidal spherical particles of amorphous molybdenum sulfide and cobalt sulfide by the homogeneous decomposition of thioacetamide in solutions containing molybdenum and cobalt salts. The use of hydrazine for accelerating the hydrolysis of thioacetamide was found to be indispensable for the preparation of uniform spherical particles of both molybdenum and cobalt sulfides. Particle size could be varied from 0.09 to 0.7 μm and 0.08 to 0.42 μm for molybdenum sulfide and cobalt sulfide, respectively, by adjusting the acidity of the mother solution over the pH range of 4 - 7. The coefficient of variation of the particles was less than 20%.

Verlinden (38) precipitated amorphous monodisperse spherical particles of yttrium hydroxycarbonate in sizes from 0.13 to 0.66 μm by the thermal decomposition of urea in a yttrium nitrate solution. The geometric standard deviation was typically less than 1.10. Again, spherical particles were produced over only a limited range of reactant compositions. The growth of the particles was described by a diffusion-controlled model and the decomposition of urea was the rate limiting step. Kayima and Hansen (39) also precipitated yttrium hydroxycarbonate particles of narrow size distribution by the same method as Verlinden. However, their particles showed definite crystallinity under electron diffraction. They also concluded that the particles grew by a diffusion controlled growth mechanism.

Gobet and Matijevic (40) prepared 0.2 μm monosized particles of cadmium selenide and lead selenide by the decomposition of selenourea. The CdSe particles were spherical and polycrystalline, whereas the PbSe particles where of cubic symmetry.

In 1979, Cornilsen and Reed (41) noted that easily filtered, spherical particles of an alumina precursor could be precipitated by the homogeneous thermal decomposition of urea in an aluminum nitrate solution. Later, Blendell et al. (42) produced monodisperse spherical particles of an alumina precursor using either urea or foramide. Particle size varied from 0.1 to 5.0 μm depending on conditions. Formamide was found to be the superior precipitating agent because it decomposed more rapidly when heated. This caused the supersaturation to increase more rapidly, creating a shorter nucleation shower. Urea, on the other hand, decomposed more slowly and appeared to cause multiple

nucleation showers due to local concentration fluctuations. This caused greater polydispersity in the size distribution.

Colloid Crystals and Dense Ordered Cakes

The observation of Willard and Tang (34), in 1953, of dried films of stannic sulfate particles that exhibited colored interference patterns, and a similar observation by Alfrey et al. (43) in 1954, that concentrated latex suspensions and also dried films of latex particles exhibited similar color patterns, gave an early indication of colloidal phenomena that was to become an important area of research many years later.

The dried latex particles tended to arrange themselves spontaneously into close-packed crystalline arrays. Under close examination with an electron microscope, the films exhibited surface features resembling grains, grain boundaries, and lattice defects similar to those present in ordinary crystalline materials. Gerould (44) observed that, at a critical suspension density, the monodisperse latex particles would sediment from the suspension onto a membrane into close-packed layers the first evidence of three-dimensional close packing of such particles as they settle from a suspension. This idea was to be used later by ceramists as a potential means of preparing dense cakes of ceramic powders that would sinter to high density at low temperature.

Luck et al. (45), in Germany, are usually credited with being the first to show that the iridescence of these ordered arrays was caused by Bragg diffraction of visible light. Kreiger and Hiltner (46) studied ordered suspensions of monodisperse latex particles more extensively by Bragg diffraction and reached several conclusions that were to become extremely important in later work on ordered suspensions.
By carefully controlling the electrolyte concentration in latex suspensions, and thus the strength of the electric double layer surrounding each particle, they showed that ordered suspensions could be created where the center-to-center differences between the particles was many times greater than the diameter of the particles and that the spacing between the particles varied with the electrolyte concentration. By systematically varying the electrolyte concentration they discovered an order-disorder transition point and stated, for the first time, that "the order-disorder transition is strongly reminiscent of the solid-liquid transition" and also that "it is hoped that further investigation will provide insight into the solid-liquid transition, and perhaps into the nature of the solid and liquid states of matter." These were prophetic statements, for indeed the work served to initiate a strong link with the field of molecular physics.

So, once again, the behavior of monodisperse colloids became a potential experimental means of examining molecular behavior - as it was years earlier in the pioneering work of Perrin on Brownian motion.

The exact cause of the ordering of the monodisperse particles in suspension is an issue which remains unresolved. Kreiger and Hiltner dismissed van der Waals forces as being the cause of the ordering

because of the very large particle-to-particle distances that could be achieved in their suspensions at very low electrolyte concentrations these distances were clearly beyond the range of van der Waals forces. Since the particles were equally charged, they assumed that ordering occurred because the particles were surrounded by equipotential surfaces surfaces - that is, each particle was located in a potential "well". This, however, did not explain disordered phases or the occurrence of an order-disorder transition. The problem was further complicated by their observation, reported by them for the first time, that under certain conditions it was possible for both ordered and disordered phases to co-exist in the same suspension. The co-existence of ordered and disordered phases remains the most difficult part of the behavior of these suspensions to explain. The work of Kreiger and Hiltner (46), reported in 1971, is a milestone in the study of what has come to be called "colloidal crystals" and also in relating the behavior of monodisperse suspensions to the solid-liquid transition for molecules.

In 1973, Hachisu et al. (47), in Japan, published the results of a simple and elegant experimental study which has become a classic reference in the field. They prepared an array of suspensions of monodisperse latexes in which they systematically varied both the solids content and the electrolyte concentration to produce a "phase diagram" a plot of solids content versus electrolyte concentration - which showed an ordered region, a disordered region, and a region where ordered and disordered phases coexisted. Such a diagram is shown in Figure 2. Thus, they confirmed Kreiger and Hiltner's observation that both kinds of phases could co-exist. They further showed that there were two

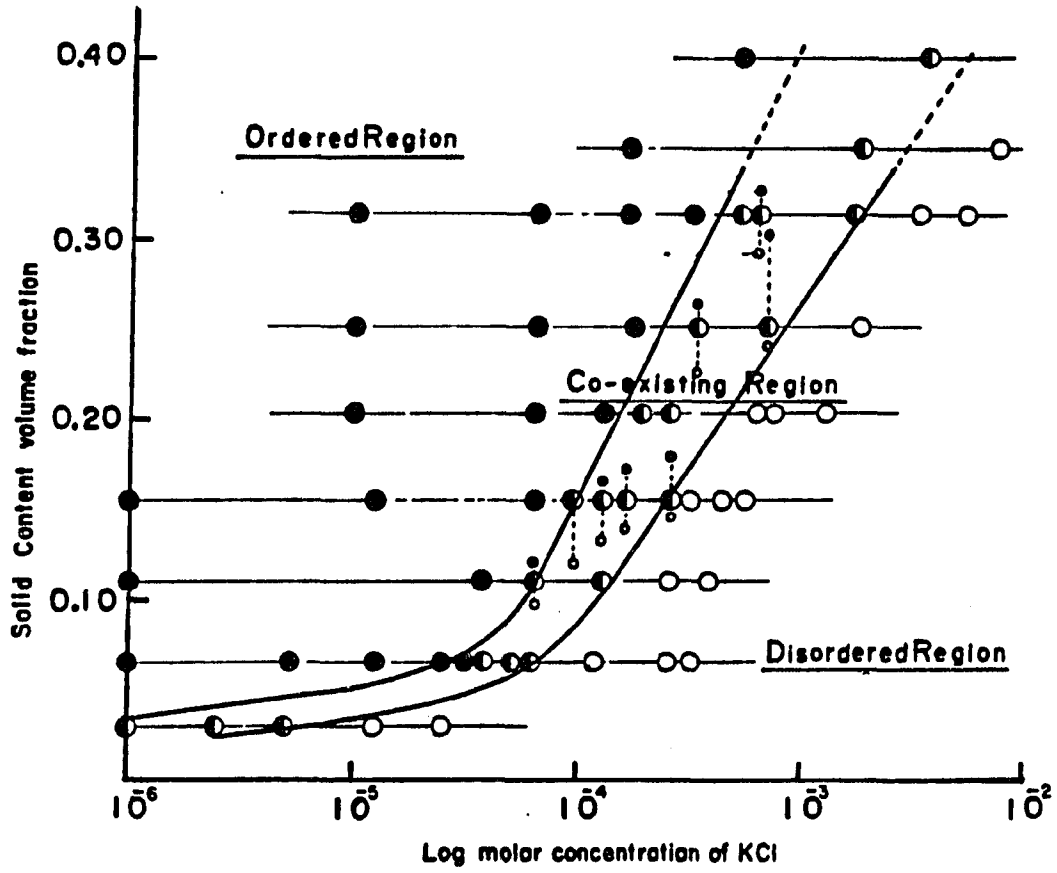

Figure 2. The phase diagram of the polystyrene latex having particle diameter of 1700 angstroms containing KCl. ●-ordered state, O-disordered state, ◐-state of co-existence. ●-volume fraction of the sediment, O-volume fraction of the supernatant and ● and O linked to a ◐-mark by dotted lines representing that these two phases coexist in a state labeled by ◐

unique transition lines, both functions of solids content and electrolyte concentration. One line indicated the disorder to co-existing transition and the other line indicated the co-existing to completely ordered transition.

The explanation for the behavior of these colloidal systems is still under discussion. The transition from a disordered state to an ordered state occurs for a decrease in the electrolyte concentration at a fixed solids concentration and also for an increase in the solids concentration at a fixed electrolyte concentration. In the first case the repulsive forces among the particles become stronger, since the decrease in the ionic strength of the solution results in expansion of the electrical double layers surrounding the particles. In spite of this, however, the transition to an ordered state is accompanied by an increase in the particle density, and furthermore, these two states can coexist under favorable transition conditions.

Three schools of thought have arisen to explain these phenomena. The first attributes it to flocculation in the secondary minimum of the DLVO particle interaction potential energy function (45). The second group (48) claims that it is due to electric repulsion among the particles. Still another group claims that there exists a coulombic attractive interaction, through the intermediary of the counter ions, that is not yet accounted for in the DLVO theory of colloid stability (49). According to the latter postulate, this additional attractive force can create another "secondary minimum" that is further from the origin than the conventional secondary minimum described by the existing DLVO theory.

The problem remains unresolved. It is of great interest because it calls into question the results of two important scientific theories the DLVO theory of colloid stability in colloid chemistry and the Kirkwood-Alder theory of phase transition in molecular physics. The latter theory relates to the behavior of interacting hard spheres in a purely repulsive environment. It has been studied by computer calculations since it was first conceived by Kirkwood in 1939 (50). There are those who believe that the transition behavior of suspensions of monodisperse colloids represents the first experimental verification of the Kirkwood-Alder theory.

Use of Monodisperse Particles in Ceramics

The phase separation which can be made to occur in monodisperse suspensions can be used to form ordered cakes, by sedimentation, at the bottom of a container. This technique was used by Bowen's ceramic engineering group at the Massachusetts Institute of Technology to form dense, ordered cakes of spherical, submicrometer ceramic powders. Their first publication on the subject, by Barringer and Bowen (1) in 1982, described the preparation and sintering of ordered compacts of TiO_2 particles prepared by the controlled hydrolysis and condensation of titanium alkoxides.

The work of Barringer and Bowen has caused a flurry of work by ceramists in the fabrication of dense ceramics from monodisperse particles. Taken in historical perspective, the method may be seen as either an evolutionary or a revolutionary development, depending upon

one's point of view. However, it certainly coincides chronologically with the beginning of a much more scientific approach to ceramic research.

The need for a more fundamental basis for ceramic processing began, about two decades ago, with the concurrent development of two new technologies - solid-state electronics and advanced energy conversion systems. In solid-state electronics, the development of densification methods which could be carried out at lower temperatures was important because it minimized diffusional interaction at interfaces in multilayer chips. At the same time, the dense layers needed to be as free of flaws as possible in order to maintain the desired electrical characteristics of the materials, and to increase the yield of the chips when they were mass-produced.

In advanced energy conversion systems, higher operating temperatures, and larger thermal cycles were encountered as the temperature of the process was raised to increase thermodynamic efficiency. This created large thermal stresses that required the use of nearly flaw free containment materials in order to provide the necessary strength and reliability.

The best way to achieve lower sintering temperatures and still maintain high quality in the manufacture of electronic ceramics is to use powders with smaller particle sizes, since such particles sinter to high density at lower temperatures. However, as particles become smaller their tendency to agglomerate becomes greater - especially at submicrometer sizes. The agglomerated powders do not pack evenly when they are pressed into green compacts. Dense regions sinter more rapidly

than less dense regions and large pores, which can be fracture-initiating flaws, often form. Thus, for conventionally prepared powders, which are quite polydisperse and have irregularly shaped particles, control of particle agglomeration becomes important. If agglomeration is carefully controlled, however, such polydisperse powders can be pressed to high and uniform green densities and can be sintered to near transparency.

Barringer and Bowen's method of using spherical, monodisperse particles and employing the principles of colloid chemistry to form dense, ordered cakes with small, uniform pores is an attractive alternative to the more conventional processing methods. This process is important for particles in the 0.1 to 1.0 μm size range. If the particles are much smaller than about 0.05 to 0.1 μm, they have a much greater tendency to bridge, leaving pores almost as large as the particles. For particles larger than about 1.0 μm the pores, even in a closely-packed body, are so large that higher sintering temperatures are required.

The use of monodisperse particles in ceramic processing is not without difficulties, however. In order to take full advantage of these unique particles, they must be packed into ordered arrays and the order must exist throughout the entire cake. If the cake contains regions of order and disorder, then differential sintering can occur, as happens with cakes containing agglomerated powders. Figure 3 shows poorly packed spheres and also the "vermiculite" or worm-shaped microstructure that occurs when such poorly packed cakes of spherical powders are sintered. Figure 4 shows a fracture surface of a close-packed green

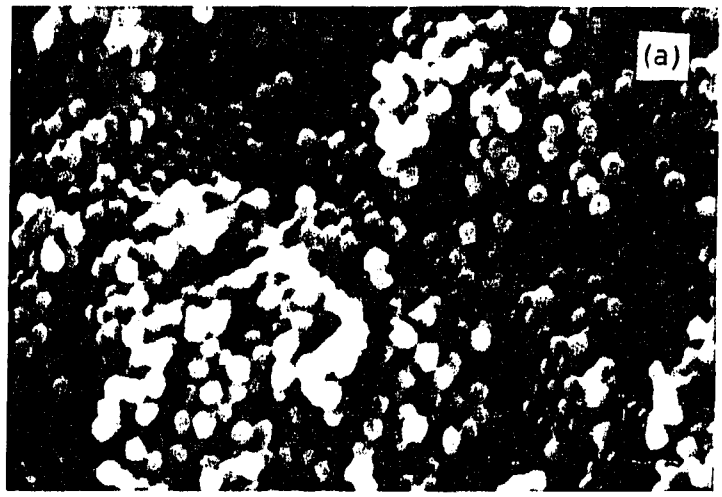

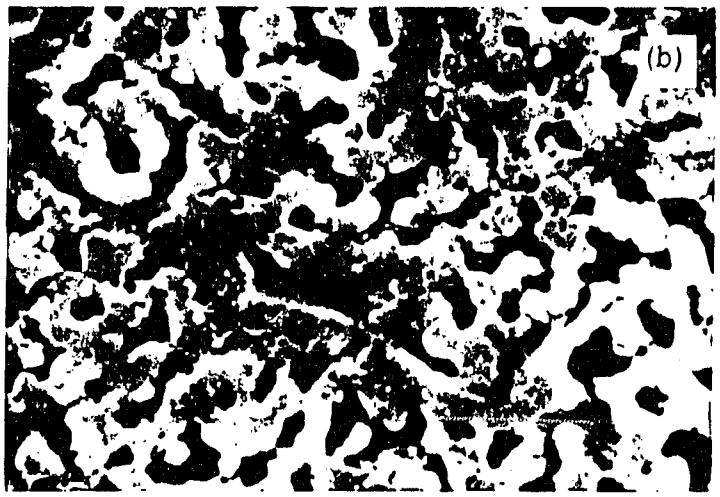

Figure 3. 3a - cake containing regions of order and disorder; 3b - vermiculite microstructure caused by differential sintering

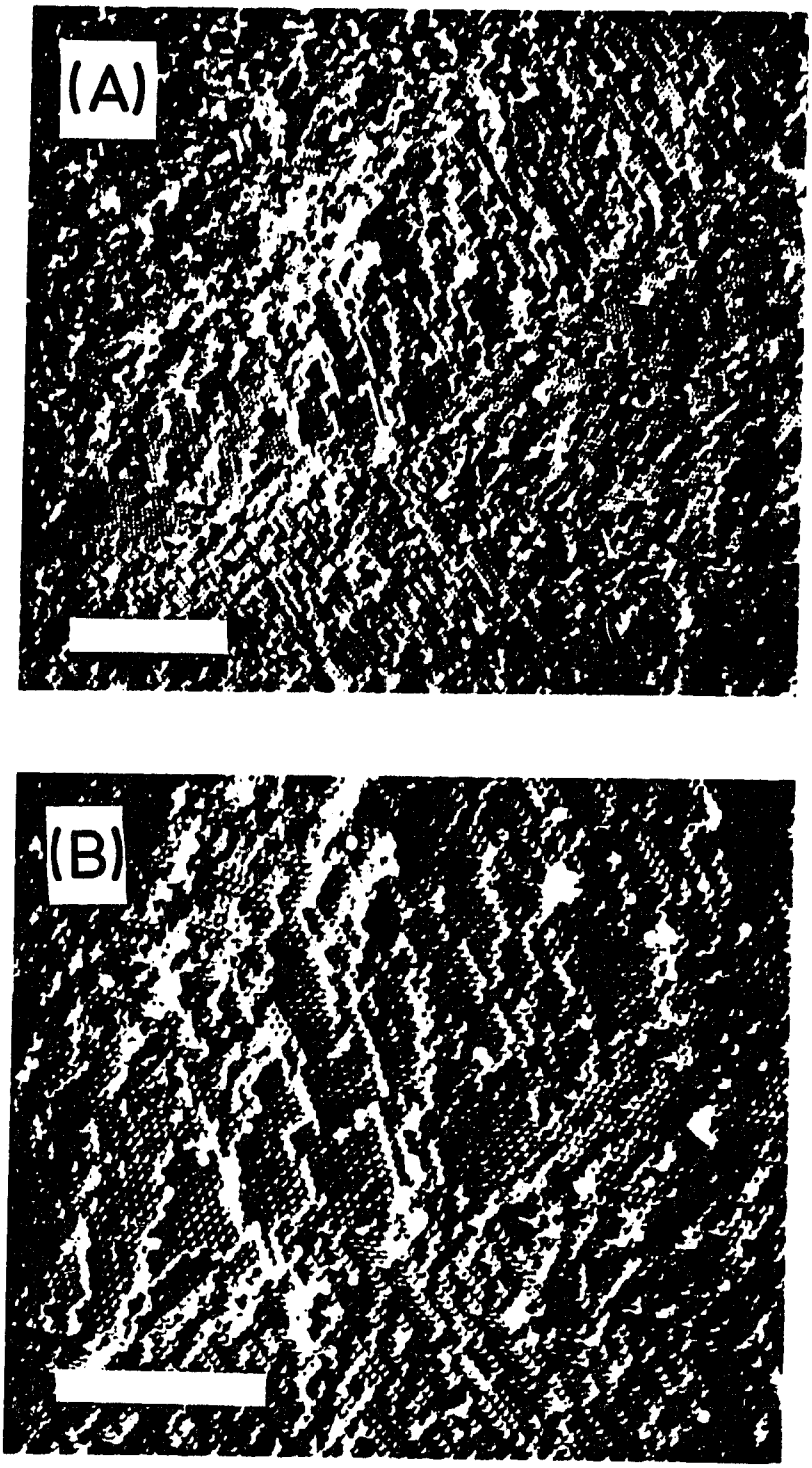

Figure 4. Fracture surfaces of close-packed green cake. 4A - bar = 5 μm; 4B - bar = 3 μm

cake that will sinter to high density.

A great deal of research effort is now being expended on ways of achieving nearly flaw free packing of spherical particles. Such efforts are those of Aksay and Schilling (51) using colloidal filtration, of Hurd et al. (52) using AC fields to induce ordering, of Russel (53) using ultrasonics, and of Iler (54) using surfactant coatings on the particles. Except for the work of Iler, these methods are designed to provide an externally impressed motion to augment the small motions of the individual particles as they vibrate in the crystal-like lattice, thus creating an annealing effect to remove lattice imperfections.

Three other major problems exist. The method, to be really commercially useful, must be capable of producing ordered cakes in complex shapes rather than in the simple geometric forms that can be obtained by sedimentation. Also, the degree of monodispersity of the particles is critical. Figure 5 shows faults created in a two-dimensional lattice by isolated oversize particles. This latter problem must, of course, be addressed when the particles themselves are prepared or else a method of removing them from the bulk powder must be found. Hachisu et al. (47) has reported some evidence that they may tend to be annealed out under proper conditions as the lattice forms, thus lending additional importance to the work being carried out on impressing externally augmented motion of the vibrating particles.

Finally, the chemical composition and surface properties of the monodisperse, spherical particles play an important role in the sintering process. Ideally, the particles should be synthesized and then formed into a green cake without ever having been removed from

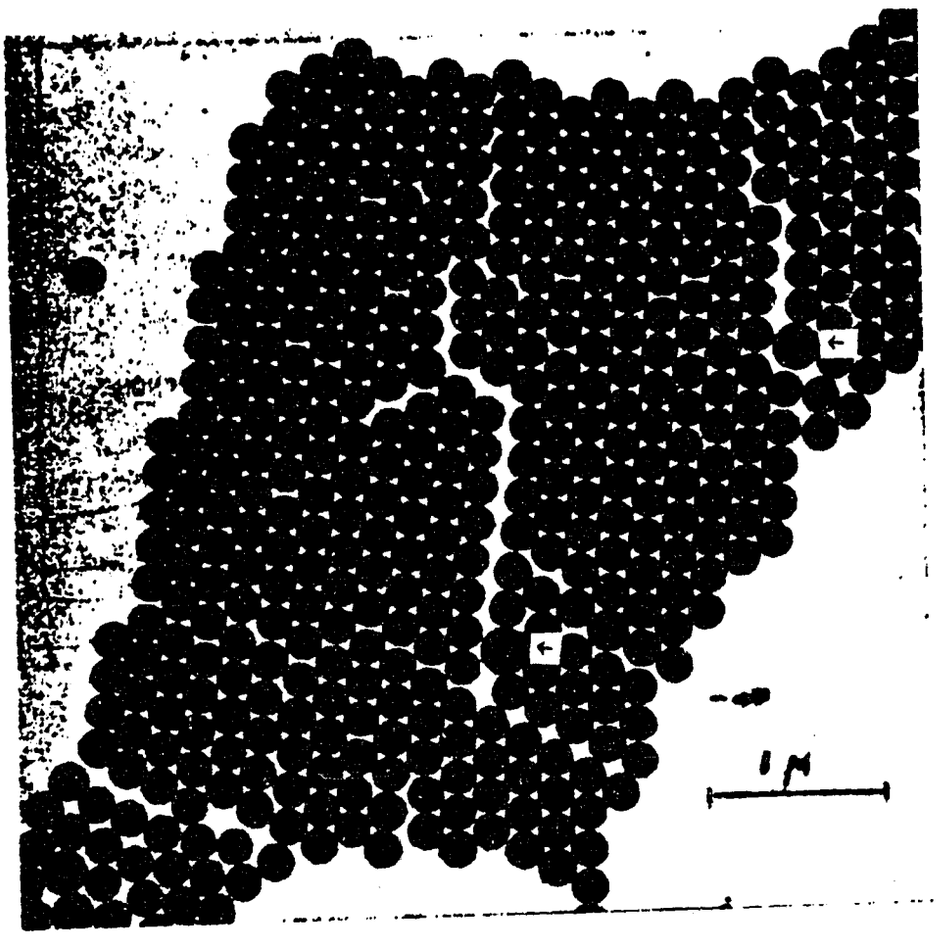

Figure 5. Electron micrograph of a monodisperse latex showing defects caused by nonuniform particles

liquid suspension. When processed this way, the particle surfaces can be kept hydrophyllic; control of their electric double-layers can be used to prevent agglomeration and to facilitate packing into ordered cakes. Most alkoxide-derived particles can be handled this way.

If the precipitated particles are, for example, hydroxides or basic salts they will be converted to oxides as the ordered cakes are heated to their sintering temperature. During this period the particles may shrink in diameter as a result of the calcination reaction. Although the cakes remain ordered, the distance between particles and hence the pore size increases. This often leads to the "wormy" or vermiculite structure described earlier for sintered cakes of poorly packed oxide particles. To overcome this problem, the precursor particles must be calcined, deagglomerated, and then re-hydrated in suspension before the ordered green cake is formed. Such a procedure is somewhat tedious, but progress has been made on the problem. Ciftcioglu and Burkhart (55) have reported sintered densities up to 96% of theoretical for yttria bodies derived from monodisperse particles that were precipitated initially as yttrium hydroxycarbonate.

Continuous Preparation Of Monosized Particles

Only very recently has work been done on the preparation of monodisperse spherical particles of inorganic materials by continuous processing. Kallay et al. (56) devised a continuous column reactor to make metal hydrous oxides by the aging of metal salt solutions, as was done batchwise by Matijevic. Ring et al. (57,58) used a packed column

to hydrolyze metal alkoxides. Haggerty (59) prepared non-oxide powders, largely silicon nitride and silicon carbide by laser heating of gaseous reactants.

In Kallay's vertically positioned column, which was thermostated and held at 100° C, an acidified $FeCl_3$ solution was used to make colloidal hematite particles. The nature of the process imposed substantial restrictions on the design of the column. A 24 hour aging time was needed and conditions approaching plug flow were necessary so that the particles would remain undisturbed as they aged. To achieve these goals, the salt solution was fed to the top of the column and laminar flow down the column was kept at a low enough value that the rate of particle settling was small relative to the flow rate. Because the solids formed settle in the direction of flow, larger particles have a shorter residence time than smaller particles; thus the size distribution of the product is sharpened as the growing particles descend through the column. The modal diameter of the product particles was 0.08μm with a standard deviation of 0.013μm (16% of the modal diameter), a result comparable to that obtained by the batch method for hematite prepared in the same laboratory (60).

Although the same technique could be applied to the generation of other metal hydrous oxides, the long residence times required would make it difficult to prepare powders in large quantities. Aging times up to several weeks have been reported to be necessary for some materials. In Kallay's work, the column was 133 cm long and only 1.2 cm in diameter. The product suspension was removed at a rate of 0.1 ml per minute. Large column diameters would surely produce thermal gradients and local

flow fluctuations that would tend to degrade the narrowness of the product size distribution. Further, only a limited variety of spherical metal hydrous oxides can be made this way.

One interesting part of Kallay's work was his use of a bed of packed silica spheres to remove foreign particles from the feed solution before it was fed to the column. The silica, which is negatively charged, attracts positively charged impurity particles, thus removing them by electrostatic attraction. The pressure drop through such a bed is much lower than would be encountered if a fine filter were used.

In the laser reactor developed by Haggerty (59) gaseous reactants are passed through an intense laser beam. The basic concept of the laser reactor is to provide a small, well-defined heating zone so that all the gas molecules are subjected to similar time-temperature histories and so that the process variables can be manipulated in a reproducible manner. A crossflow design was most successful for experimental work because the process variables could be controlled accurately. In the crossflow reactor a laser beam having a Gaussian-shaped intensity profile orthogonally intersects a premixed reactant gas stream with a parabolic velocity profile. The pressure in the reactor is kept at 0.08 to 0.09 atm. by a throttling valve and a mechanical vacuum pump. The product particles may be collected by a filter or by an electrostatic precipitator. To insure uniform laser intensities, the gas stream must be kept optically thin in the crossflow reactor, thus it is an inefficient design. Only 2 - 15% of the incident light is absorbed by the reactants. A production design would require a counterflow system or other arrangement, such as multiple, radially

opposed beams, to capture more of the light and make the reactor more efficient. Also there needs to be a reasonable match between the wavelengths emitted by the laser and those absorbed by the reactant gases. Haggerty used a CO_2 laser.

For silicon nitride and silicon carbide, the particles were nearly spherical and had little porosity. Particle mean diameters were in the 100 - 500 Angstrom range and the distribution had a typical coefficient of variation of about 25%. The reactions were very fast, with rapid heating rates (10^6 ^oC/sec), short reaction times ($5x10^{-4}$ sec) and rapid cooling rates (10^5 ^oC/sec). It is not yet clear how many different kinds of spherical, monodisperse powders can be made this way, or how much the standard deviation of the particle size distribution can be narrowed by further work. In some cases, chainlike agglomerates of the spherical particles were observed on the collecting filter, but the strength of these agglomerates, or the magnitude of any neck-bonding among the particles is not yet fully known. Since the particles are produced dry, their surface history when they are suspended in a liquid medium prior to attempted sedimentation into dense compacts is also not known.

Ring et al. (57,58) used a packed bed reactor and a static mixer reactor for the production of narrow sized and unagglomerated TiO_2 powders by alkoxide hydrolysis. Residence times ranged from about 30 seconds to about 1000 seconds, corresponding to flow rates of 200 and 5 ml/sec respectively. The mean particle size was typically about 0.3 μm regardless of residence time. The geometric standard deviation was generally between 1.1 and 1.3 depending on the residence time. Longer

residence times tended to give larger geometric standard deviations. There was little difference between the size distributions obtained from the packed bed reactor and the static mixer reactor. Ring used a correlation developed by Bischoff (61), and presented in Levenspiel (62), which related the geometry of the packed bed reactor to a number of stirred tank reactors in series. With this correlation, coupled with a model for the particle size distribution coming from stirred tank reactors in series by Abegg and Balakrishnan (63), he developed a model for the production of the TiO_2 particles from the packed bed reactor. How well Ring's model actually agrees with his experimental results is uncertain because samples were taken from the reactor after only 1.5 residence times. After that, the particles were allowed to age for an hour before specimens were prepared for size analysis by electron microscopy.

PRECIPITATION

Historically, precipitation has been used simply as a means of recovering material from solution, or as a means of separating one substance from another (selective precipitation). The goals were to produce a precipitate which could be filtered and washed easily, and to remove the desired substance from the solution as completely as possible. The detailed characteristics of the precipitate particles were of only secondary interest. In more recent years, however, much greater attention has been given to the properties of the individual particles. A tremendous amount of control over the size, size distribution, porosity, state of agglomeration, degree of crystallinity, and morphology of the particles in a precipitate can be achieved by proper selection of the processing conditions used in preparing the precipitate. Those industries which have had the greatest interest have been those involved in cosmetics and pigments, and more recently, catalysts and ceramics.

Precipitation, in the sense of the present discussion, is commonly carried out by the chemical reaction of two or more reactants. As the reaction proceeds, the concentration of the precipitating species increases and rises above the saturation level. After an induction period, the length of which depends upon the conditions under which the precipitation is being carried out, many small particles begin to appear and the solution becomes turbid. During this period, nucleation has

occurred and the small nuclei have grown in size until they can scatter sufficient visible light to produce the observed turbidity. The particles then continue to grow as additional material is generated by the reaction. The increase in particle size may take place by deposition on the surfaces of existing particles, by particle aggregation, or by both deposition and aggregation. If, in addition, the supersaturation remains high enough, additional nuclei may be formed.

Precipitation may thus be viewed as a process that involves nucleation, growth by solute deposition (usually called crystal growth even though the deposit may be only partially crystalline or even amorphous), and aggregation. The change of phase may take place by nucleation or crystal growth. The increase in the size of the particles, if a particle is defined as a contiguous amount of the solid phase which moves as a single entity in the suspension, may occur by crystal growth or by aggregation.

Nucleation

Nucleation, the necessary first step in the precipitation process, may be homogeneous, heterogeneous, or secondary (64,65,66,67), depending largely upon the supersaturation of the solution. Homogeneous nucleation occurs spontaneously, does not require the presence of surfaces of any kind, and requires the highest level of supersaturation. Heterogeneous nucleation is prompted by the presence of foreign surfaces such as those on small impurity particles in the solution, and can occur

at lower levels of supersaturation. The free energy change required for nucleation to occur at the foreign surface is less than that required for homogeneous nucleation; in this sense, the surface may be considered to catalyze the nucleation process (64,65,66,67). Secondary nucleation is induced by suspended crystals of the solute. Crystal-crystal contact, as well as noncrystal-crystal contact, can give rise to new nuclei. Secondary nucleation also may occur at relatively low levels of supersaturation and is generally a function of suspension density and energy input to the system (65,66,67).

For homogeneous nucleation to occur, the formation of the solid phase must produce a substantial decrease in the excess free energy. In the classical interpretation, the supersaturated solution contains clusters of molecules or ions of solute which are continuously forming and redispersing. Their free energy is made up of two parts - a volume free energy resulting from bond formation and a surface free energy resulting from the formation of a new surface. The surface free energy is a positive quantity and is proportional to the square of the cluster radius. The volume free energy is negative and is proportional to the cube of the cluster radius. As the radius increases, the overall free energy, ΔG, reaches a maximum value when the cluster achieves some critical size, r_c. This size corresponds to the smallest possible stable nucleus. Particles which do not reach the critical radius tend to dissolve and particles larger than the critical radius tend to grow. Thus, an energy barrier, ΔG, must be overcome before homogeneous nucleation can occur.

The critical radius can be estimated from Nielsen's equation (68),

$$r_c = \frac{2\sigma\bar{v}}{RT \ln S} \qquad (3)$$

where σ is the crystal surface tension, $\bar{v}$ is the molar volume, R is the gas constant, T is the absolute temperature, and S is the ratio of the supersaturation solution concentration to the equilibrium concentration. Nielsen has pointed out that for many substances, the value of the critical radius is in the range from 5 to 20 Angstroms. As supersaturation increases, the critical radius decreases and the nucleation rate increases.

Since homogeneous nucleation requires high supersaturations, the presence of a large particle suspension density is often taken as an indication that homogeneous nucleation has occurred.

Both Nielsen (68) and Walton (69) have found that the upper limit of the number of heteronuclei normally present in aqueous solutions is in the range of 10^6 to 10^8 nuclei/ml. Thus, precipitation processes yielding fewer particles than this are most likely the result of heterogeneous nucleation. Further, if the number of precipitate particles is essentially independent of the initial reactant concentration, then heterogeneous nucleation must be suspected of being the dominant nucleation mechanism. Such deductions, of course, also presume that coagulation of the primary particles into larger aggregates has not occurred.

Homogeneous Precipitation

The advantages of precipitation from homogeneous solution have been known since Willard and Tang (33) used it to prepare dense precipitates and LaMer and Dinegar (12) used it to make monodisperse sulphur sols. Only more recently has it been used in technological applications where the unique ability to control particle morphology can be fully exploited. In general, homogeneous precipitation may be viewed as a way of regulating the relative importance of nucleation and crystal growth as the process proceeds. By slowly releasing the precipitant through the decomposition of a dissolved precursor, the phenomena of nucleation and crystal growth can be separated. This permits one to cause all the nuclei to form at essentially the same time, as explained earlier, and then to have all the resulting particles grow at the same rate, producing a population of monodisperse particles.

LaMer and his colleagues explained the formation of their nuclei in terms of homogeneous nucleation; but as the process has come to be examined in greater detail, it seems most probable that heterogeneous rather than homogeneous nucleation initiates homogeneous precipitation (69). The most illuminating discussion of this has only become available very recently in the experimental work of Kayima and Hansen (39). They prepared spherical, monodisperse particles of yttrium hydroxycarbonate by the decomposition of urea in the presence of yttrium nitrate. Both seeded and unseeded precipitations were studied.

Kayima and Hansen found, using silica seeds about 7 nm in size, that below a seed concentration of 4×10^{10} particles/ml pure

heterogeneous nucleation could not occur. When a greater number of seeds were used, the solute was deposited only on the seed crystals; no new particles were formed. Under such conditions, the available solid surface area in the precipitator was great enough to prevent the supersaturation from building up to a sufficiently high level for homogeneous nucleation to occur.

When fewer seed crystals were used, the final particle density rose to very nearly 4×10^{10} particles/ml. A likely explanation for this phenomenon is that additional nuclei were formed, presumably by homogeneous nucleation, to create enough solid surface area that the rate of crystal growth was great enough to consume all of the new material formed by the precipitation reaction. They called 4×10^{10} particles/ml the "critical number concentration", or CNC, of silica seeds below which pure heterogeneous precipitation could not occur.

These conclusions were further supported by their experiments with unseeded systems, in which 3×10^{10} particles/ml were produced. This number was surprisingly close to the CNC observed for seeded systems. They concluded that above the CNC only heterogeneous nucleation occurred and that below the CNC heterogeneous nucleation followed by homogeneous precipitation took place. The particle population which resulted when both processes occurred was always more polydisperse, most likely a result of the occurrence of heterogeneous and homogeneous nucleation at different times; but the polydispersity was moderated by the fact that particle growth fit a diffusion-controlled model in which the smaller particles grew at a faster rate than the larger ones. Since the decomposition kinetics of urea in aqueous solution are well known, they

also were able to determine that the decomposition of urea was the rate-limiting reaction.

In earlier work on the same system, Verlinden (38) also found urea decomposition to be the rate-limiting reaction and that particle growth fit a diffusion-controlled model. In both cases, analyses of the precipitates showed them to be yttrium hydroxycarbonate, $Y(OH)CO_3 \cdot H_2O$, but Kayima and Hansen obtained a crystalline pattern by electron diffraction whereas Verlinden did not.

Zeta potential measurements by Kayima and Hansen showed that H^+ and OH^- are the potential determining ions for the yttrium hydroxycarbonate particles and that the isoelectric point (IEP) was reached at a pH of 7.4. They further found that at the onset of turbidity, an early point in the precipitation, the pH was 6.1, and that the pH increased as the batch precipitation proceeded, probably passing through the IEP and producing the unstable, coagulated sol which they obtained if the precipitation reaction was allowed to continue too long. If the ionic strength of the liquid was too high, coagulation also was observed as a result of compression of the electric double layers surrounding the particles. Their results emphasize the need to regulate both pH and ionic strength during homogeneous precipitation if coagulation is to be avoided. Figure 6 shows both coagulated spheres and uncoagulated spheres, produced under different conditions. If precipitation is continued beyond the coagulation point, neck growth between the particles takes place and the advantages of producing monodisperse spheres are lost.

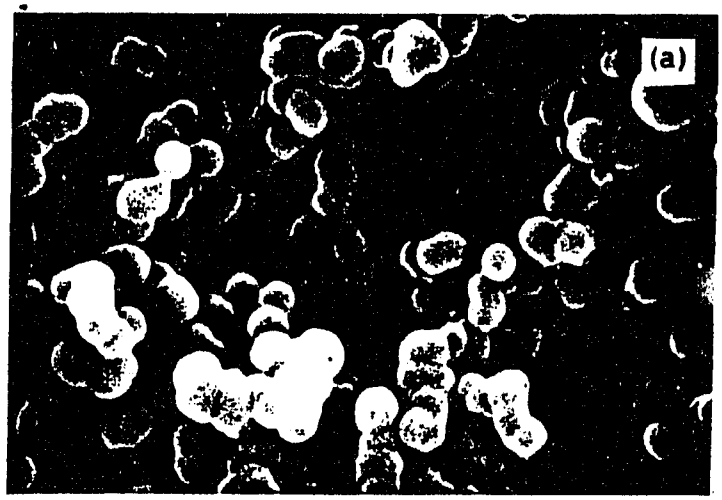

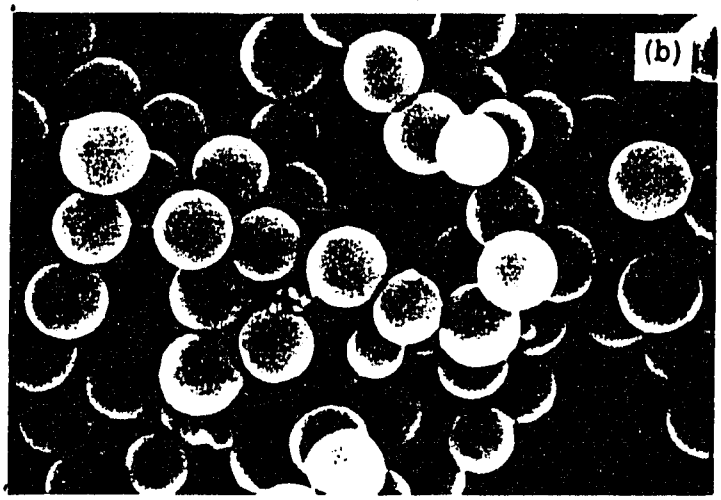

Figure 6. 6a - coagulated spheres; 6b - uncoagulated spheres

Particle Growth

Particle growth in suspension can be thought of as a two step process. The first step is the transport of solute to the particle surface followed by a surface reaction step. In the field of crystallization, this latter step is often referred to as the surface integration step since the solute must be oriented in conformity with the crystal structure. This is often the rate-limiting step in crystal growth. In the case of an amorphous particle, there is no orientation step since there is no crystal structure. Therefore, the surface reaction step will tend to occur much more rapidly in the case of a growing amorphous particle than in the case of a growing crystal.

Molecular and convective transport

If the rate of reaction at the particle surface is fast relative to the transport of ions through the solution, then transport through the solution will control the growth rate. Both convective transport and molecular diffusion can be important in the case of an agitated suspension of solids.

The Frossling equation (70) can be used to determine the relative importance of convective transport vs. molecular diffusion.

$$Sh = 2 + 1.10Re^{1/2}Sc^{1/3} \qquad (4)$$

where $Sh = k_d D_p/D$, Sherwood number

k_d = mass transfer rate constant

D_p = diameter of particle

D = molecular diffusivity

$Re = D_p u_s/\nu$, particle Reynolds number

u_s = particle slip velocity

ν = kinematic viscosity

$Sc = \nu/D$, Schmidt number

The slip velocity, u_s, is the difference in motion between the particles and the circulating fluid. If the particles are large and heavy, there will be a significant difference between the motion of the particles and the circulating fluid. If the particles are small and light, they will tend to move, with little or no slip, along with the circulating fluid.

Miller (71) has suggested an empirical equation from which the slip velocity may be determined in an agitated vessel:

$$\frac{u_s}{u_t} = 6.44 \times 10^{-4} (\text{rpm})^{1.239} \tag{5}$$

where u_t is the terminal settling velocity of the particle which can be obtained from Stokes' law,

$$u_t = \frac{g_c L^2 (\rho_c - \rho)}{18\mu} \tag{6}$$

where g_c is the gravitational constant, L is the particle diameter, ρ_c is the density of the particle, ρ is the density of the fluid, and μ is the fluid viscosity.

The first term on the right hand side of Equation 4 is the mass transfer contribution of molecular diffusion. The second term is the mass transfer contribution of convective transport. If the numerical value of the convective transport term in the Frossling equation is substantially less than 2, then molecular diffusion will be the dominant mass transfer process. On the other hand, if the convective transport term is much greater than 2 then convective transport will dominate.

For the yttrium nitrate-urea system, to be studied in the present work, one can estimate the relative importance of molecular and convective transport as follows. For a particle diameter of 1 μm, a particle density of 2.8 g/cm^3, water at 90° C, and an impeller speed of 750 rpm, the term $1.10Re^{1/2}Sc^{1/3}$ in Equation 4 is equal to 2.5×10^{-2}. Therefore, molecular diffusion will be the dominant mass transfer process.

Particle growth rate

If diffusion is the rate limiting process for particle growth, then one can predict the growth rate from Fick's law. By Fick's law, the molecular flux J is related to the concentration gradient dC/dx by

$$J = D\left(\frac{dC}{dx}\right) \tag{7}$$

where x is the length of the diffusion path, C is the concentration of the diffusing species and D is the diffusion coefficient. The rate of material diffusing to a spherical surface, distance r from the center is

given by

$$\frac{dm}{dt} = 4\pi r^2 D \frac{dC}{dr} \tag{8}$$

where m is moles of diffusant.

If a steady state concentration gradient is set up much more quickly than the rate at which the particle grows, then dm/dt may be considered to be constant and Equation 8 can be integrated to give

$$4\pi D \int_{C_1}^{C_2} dc = \frac{dm}{dt} \int_{r_1}^{r_2} \frac{dr}{r^2} \tag{9}$$

or,

$$\frac{dm}{dt} = \frac{4\pi D (C_2 - C_1)}{\frac{1}{r_1} - \frac{1}{r_2}} \tag{10}$$

If $C_1 = C_e$ (equilibrium concentration) at $r_1 = r$ (the surface of the sphere) and $C_2 = C$ (the bulk liquid concentration) at $r_2 = \infty$, then

$$\frac{dm}{dt} = 4\pi r D (C - C_e) \tag{11}$$

The growth rate can be found by multiplying both sides of Equation 11 by the molar volume $\bar{v}$ and dividing by the particle surface area, $4\pi r^2$ to yield,

$$\frac{dr}{dt} = \frac{D\bar{v}(C - C_e)}{r} \qquad (12)$$

This equation has been derived by many different authors (9,65,68,72). It neglects the influence of the growth of the particle on the concentration gradient, and the mutual influence of all the individual diffusion fields.

Frank (73) and Nielsen (74) both solved the problem of radially symmetric phase growth controlled by diffusion without neglecting the influence of the growth of the particle on the concentration gradient. In the case of dilute solution their results reduce to Equation 12. It also has been found that the individual diffusional fields of particles in suspension can be treated individually when the mean distance between particles is larger than about 10 times the particle diameter (75,13).

PRECIPITATION REACTOR MODELS

Four types of continuous reactors will be examined in this section. They are:

1. stirred tank reactor
2. laminar flow reactor
3. packed bed reactor
4. semi-batch reactor.

Although the laminar flow reactor was not studied in this research, it is examined in this section so that it can be compared with the packed bed reactor. A laminar flow reactor is simply a packed bed reactor with no packing material.

In order to facilitate the formulation of mathematical models for each of these three reactors it is necessary to define a continuous variable to represent the distribution of particle sizes. The population density, n(L), is defined such that

$$\Delta N = \int_{L_1}^{L_2} n(L)\, dL \tag{13}$$

where ΔN is the number of particles in the size range L_1 to L_2, L is some characteristic particle length, and n is some function of L (66). In the case of spherical particles, L is taken to be the particle diameter. Alternately, n can be defined as

$$\lim_{\Delta L \to 0} \frac{\Delta N}{\Delta L} = \frac{dN}{dL} = n(L) . \tag{14}$$

In the sections that follow, only a summary of each model is given. The detailed derivations of the equations are given in Appendices A, B, C, and D.

Stirred Tank Reactor

Randolph and Larson (66) have derived the population balance for a stirred tank reactor operating at steady state with the following assumptions: (a) perfect mixing, (b) no particle classification at withdrawal, and (c) negligible particle breakage. A reactor which conforms to these assumptions is called a mixed suspension, mixed product removal (MSMPR) reactor. Under these conditions the population balance is,

$$\frac{d(Gn)}{dL} + \frac{n}{\tau} - \frac{n_i}{\tau} = 0 \tag{15}$$

where G is the particle growth rate, n_i is the population density of particles in the feed stream, and τ is the average residence time of particles in the reactor. If there are no particles in the feed stream, and if the growth rate is constant, Equation 15 reduces to

$$G\frac{dn}{dL} + \frac{n}{\tau} = 0 \tag{16}$$

which has the simple exponential function,

$$n = n^{o}\exp(-\frac{L}{G\tau}) \tag{17}$$

as a solution. The constant n^{o} is the nuclei population density (mathematically, the number density of particles of zero size). The growth rate and nuclei population density are easily obtained for such a reactor. A plot of experimental values of ln n vs. L, will give a straight line of slope $-1/G\tau$ and intercept of ln n^{o}.

Diffusion-controlled growth

If growth is diffusion-controlled, as is expected for homogeneous precipitation processes, then the growth rate G varies with particle diameter, L, and may be expressed as,

$$G = \frac{dL}{dt} = \frac{4D\bar{v}(C - C_e)}{L} = \frac{k}{L} \tag{18}$$

where k is a constant when the reactor is operating at steady state. If there are no particles in the feed stream ($n_i = 0$) and this expression for G is used in Equation 15, the solution is,

$$n = \frac{n^{o}}{L_o}\exp(\frac{L_o^2}{2k\tau})\ L\ \exp(-\frac{L^2}{2k\tau}) \tag{19}$$

where L_o is the critical nucleus size. At steady state, the term n^{o}/L_o $\exp(L_o^2/2k\tau)$ is constant and the solution may be written as

$$n = cL \exp(-\frac{L^2}{2k\tau}) \tag{20}$$

In most cases the population density, n, has units of number of particles per unit volume per unit length. Sometimes, however, it is more convenient to express n in terms of % particles per unit length. This is usually the case when the particle sizing technique one is using gives results in terms of % particles per unit length as with TEM or with sedimentation type particle size analyzer data. Since,

$$\int_0^\infty ndL = ck\tau = 100\% \tag{21}$$

Equation 19 can be written

$$n = 100\% \left[\frac{L}{k\tau} \exp(-\frac{L^2}{2k\tau}) \right] \tag{22}$$

Thus, for diffusion-controlled growth, the particle size distribution depends on the residence time τ and the growth constant $k(=4D\bar{v}(C-C_e))$. Since k and τ always appear as a product, Equation 22 should be regarded as having only a single parameter. Thus, both the shape of the distribution and also the mean size will both change with a change in the product, $k\tau$. Figure 7 shows a plot of n vs. L for various values of $k\tau$. The particle size distribution curve exhibits a maximum, since n must approach zero as L approaches zero and the curve must pass through the origin. The shape of the particle size distribution curve is a combination of the effect of the residence time distribution for a

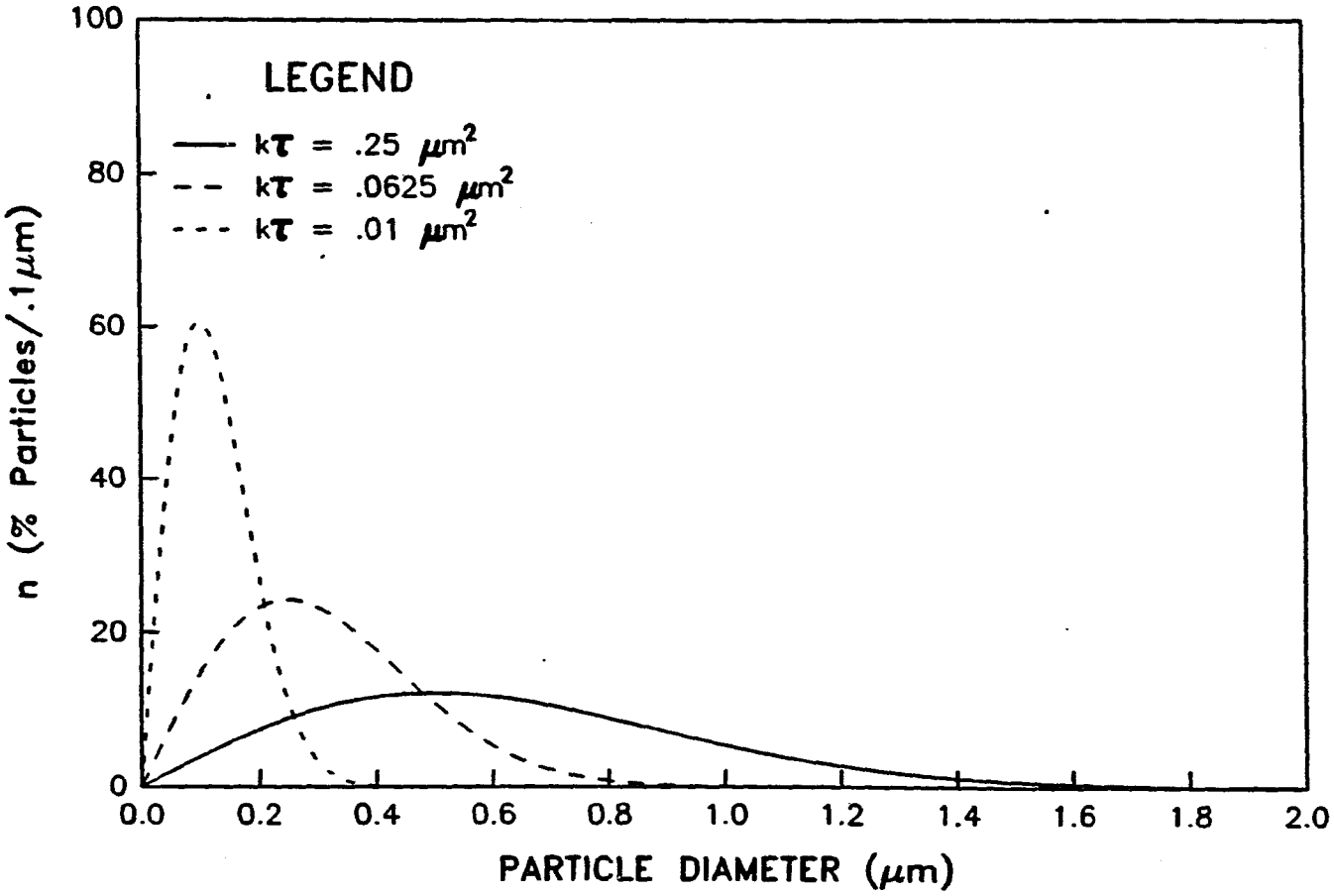

Figure 7. Population density vs. particle diameter for various values of kτ

MSMPR reactor and the fact that the particle growth rate is inversely proportional to particle size, i.e., small particles grow faster than large particles.

There are several important statistical parameters, obtainable from the population density function (66,76), that are useful in characterizing the particle population. The mean particle size, $\bar{L}$, is

$$\bar{L} = \left(\frac{\pi k\tau}{2}\right)^{1/2} \tag{23}$$

and, the variance, σ^2, is

$$\sigma^2 = 2k\tau\left(1 - \frac{\pi}{4}\right) \tag{24}$$

A dimensionless measure of the relative spread of a distribution is the coefficient of variation, C.V., defined as the ratio of the standard deviation of the distribution to the mean particle size,

$$C.V. = \left(\frac{\sigma}{\bar{L}}\right) \times 100\% \tag{25}$$

For a MSMPR reactor with size independent growth, the coefficient of variation is 100%. For diffusion-controlled growth it is,

$$C.V. = \frac{\left(2k\tau\left(1 - \frac{\pi}{4}\right)\right)^{1/2}}{\left(\frac{\pi k\tau}{2}\right)^{1/2}} \times 100\% = \left(\frac{4 - \pi}{\pi}\right)^{1/2} \times 100\% = 52.3\% \tag{26}$$

Equations 23, 24, and 26 show that the mean and variance of the particle size distribution are proportional to $(k\tau)^{1/2}$ and $k\tau$ respectively, but the coefficient of variation is independent of these variables. Thus, while $\bar{L}$ and σ^2 increase with increasing values of $k\tau$, the relative spread of the size distribution remains constant, independent of the operating parameters.

For the sake of comparison, the coefficient of variation of "monodisperse" yttria precursor powder prepared by Kayima and Hansen (39) via a batch process ranged from 9.2% to 16.4%.

The particle size at which the population density is a maximum is known as the mode of the distribution, L_M. It is found by taking the derivative of Equation 22 with respect to L and setting it equal to zero. This yields,

$$L_M = (k\tau)^{1/2} \tag{27}$$

By comparing Equations 23 and 27 we see that the mean particle size $\bar{L}$ and the modal particle size L_M have the same dependence on $k\tau$ but that L_M is slightly smaller than $\bar{L}$.

The importance of Equation 27 is that it can be used easily to determine the concentration of the rate-limiting diffusant in a MSMPR reactor. If one assumes that the concentration of the diffusing species at the surface of the particle is negligible compared to the concentration of the species in the bulk solution, then $k = 4D\bar{v}C$. Substituting this expression for k into Equation 16 and solving for C gives

$$C = \frac{L_M^2}{4D\bar{V}\tau} \tag{28}$$

Thus, given reasonable estimates of D and $\bar{v}$, the concentration of the rate-limiting diffusant can be determined from the value of L_M obtained from a plot of n vs. L. Conversely, if one knows the concentration of the diffusing species as well as D and $\bar{v}$, then it is possible to predict, a priori, the shape of the particle size distribution that will be produced.

Laminar Flow Reactor

In a simplified analysis of a tubular laminar flow reactor, it can be assumed that dispersion due to axial and radial diffusion of the particles is negligible. In this case, the particles flow through a tube with a parabolic velocity profile given by,

$$u(\rho) = \frac{2Q}{\pi\rho_o}\left[1 - \left(\frac{\rho}{\rho_o}\right)^2\right] \tag{29}$$

where, $u(\rho)$ = fluid velocity as a function of radial position

Q = flow rate

ρ_o = tube radius

ρ = radial position measured from the center of the tube

If one further assumes that nucleation takes place only at the entrance of the tube, then the residence time of a growing particle in

the reactor is a function of its radial position, since the velocity varies in a parabolic fashion across the tube. Dispersion of the particles by radial diffusion would tend to narrow the size distribution while axial diffusion and nucleation throughout the tubular reactor would tend to broaden the size distribution.

If the particles grow by diffusion, G=k/L and, as explained earlier, k may be assumed constant under steady-state operation. Under these conditions, the population density distribution for particles leaving the reactor can be shown to be,

$$n = \frac{4(k\tau)^2}{L^5} \tag{30}$$

Figure 8 shows a plot of n vs. L for diffusion-controlled growth in a laminar flow reactor. Like the expression for the size distribution in a MSMPR reactor, Equation 22, Equation 30 has one adjustable parameter, $k\tau$. The minimum particle size, L_{min}, is equal to $(k\tau)^{1/2}$. This is the size of a particle which travels down the center streamline of the reactor. The mean particle size, $\bar{L}$, is given by Equation 58

$$\bar{L} = \frac{4}{3}(k\tau)^{1/2} \tag{31}$$

The variance is

$$\sigma^2 = \frac{2}{9}(k\tau) \tag{32}$$

and the coefficient of variation is

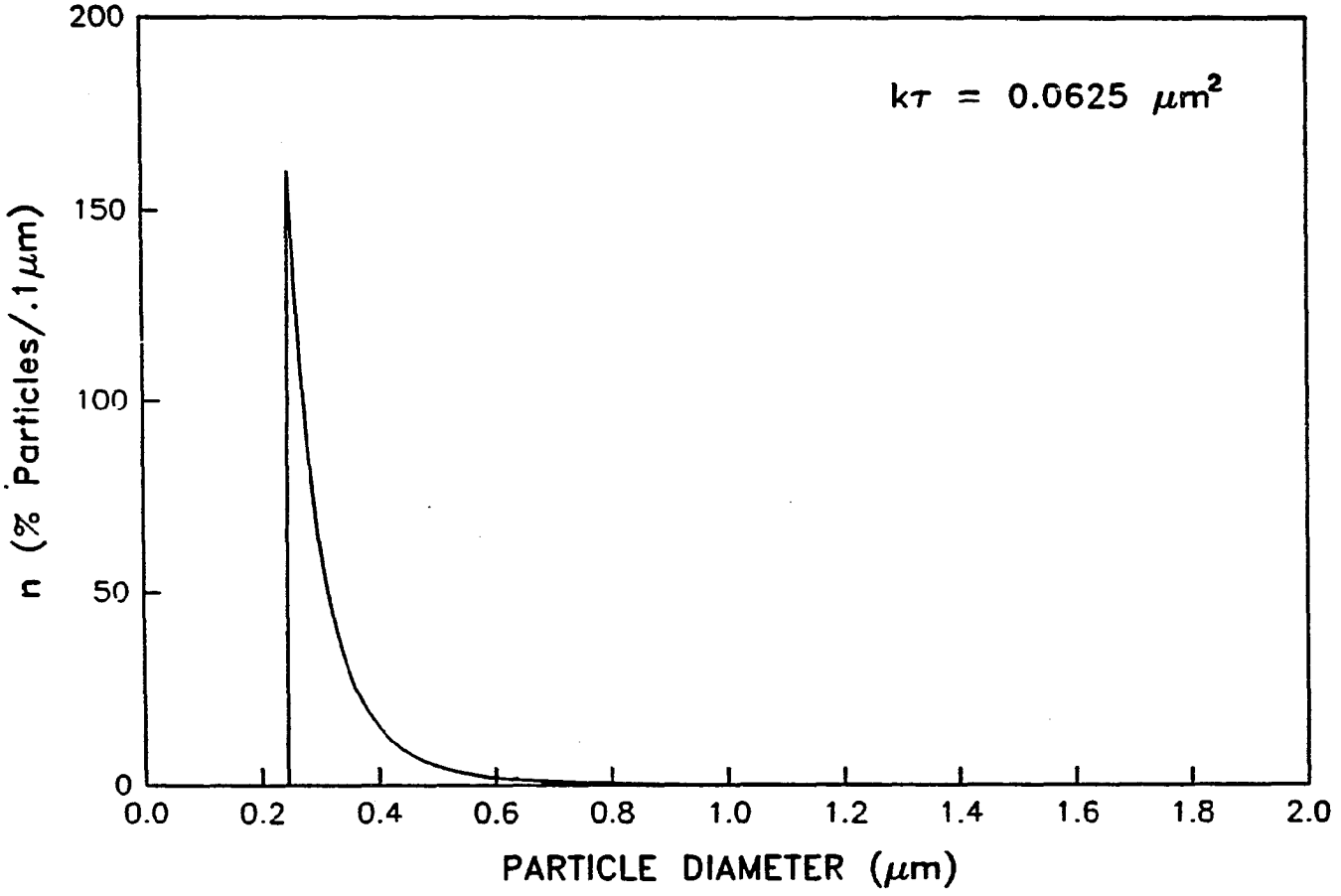

Figure 8. Population density vs. particle diameter for a laminar flow reactor

$$C.V. = \frac{(2/9)^{1/2}}{4/3} \times 100\% = 35.4\% \qquad (33)$$

This is significantly better than the coefficient of variation for the stirred tank reactor, which was shown in the previous section to be, 52.3%.

The laminar flow reactor does not produce the fine particles that the stirred tank reactor does; the minimum residence time occurs for those particles flowing through the center of the reactor where the velocity is a maximum. However, the exponential decay in population density of the stirred tank reactor means that it will have fewer very large particles than the laminar flow reactor.

As was the case for the the stirred tank reactor, the concentration of the rate limiting diffusant can be estimated by determining some characteristic parameter of the size distribution such as the mean or modal particle size. In the case of the laminar flow reactor, it is easiest to use the minimum particle size. Once the minimum particle size is known the constant k can be determined. The concentration of the the rate-limiting species can then be estimated from a knowledge of k.

Packed Bed Reactor

For continuous precipitation of monosized particles it is necessary to have a reactor with a very narrow residence time distribution typical of plug flow. Plug flow can be approximated by a large number of

stirred tank reactors in series. The residence time distribution (RTD) for m stirred tank reactors in series can be found in a number of texts on chemical reactor design (62,77,78). The variance of the residence time distribution is

$$\sigma^2 = \frac{1}{m} \tag{34}$$

For very large values of m the RTD curve becomes increasingly symmetrical and approaches a normal curve (77). The tanks-in-series model is sometimes used to account for deviations from plug flow of tubular vessels and packed beds. Abegg and Balakrishnan (63) used the tanks-in-series concept as a mixing model to calculate the types of crystal size distributions which can result when the active volume of a crystallizer is not well mixed. They derived the following expression for the particle size distribution in terms of the number of tanks, m.

$$n_m = n^o\left[\frac{(ZL)^{m-1}}{(m-1)!}\right]\exp(-ZL) \tag{35}$$

where n_m is the crystal size distribution of the m^{th} tank, n^o is the nuclei population density of the first tank, and $Z = m/G\tau$. In deriving Equation 35 they assumed that nucleation occurs only in the first tank, and that the particle growth rate G, is independent of size. Abegg and Balakrishnan (63) also derived the particle size distribution for m stirred tank reactors in series assuming that the nucleation rate was equal in all tanks. That expression is

$$n_m = n^o\left[\sum_{a=1}^{m} \frac{(ZL)^{a-1}}{(a-1)!}\right]\exp(-ZL) \tag{36}$$

Another model which is used to account for deviations from plug flow is the dispersion model (62,77,78). In an equation analogous to Fick's law, all the contributions to backmixing of fluid flowing in the x direction can be described as follows:

$$\frac{dc}{dt} = D_a\frac{\partial^2 C}{\partial x^2} \tag{37}$$

where the parameter D_a, which is called the longitudinal or axial dispersion coefficient, uniquely characterizes the degree of backmixing during flow.

In dimensionless form where $z = (ut + x)/l$ and $\theta = tu/l$ Equation 37 becomes

$$\frac{\partial C}{\partial \theta} = \left(\frac{D_a}{ul}\right)\frac{\partial^2 C}{\partial z^2} - \frac{\partial C}{\partial z} \tag{38}$$

where the dimensionless group D_a/ul, called the vessel dispersion number, describes the extent of axial dispersion. As $D_a/ul \to 0$, the dispersion is negligible, hence plug flow occurs. As $D_a/ul \to \infty$, the dispersion becomes large and mixed flow results. For a closed vessel, the variance of the residence time distribution is (62,77)

$$\sigma^2 = 2\frac{D_a}{ul} - 2\left[\frac{D_a}{ul}\right]^2 \left(1 - e^{\frac{ul}{D_a}}\right) \tag{39}$$

At small values of the dispersion number (< .1) plug flow is approached and Equation 39 becomes

$$\sigma^2 = \frac{2D_a}{ul} \tag{40}$$

This dispersion model gives residence time distributions that are identical to the tanks-in-series model (57,77). Ring (57) used the similarity of RTD results to analyze a packed bed reactor that produced $TiO_2 \cdot xH_2O$. He used a correlation developed by Bischoff (61) and presented in Levenspiel (62) for dispersion intensity as a function of Reynolds number for packed bed flow. This correlation gives the intensity of dispersion, $D_a\varepsilon/(ud_p)$, as a function of Reynolds number $d_p u\rho/\mu$ where d_p is the diameter of the packing material and ε is the void fraction. The dispersion number D_a/ul is calculated from the intensity of dispersion and the geometric shape factor for the packed bed $(d_p/(\varepsilon d))(d/l)$ where d is the diameter of the reactor and l is the reactor length.

$$\frac{D_a}{ul} = \left[\frac{D_a\varepsilon}{ud_p}\right]\left[\frac{d_p}{\varepsilon d}\,\frac{d}{l}\right] \tag{41}$$

At low Reynolds numbers, $D_a\varepsilon/ud_p$ is essentially constant at about 2.0. Therefore, the dispersion number may be determined using the simpler

expression,

$$\frac{D_a}{ul} = \frac{2d_p}{\varepsilon l} \tag{42}$$

Once D_a/ul was found from the correlation, the equivalent number of stirred tank reactors in series, m, was determined by combining Equations 34, 40 and 42 to get

$$m = \frac{\varepsilon l}{4d_p} \tag{43}$$

After finding a value of m, the number of series reactors approximated by the packed bed reactor, Ring used Equations 35 and 36 to predict the size distribution of $TiO_2 \cdot xH_2O$ particles produced by his packed bed reactor. He found that the model which assumes equal nucleation rates in all tanks (Eq. 36) to be the best fit to his experimental data.

Ring (57) implicitly assumed that particle growth rate was size independent, an assumption that contradicts most experimental data for alkoxide hydrolysis by homogeneous precipitation. In this research, however, particle growth is assumed to be diffusion-controlled. The size distribution for m stirred tank reactors in series with diffusion-controlled growth and nucleation only in the first tank is

$$n_m = 100\% \left[\frac{B^m L^{2m-1}}{2^{m-1}(m-1)!}\right] \exp\left(-\frac{BL^2}{2}\right) \tag{44}$$

where $B = m/k\tau$. Figure 9 shows the particle size distributions predicted by Equation 44 for different numbers of stirred tank reactors

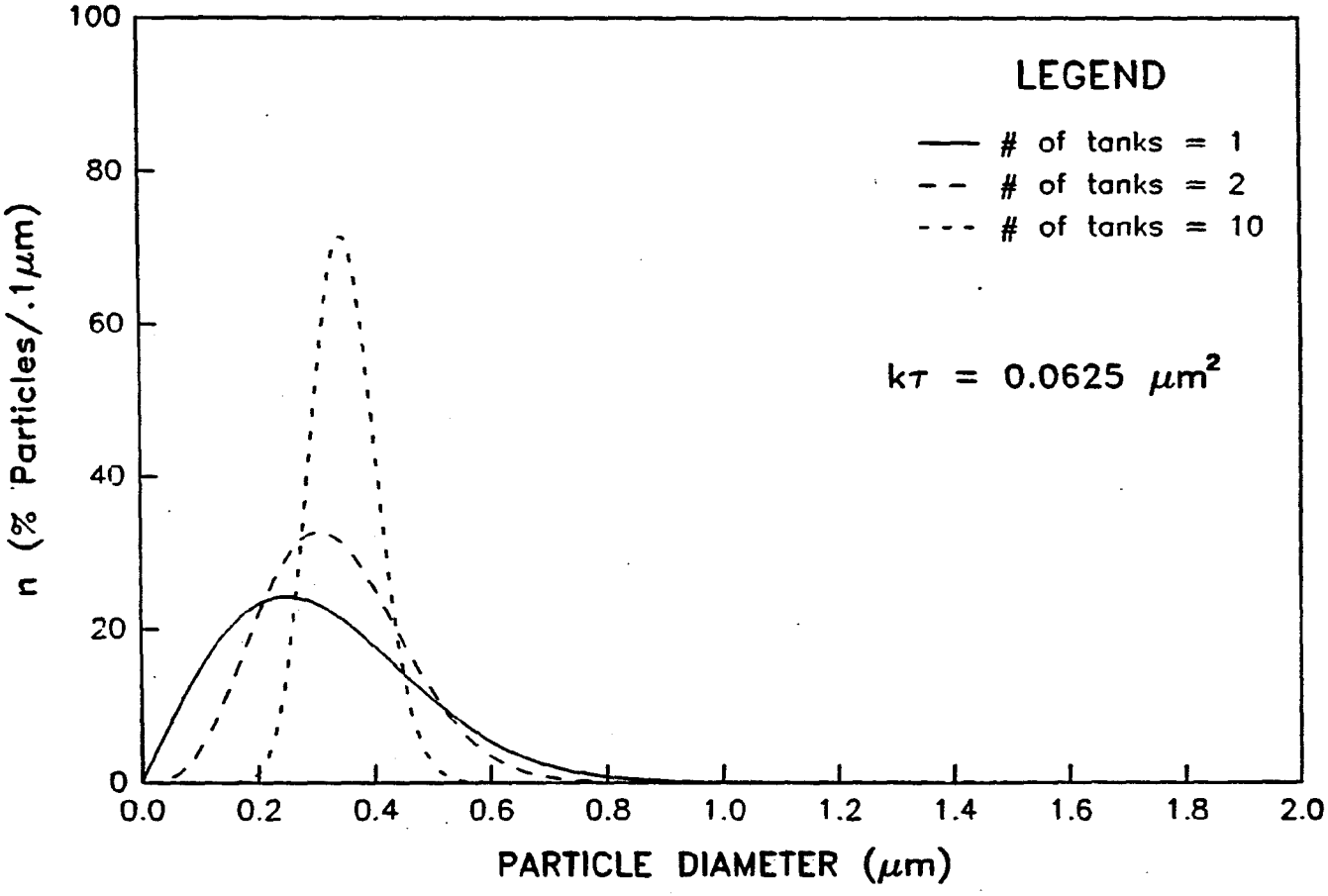

Figure 9. Population density vs. particle diameter for the packed bed reactor model assuming nucleation occurs only in the first tank

in series. As the number of tanks in series increases, the particle size distribution becomes more narrow and more symmetrical.

For the case of equal nucleation in all tanks the size distribution coming from the m^{th} tank is

$$n_m = \frac{100\%}{k\tau} \sum_{a=0}^{m-1} \frac{B^a L^{2a+1}}{2^a a!} \exp\left(-\frac{BL^2}{2}\right) \qquad (45)$$

Figure 10 shows the particle size distributions predicted by Equation 45 for different numbers of stirred tank reactors in series. This model predicts that the decrease in the coefficient of variation with increasing numbers of tanks will be significantly less than the model in which it is assumed that nucleation occurs only in the first tank. Also, because new nuclei are assumed to be forming continuously, the particle size distribution remains unsymmetrical as the number of tanks increases. Equations 44 and 45 are two parameter models, both $k\tau$ and m can be varied.

The mean, variance, and coefficient of variation for the packed bed reactor are given in Table 1 along with the statistical parameters for the MSMPR and laminar flow reactors.

The importance of the packed bed reactor is that it allows one to produce a desired size distribution by adjusting the geometric parameters of the reactor (i.e., length, diameter, packing size). As was stated in the introduction, controlling the size distribution of ceramic powders is crucial in the production of high performance ceramics. In particular, having a ceramic powder with a narrow size distribution is thought to be the key to improving the fracture

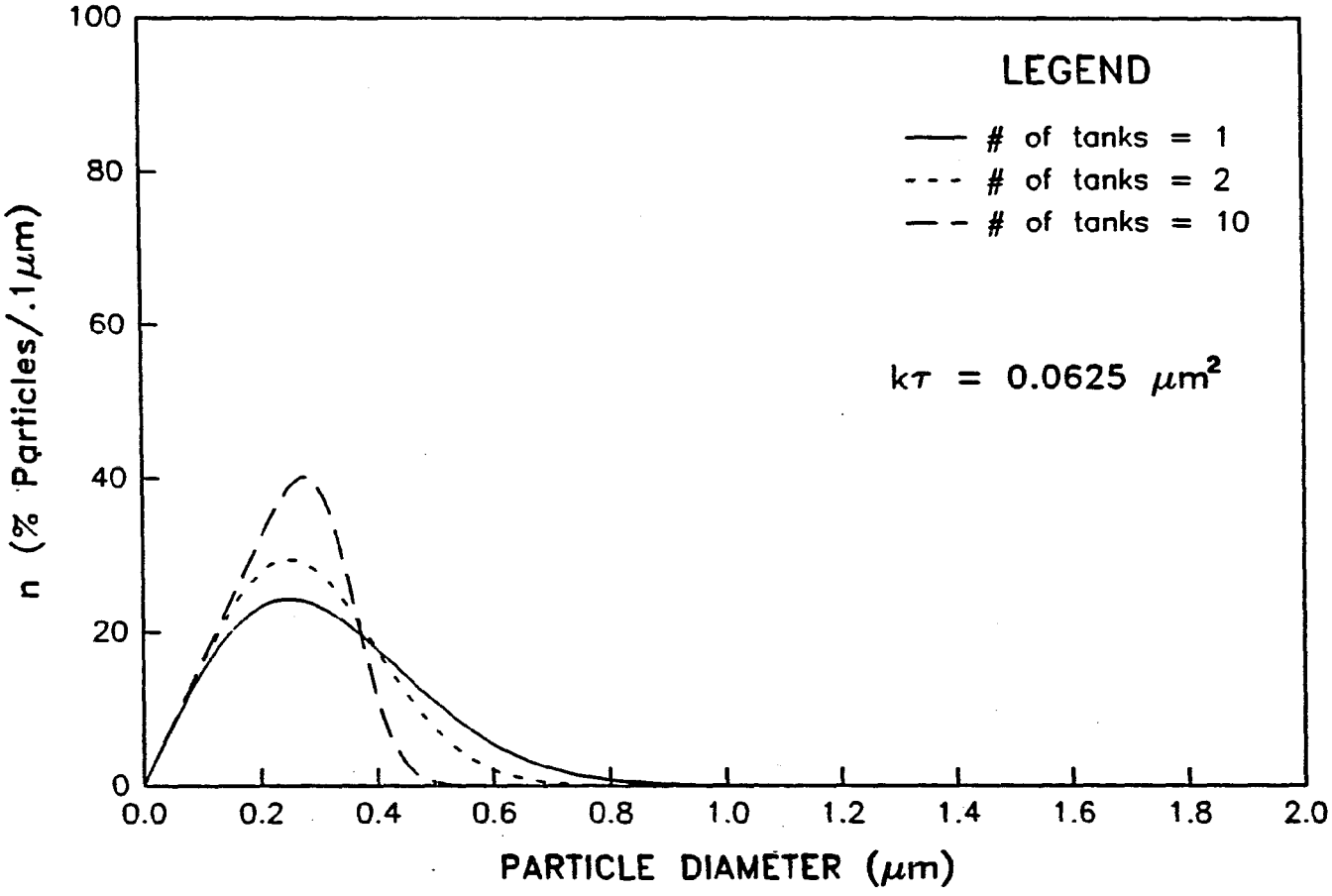

Figure 10. Population density vs. particle diameter for the packed bed reactor model assuming equal nucleation in all tanks

Table 1. Summary of MSMPR, laminar flow, and packed bed models

	MSMPR	LAMINAR FLOW	PACKED BED (nucleation in first tank only)	PACKED BED (equal nucleation in all tanks)
n	$\frac{L}{k\tau}\exp\left(-\frac{L^2}{2k\tau}\right)$	$\frac{4(k\tau)^2}{L^5}$	$\left[\frac{B^m L^{2m-1}}{2^{m-1}(m-1)!}\right]\exp\left[-\frac{BL^2}{2}\right]$	$\frac{1}{k\tau}\sum_{a=0}^{m-1}\frac{B^a L^{2a+1}}{2^a a!}\exp\left[-\frac{BL^2}{2}\right]$
$\bar{L}$	$\left(\frac{\pi k\tau}{2}\right)^{1/2}$	$\frac{4(k\tau)^{1/2}}{3}$	$\frac{(2m-1)!!}{2^m(m-1)!}\cdot\left(\frac{2\pi}{B}\right)^{1/2}$	$\frac{2^{1/2}}{mB^{1/2}}\sum_{a=0}^{m-1}\frac{\Gamma(a+3/2)}{a!}$
σ^2	$2k\tau(1-\pi/4)$	$\frac{2k\tau}{9}$	$\frac{2}{B}\left[m-\left(\frac{(2m-1)!!}{2^m(m-1)!}\right)^2\cdot\pi\right]$	$\frac{2}{m^2B}\left\{m\sum_{a=0}^{m-1}\frac{\Gamma(a+2)}{a!}-\left[\sum_{a=0}^{m-1}\frac{\Gamma(a+3/2)}{a!}\right]^2\right\}$
$\frac{\sigma}{\bar{L}}$	$\frac{(4-\pi)^{1/2}}{\pi^{1/2}}$	$\frac{(2/9)^{1/2}}{4/3}$	$\frac{2^m(m-1)!\left[m-\pi\left(\frac{(2m-1)!!}{2^m(m-1)!}\right)^2\right]^{1/2}}{(2m-1)!!\cdot\pi^{1/2}}$	$\frac{\left[m\sum_{a=0}^{m-1}\frac{\Gamma(a+2)}{a!}-\left[\sum_{a=0}^{m-1}\frac{\Gamma(a+3/2)}{a!}\right]^2\right]^{1/2}}{\sum_{a=0}^{m-1}\frac{\Gamma(a+3/2)}{a!}}$

$$B=\frac{m}{k\tau}$$

$$(2m-1)!!=(2m-1)(2m-3)(2m-5)\cdots5\cdot3\cdot1$$

toughness of ceramic components. At this point no one has ever said how narrow a size distribution must be in order to obtain an acceptable packing of the ceramic powder. Ring (57) has stated that a geometric standard deviation of 1.2 or less is necessary, but he gives no justification for this conclusion.

Semi-Batch Reactor

Roth et al. (79) have shown that the semi-batch operation of a continuous stirred tank reactor can be used to produce levels of macromixing that range between the two limiting cases of plug flow and complete backmixing. This makes the semi-batch reactor very attractive as a means of producing a particle size distribution with a given degree of monodispersivity, since the size distribution can be adjusted by merely changing the operating parameters.

The operation of a semi-batch reactor consists of three separate modes which are repeated in sequence. In the first mode, reactant is fed into the reactor at a constant flow rate and the volume of the reactor increases linearly from the minimum volume, V_o, to the maximum volume, V_m. After the filling mode comes the batch mode, during which there is no flow in or out of the reactor. Finally, there is the emptying mode, in which product is removed from the reactor at a constant flow rate until the reactor volume has decreased from V_m to V_o. The duration of the filling and emptying modes have been assumed to be equal. This simplifies the analysis but does not severely restrict the number of possible operating policies (79). The semi-batch operating

cycle is shown in Figure 11.

It has been shown (79) that, after an infinite number of cycles, the residence time distribution for a semi-batch reactor can be expressed as

$$f(\theta) = \sum_{z=0}^{\infty} (V)^z \frac{(\theta-\theta_B-z\theta_T)}{\theta_F} [U(\theta-\theta_B-z\theta_T) - U(\theta-\theta_B-\theta_E-z\theta_T)]$$

$$+ \sum_{z=0}^{\infty} (V)^z [1- \frac{(\theta-\theta_B-\theta_E-z\theta_T)}{\theta_F}] [U(\theta-\theta_B-\theta_E-z\theta_T) - U(\theta-(z+1)\theta_T)] \quad (46)$$

where

$$U(x)=1 \quad (x\geq 0)$$

$$=0 \quad (x<0) \quad (47)$$

and

dimensionless time, $\theta = Q_S t/V_m$
volume fraction, $V = V_O/V_m$
Q_S = flow rate during filling mode
t = time
V_m = maximum reactor volume
V_O = minimum reactor volume
θ_B, θ_E, θ_F, and θ_T are the dimensionless batch, emptying, filling, and total cycle time, respectively.

By knowing the residence time distribution for the reactor and by knowing an expression for the growth rate of particles in the reactor ($dL/dt=k/L$), one can arrive at the particle size distribution produced by the reactor under various operating conditions.

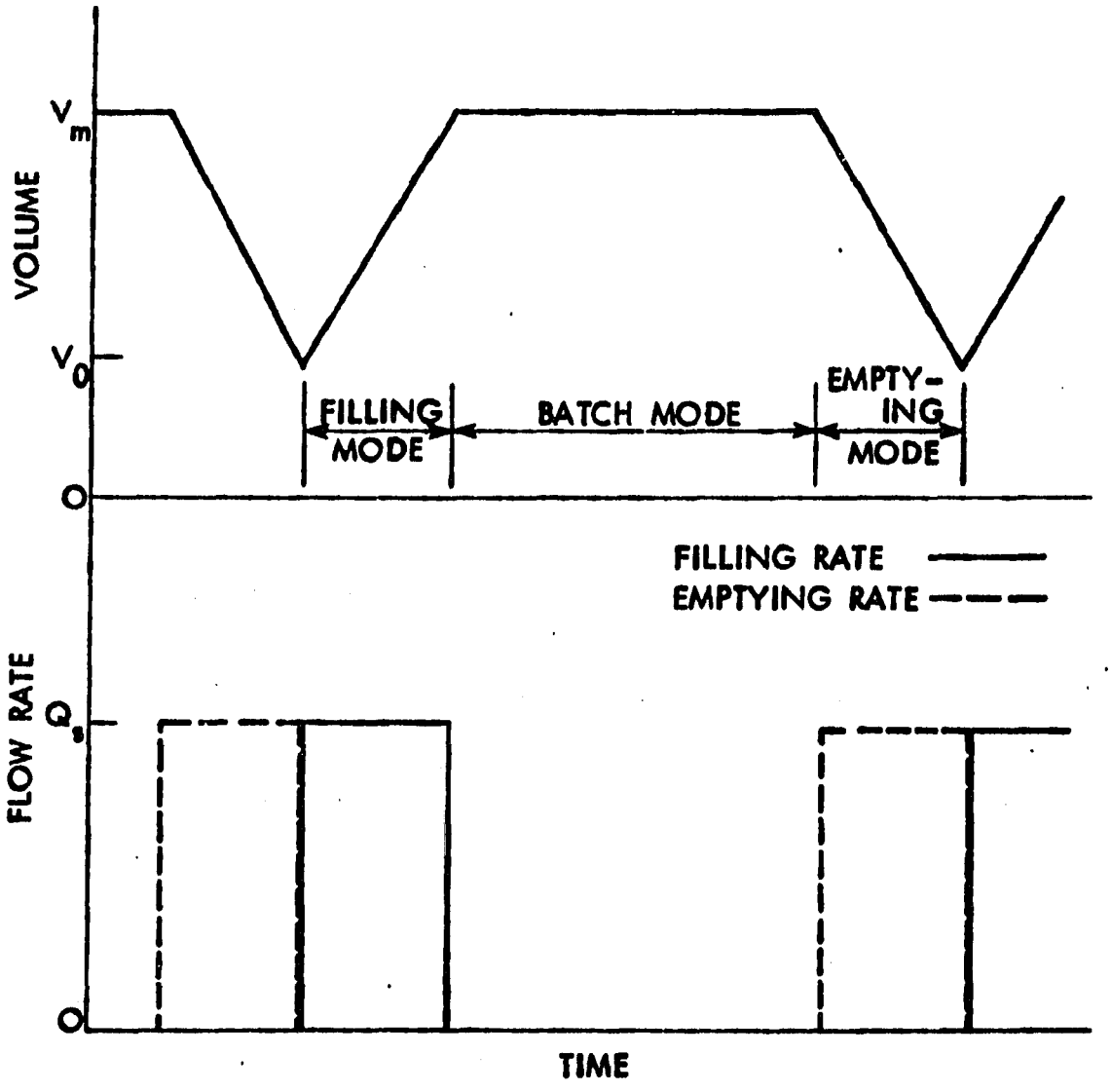

Figure 11. Semi-batch reactor operating cycle(79)

$$n = \frac{4L(1-V)}{k[(1-\sigma_B)t_T]^2}\left\{\sum_{z=0}^{\infty} V^z\left(\frac{L^2}{2k} - (\sigma_B+z)t_T\right)\left[U\left(\frac{L^2}{2k} - (\sigma_B+z)t_T\right)\right.\right.$$

$$\left. - U\left(\frac{L^2}{2k} - \frac{1}{2}(\sigma_B+2z+1)t_T\right)\right] + \sum_{z=0}^{\infty} V^z\left[\frac{t_T(1-\sigma_B)}{2} - \frac{L^2}{2k} - \frac{1}{2}(\sigma_B+2z+1)t_T\right]$$

$$\left.\left[U\left(\frac{L^2}{2k} - \frac{1}{2}(\sigma_B+2z+1)t_T\right) - U\left(\frac{L^2}{2k} - (z+1)t_T\right)\right]\right\} \qquad (48)$$

where t_T is the total cycle time and σ_B is the batch fraction which is equal to the batch time divided by the total cycle time. Equation 48 is a four parameter model. The adjustable variables are t_T, k, σ_B, and V. Figures 12 and 13 show how the particle size distribution varies as a function of batch fraction and volume fraction respectively. As the batch fraction increases, the individual peaks sharpen and as volume fraction increases, the number of peaks with a significant fraction of particles increases.

The mean particle size, $\bar{L}$, for a semi-batch reactor with diffusion controlled growth is

$$\bar{L} = \frac{4(1-V)(kt_T)^{1/2}}{(1-\sigma_B)^2}\left\{\sum_{z=0}^{\infty} V^z\left[\frac{1}{10}(T_1^5 - T_2^5) - \frac{1}{3}(T_1^3 - T_2^3)(\sigma_B + z)\right]\right.$$

$$\left. + \sum_{z=0}^{\infty} V^z\left[\frac{1}{3}(T_3^3 - T_1^3)(z+1) - \frac{1}{10}(T_3^5 - T_1^5)\right]\right\} \qquad (49)$$

where

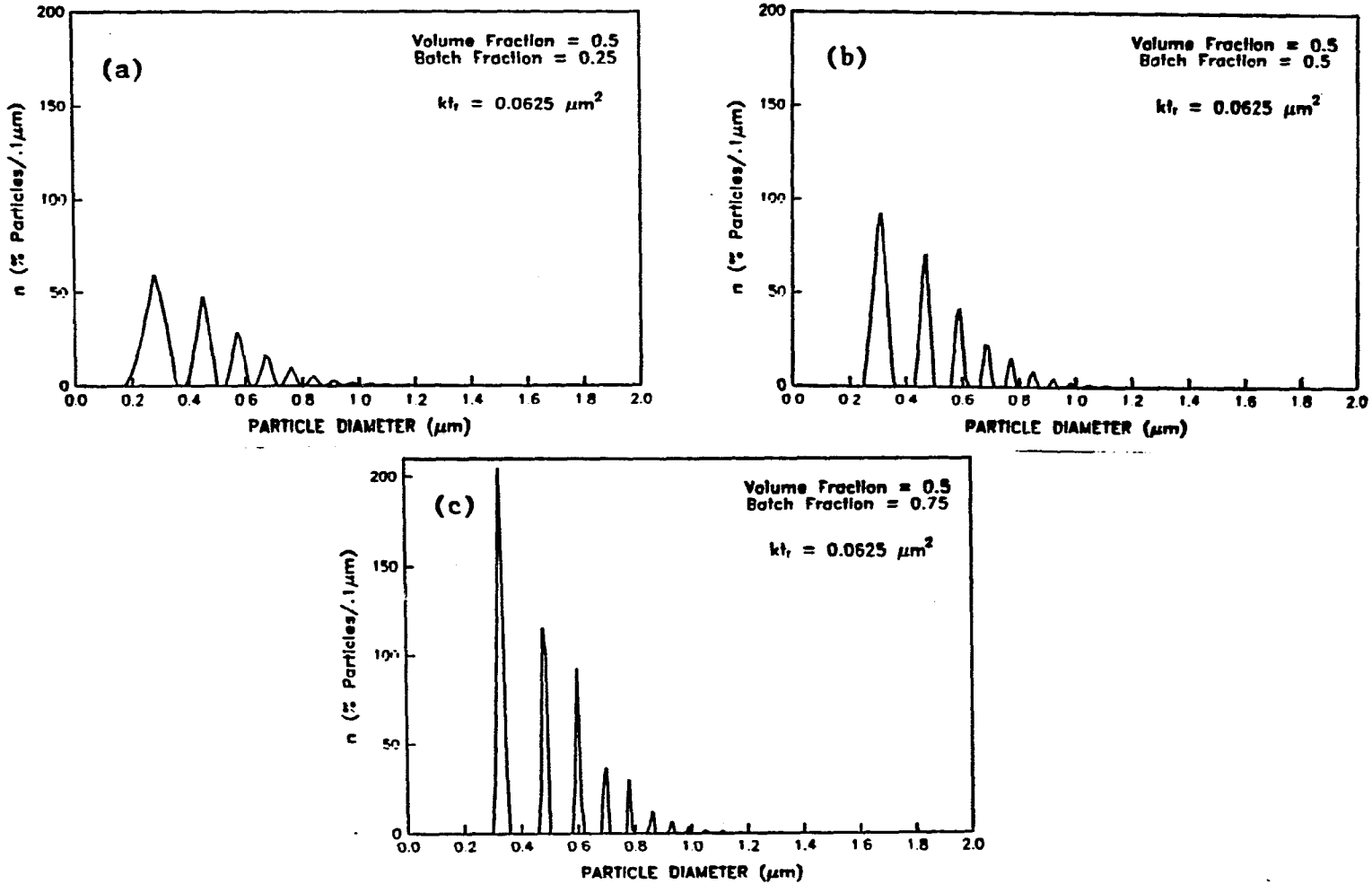

Figure 12. Figures 12a - 12c show how the particle size distribution from a semi-batch reactor would vary as a function of batch fraction

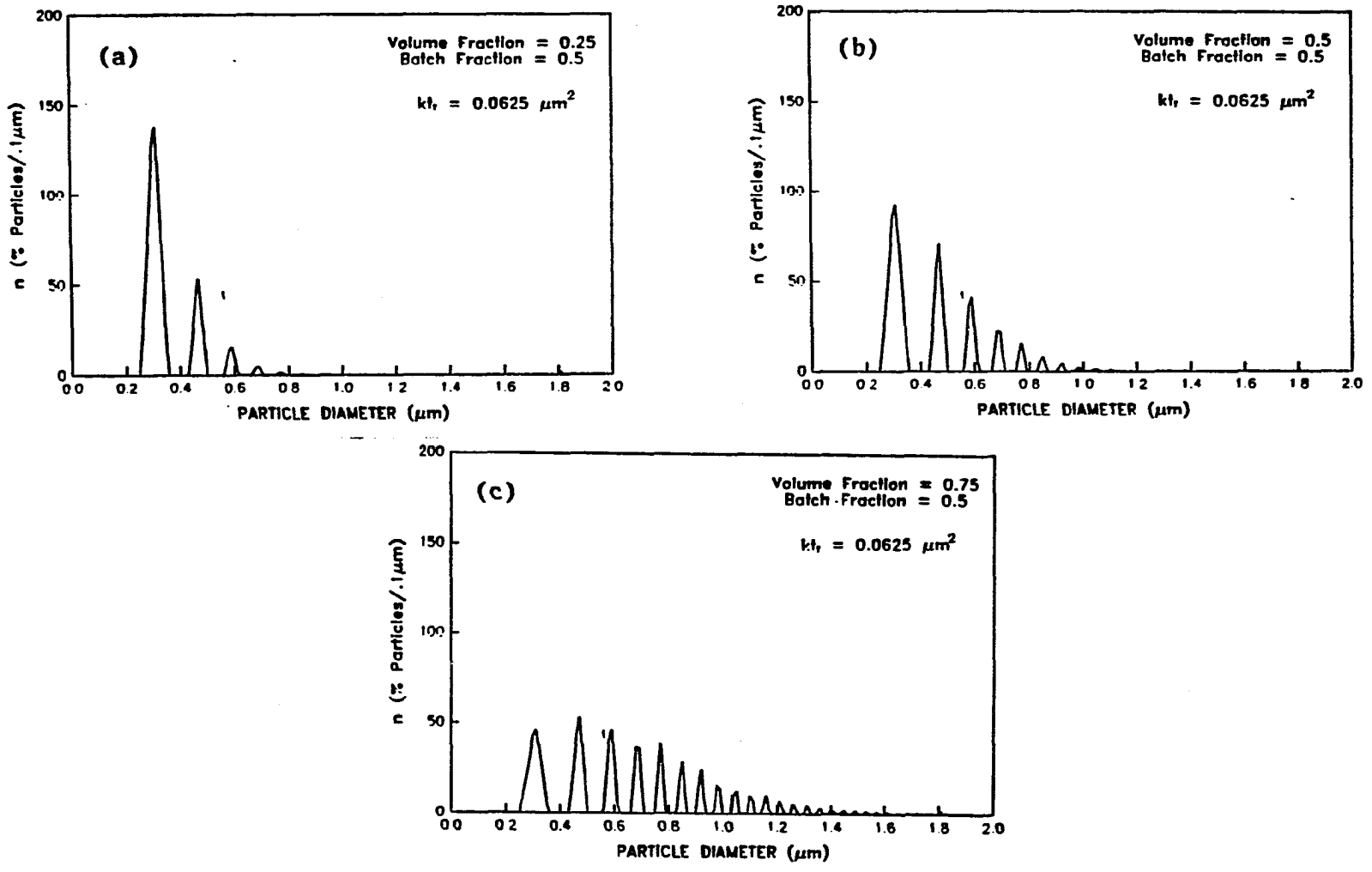

Figure 13. Figures 13a - 13c show how the particle size distribution from a semi-batch reactor would vary as a function of volume fraction

$$T_1 = (\sigma_B + 2z + 1)^{1/2} \tag{50}$$

$$T_2 = (2\sigma_B + 2z)^{1/2} \tag{51}$$

$$T_3 = (2z + 2)^{1/2} \tag{52}$$

The variance, σ^2 of the distribution is

$$\sigma^2 = \frac{4(1-V)kt_T}{(1-\sigma_B)^2} \left\{ \sum_{z=0}^{\infty} V^z \left[\frac{1}{12} (T_1^6 - T_2^6) - \frac{1}{4} (T_1^4 - T_1^4)(\sigma_B + z) \right] \right.$$

$$\left. + \sum_{z=0}^{\infty} V^z \left[\frac{1}{4} (T_3^4 - T_1^4)(z+1) - \frac{1}{12} (T_3^6 - T_1^6) \right] \right\} - (\bar{L})^2 \tag{53}$$

The mean of the particle size distribution is proportional to $(kt_T)^{1/2}$ and the variance is proportional to kt_T. This is the same dependence that the MSMPR, laminar flow, and packed bed reactors have on $k\tau$. Like those other reactors, the coefficient of variation is independent of kt_T as shown in Table 2 along with a summary of the other equations for the semi-batch reactor.

Figure 14 shows how the coefficient of variation, $\sigma/\bar{L}$ x 100%, varies with volume fraction, V, for various values of batch fraction, $\sigma_B = t_B/t_T$. As V approaches 1, the reactor will have the same level of macromixing as a MSMPR reactor, and the coefficient of variation of the particle size distribution will approach 52.3%. As the batch fraction, σ_B, goes to 1, the semi-batch reactor becomes a batch reactor with instantaneous filling and removal times. In this case, Roth et al. (79) have shown that the semi-batch reactor will have a residence time distribution that is identical with a recycle plug flow reactor with a

Table 2. Summary of semi-batch reactor model

n	$\frac{4L(1-V)}{k[(1-\sigma_B)t_T]^2}\left[\sum_{z=0}^{\infty} V^z\left(\frac{L^2}{2k}-(\sigma_B+z)t_T\right)\left|U\left(\frac{L^2}{2k}-(\sigma_B+z)t_T\right)\right.\right.$ $\left.-U\left(\frac{L^2}{2k}-\frac{1}{2}(\sigma_B+2z+1)t_T\right)\right]+\sum_{z=0}^{\infty} V^z\left[\frac{t_T(1-\sigma_B)}{2}-\frac{L^2}{2k}-\frac{1}{2}(\sigma_B+2z+1)t_T\right]$ $\left.\left[U\left(\frac{L^2}{2k}-\frac{1}{2}(\sigma_B+2z+1)t_T\right)-U\left(\frac{L^2}{2k}-(z+1)t_T\right)\right]\right]$
L	$\frac{4(1-V)(kt_T)^{1/2}}{(1-\sigma_B)^2}\left\{\sum_{z=0}^{\infty} V^z\left[\frac{1}{10}(T_1^5-T_2^5)-\frac{1}{3}(T_1^3-T_2^3)(\sigma_B+z)\right]\right.$ $\left.+\sum_{z=0}^{\infty} V^z\left[\frac{1}{3}(T_3^3-T_1^3)(z+1)-\frac{1}{10}(T_3^5-T_1^5)\right]\right\}$
σ^2	$\frac{4(1-V)kt_T}{(1-\sigma_B)^2}\left\{\sum_{z=0}^{\infty} V^z\left[\frac{1}{12}(T_1^6-T_2^6)-\frac{1}{4}(T_1^4-T_1^4)(\sigma_B+z)\right]\right.$ $\left.+\sum_{z=0}^{\infty} V^z\left[\frac{1}{4}(T_3^4-T_1^4)(z+1)-\frac{1}{12}(T_3^6-T_1^6)\right]\right\}-(L)^2$
$\frac{\sigma}{L}$	$\frac{(1-\sigma_B)\left[\{\Psi\}-\frac{4(1-V)}{(1-\sigma_B)^2}\{\Phi\}^2\right]^{1/2}}{2(1-V)^{1/2}\{\Phi\}}$

$T_1 = (\sigma_B+2z+1)^{1/2}$

$T_2 = (2\sigma_B+2z)^{1/2}$

$T_3 = (2z+2)^{1/2}$

$$\{\Phi\} = \left\{\sum_{z=0}^{\infty} V^z\left[\frac{1}{10}(T_1^5-T_2^5)-\frac{1}{3}(T_1^3-T_2^3)(\sigma_B+z)\right]\right.$$
$$\left.+\sum_{z=0}^{\infty} V^z\left[\frac{1}{3}(T_3^3-T_1^3)(z+1)-\frac{1}{10}(T_3^5-T_1^5)\right]\right\}$$

$$\{\Psi\} = \left\{\sum_{z=0}^{\infty} V^z\left[\frac{1}{12}(T_1^6-T_2^6)-\frac{1}{4}(T_1^4-T_1^4)(\sigma_B+z)t_T\right]\right.$$
$$\left.+\sum_{z=0}^{\infty} V^z\left[\frac{1}{4}(T_3^4-T_1^4)(z+1)-\frac{1}{12}(T_3^6-T_1^6)\right]\right\}$$

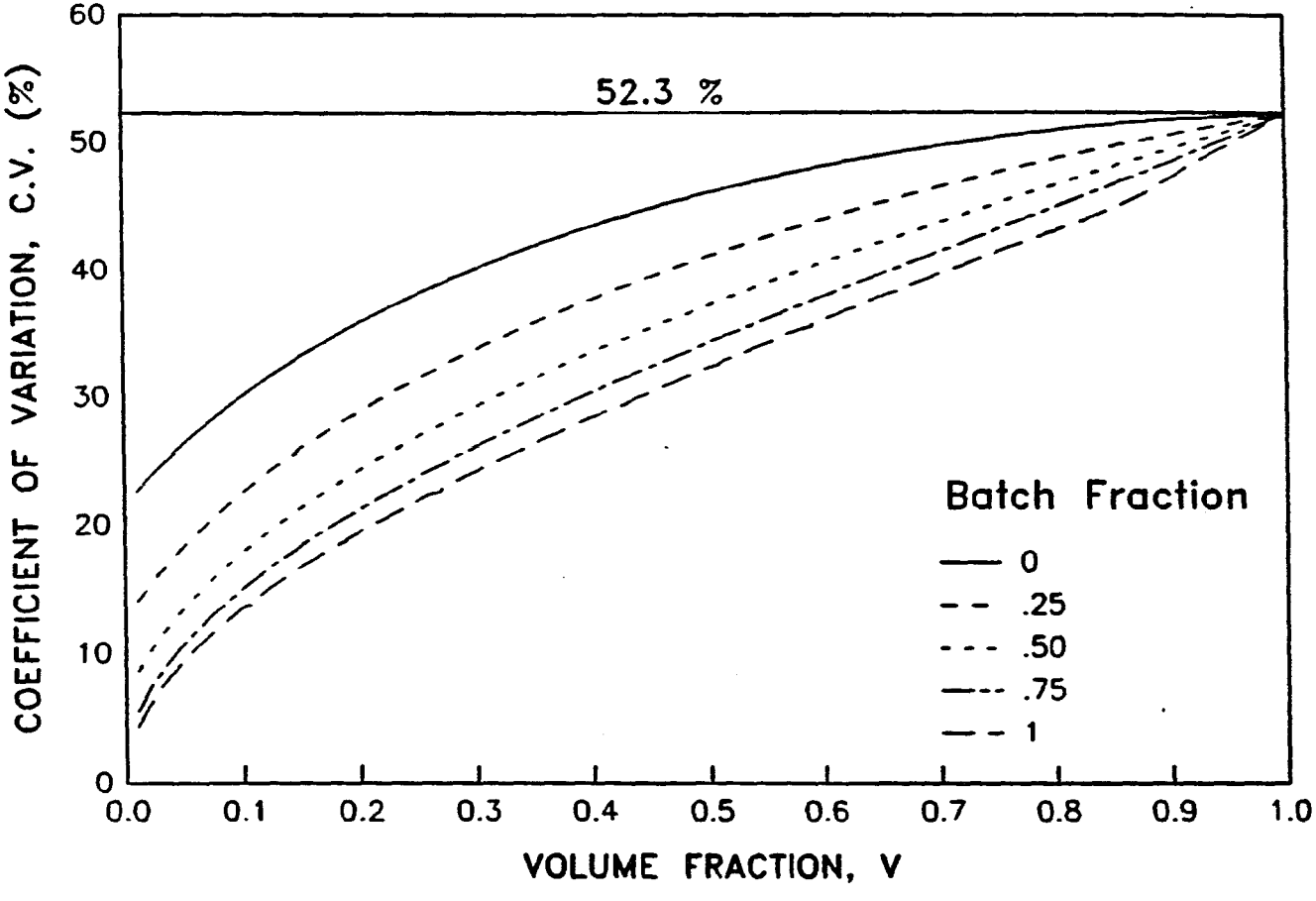

Figure 14. Coefficient of variation vs. volume fraction for various values of batch fraction

recycle ratio of R = V/(1-V) and also identical with a tanks-in-series model with 1/V tanks.

From Figure 14 it is clear that, if one wants to produce particles with as narrow a size distribution as possible, the best policy for operating a semi-batch reactor would be to operate with σ_B as close to 1 as possible and with V as small as possible. This makes sense physically since, in this case, the reactor would would be acting like a plug flow reactor.

The semi-batch reactor has two advantages over the packed bed reactor. First, no special packing material is needed as is the case with the packed bed reactor where fouling can occur if the precipitate adheres to the packing material. Second, the size distribution of the semi-batch reactor can be modified by simply changing the volume fraction and/or the batch fraction of the reactor, whereas it is necessary to physically change the packed bed reactor (by changing the diameter of the packing material and/or the reactor length) in order to effect a change in the particle size distribution.

EXPERIMENTAL EQUIPMENT AND PROCEDURES

Reagents

The feed solutions for the reactors in this research were 0.01-0.03 M in yttrium nitrate and 0.15-0.50 M in urea, $CO(NH_2)_2$. Yttrium nitrate, $Y(NO_3)_3 \cdot xH_2O$, was supplied by Research Chemicals and was 99.9% pure. The reagent grade urea was obtained from Fischer Scientific Company. The yttrium nitrate and urea were dissolved in deionized water. Upon heating, urea undergoes a first order decomposition to ammonia and carbon dioxide which results in the precipitation of spherical particles of yttrium hydroxycarbonate, $Y(OH)CO_3 \cdot H_2O$.

Experimental Equipment

Mixed-suspension mixed-product removal reactor

A mixed-suspension mixed-product removal (MSMPR) reactor was used to investigate the growth mechanism of the yttrium hydroxycarbonate particles. A schematic diagram of this precipitation system is shown in Figure 15. Masterflex peristaltic pumps were used to feed reactants and products to and from the MSMPR reactor. Small foreign particles in the feed stream were removed by a 0.2 μm Ultipor filter.

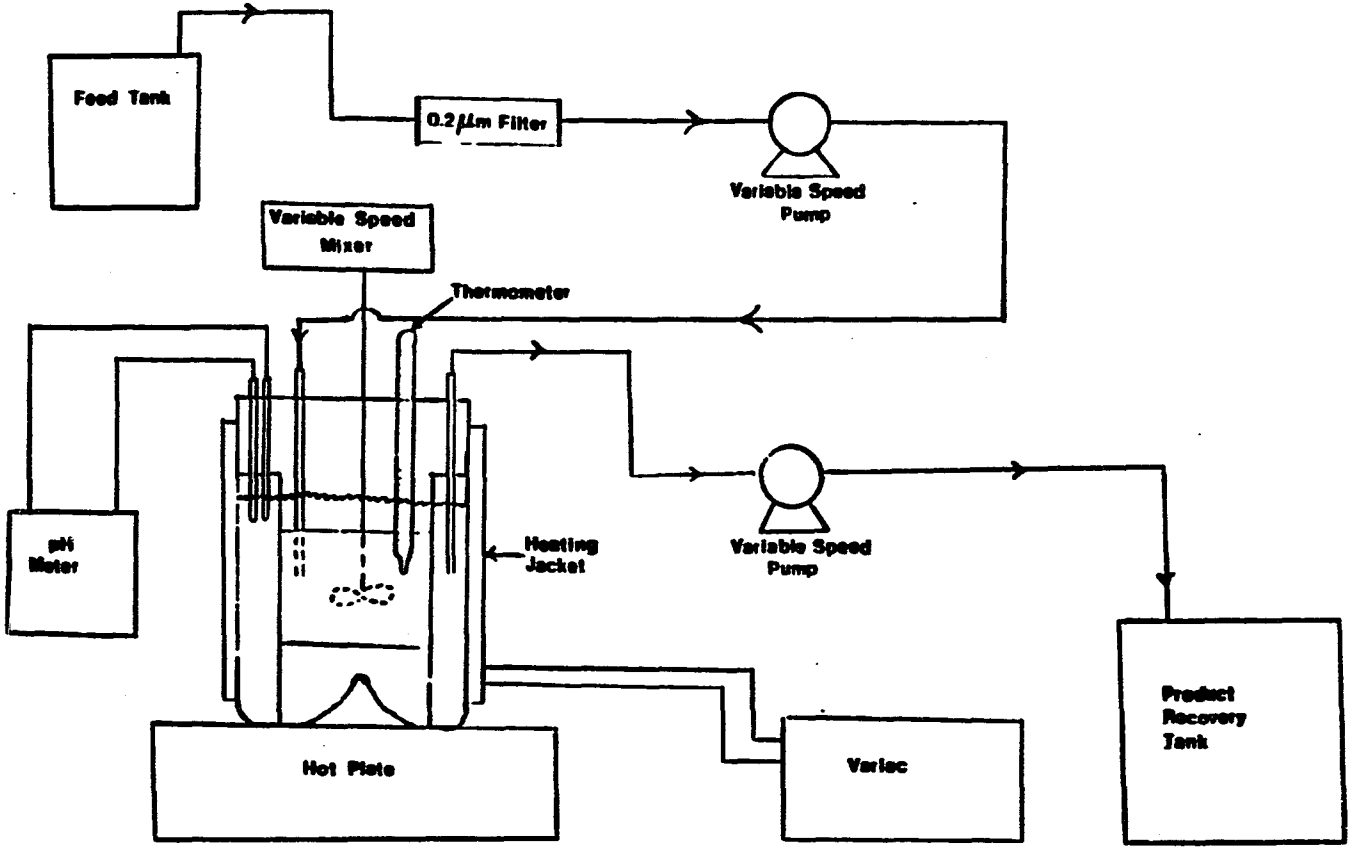

Figure 15. Schematic diagram of MSMPR reactor system

The precipitation vessel, shown in Figure 16, was made of borosilicate glass. The curved bottom was pushed up at the center to form a conical baffle which minimized dead water zones and helped to keep the precipitate particles suspended. A stainless steel draft tube was supported by four vertical stainless steel baffles. The draft tube served to direct the downward flow produced by the impeller. The conical baffle caused an upward flow; the four vertical baffles divide this upward flow into four regions, reducing the tendency of the particle suspension to swirl around the annular region. The top of the reactor, made of plexiglas, contained openings for a feed tube, a product removal tube, a thermometer, an impeller, and pH electrodes. An O-ring seal was used at the junction of the plexiglas top and the borosilicate glass vessel. A rubber gasket was used at the point where the impeller passed through the plexiglas top.

Feed was introduced into the center of the draft tube where rapid dispersion occurs. The product removal tube was located in the annular section of the reactor. Intermittent product removal (typically used in reactors of this type) was not necessary because of the small size of the particles formed during the precipitation. When particle size is small compared to the size of the product removal tube, particle classification is negligible (80).

The O-ring seal and the rubber gasket did not make the reaction vessel air-tight; small amounts of steam escaped at the point where the impeller entered the reactor and only light finger pressure was necessary to lift the top off the reactor. Therefore, the pressure of the air above the liquid in the reactor was approximately atmospheric.

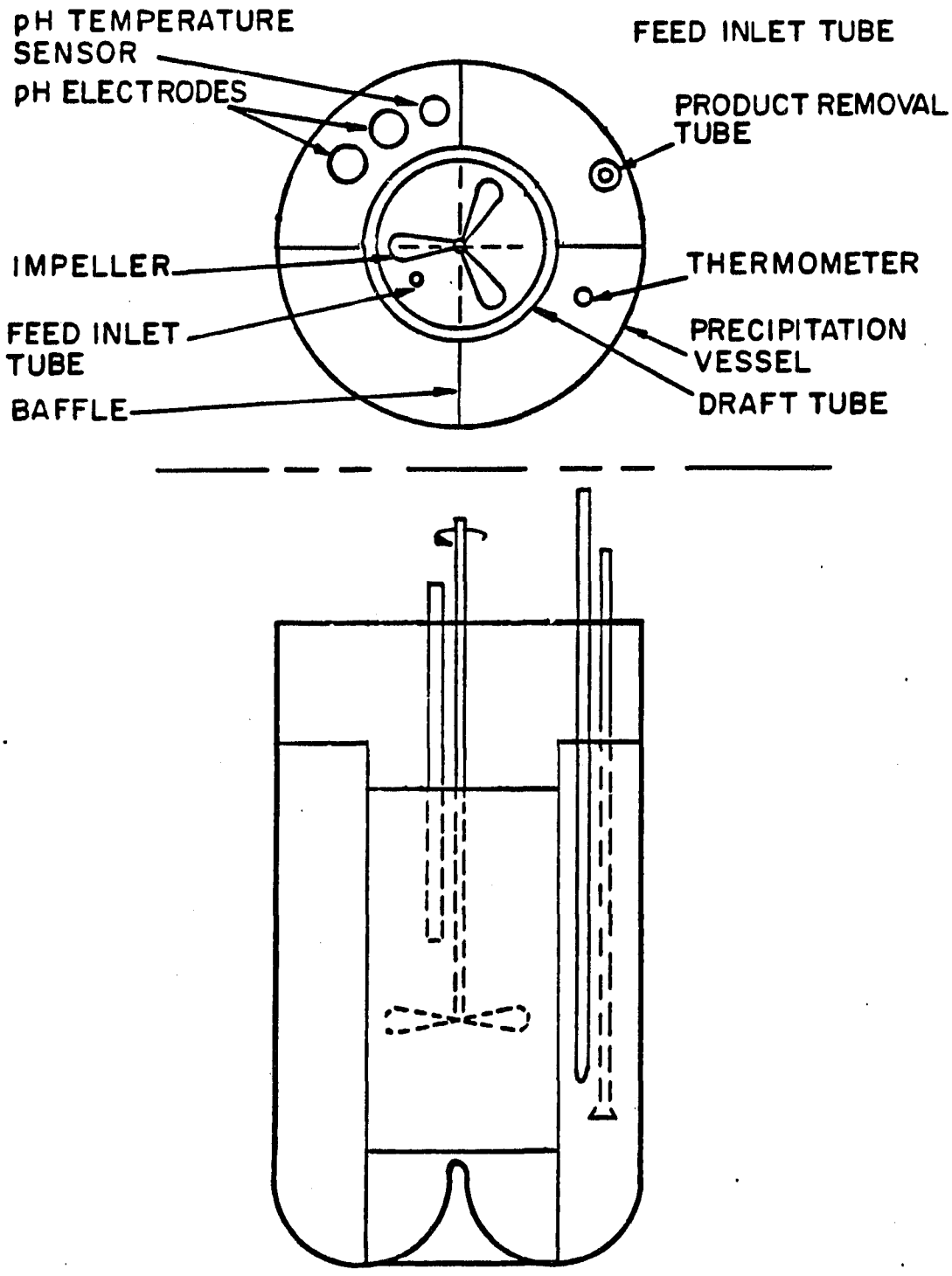

Figure 16. Diagram of precipitation reactor showing the arrangement of auxiliary equipment inserted into the vessel

Water could be seen condensing in the reactor, so the air above the reactor was probably saturated with water vapor.

The working volume in the reactor was 1.5 liters. The feed and product removal pumps were synchronized so as to maintain a constant liquid level in the reactor. The reactor rested on a hot plate and was wrapped with heating tape. The hot plate and the Variac controlling the heating tape were set at an appropriate level for maintaining a constant temperature for a given flow rate. The temperatures used in this research were 90°C, 95°C, and 100°C. Impeller speed was held constant at 750 rpm for all of the experimental runs.

Before each experimental run, the MSMPR reactor and the feed and product lines were cleansed with a dilute acid solution to remove any traces of precipitate adhering to the walls of the reactor or to the inside wall of the tubing. This was followed by a rinse with deionized water.

Tubular reactor

The tubular reactor system, shown diagrammatically in Figure 17, was used for the packed bed experiments. The reactor consisted of a central glass column 10 mm in diameter which was surrounded by a glass jacket. The length of the column was 490 mm. The outer diameter of the jacket was 20 mm. The temperature in the glass column was kept constant by circulating hot oil from a constant temperature bath through the glass jacket. A peristaltic pump was used to feed the reactants into the column.

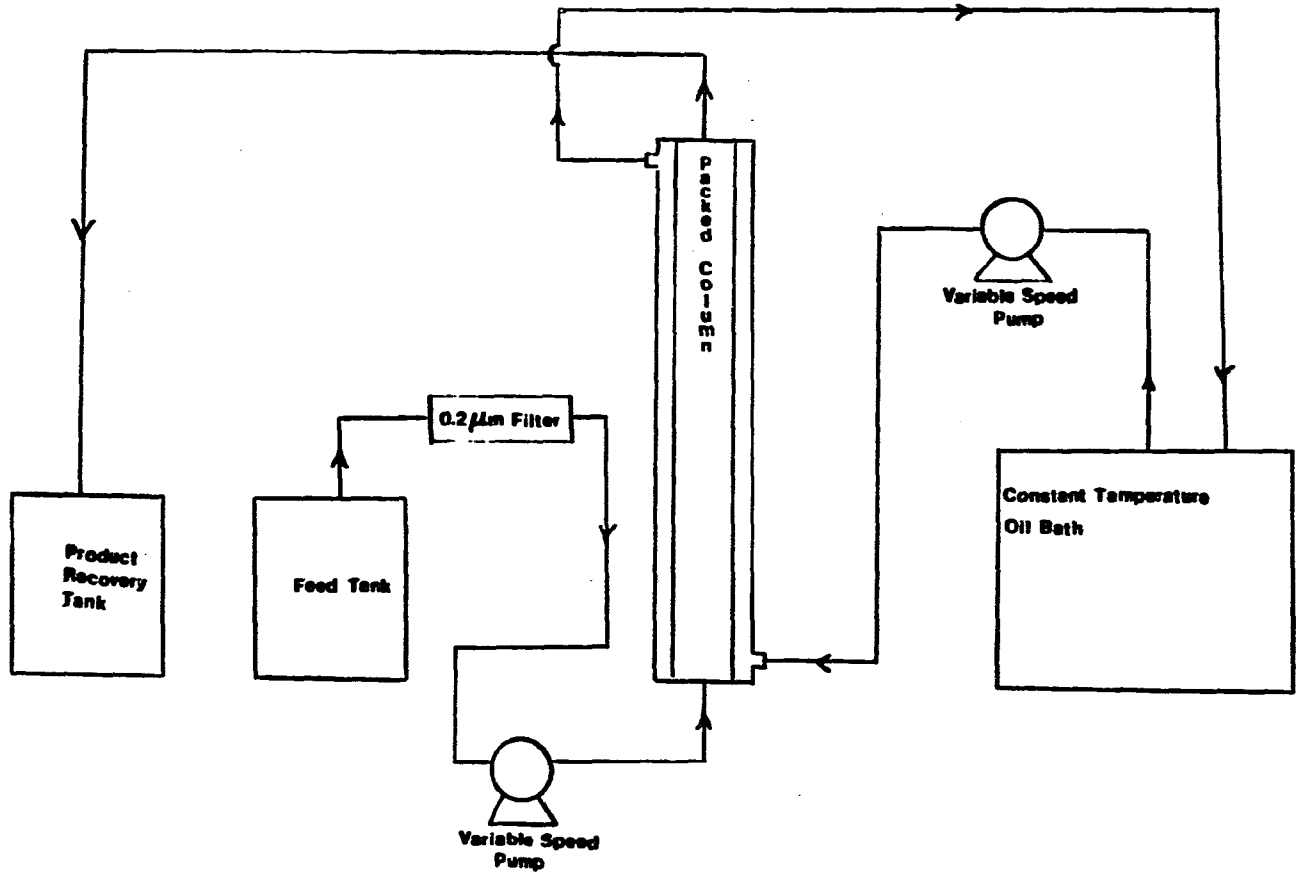

Figure 17. Schematic diagram of tubular reactor system

Initially, the feed stock was 0.02 M in yttrium nitrate and 0.25 M in urea. The feed stock was then heated until a bluish tint appeared, indicating that nucleation had taken place. This solution was immediately cooled in an ice bath to room temperature to quench any further decomposition of urea. This nucleated feed was then pumped through the packed column with a peristaltic pump. TEM measurements indicated that the feed particles were about 0.05 μm in diameter. Teflon beads with a diameter of 3.175 mm were used as the packing material for the packed bed reactor. Glass beads of various sizes were also tried. The sizes ranged from 3 mm to 0.1 mm. It was found that for glass beads below about 1 mm in diameter, significant plugging of the reactor occured due to particles adhering to the surface of the glass beads. In order to prevent this problem, the glass beads were treated with Prosil-28, an organosilane which makes glass surfaces water repellent. Unfortunately, this seemed to have no effect on the plugging problem. It seems that if the packing material is large enough, the plugging problem goes away. Therefore, it appears that the best way to increase the number of stirred tank reactors in series approximated by the packed bed reactor, is to increase the height of the bed and not decrease the size of the packing material. For this reason, the same size beads were used for all the packed bed experiments and two different bed heights (490 mm and 250 mm) were used instead.

Semi-batch reactor

The semi-batch reactor had a design similar to the MSMPR reactor except that there was no center draft tube and there was a preheat tank which fed in to the reactor. There was no draft tube because when the liquid level in the reactor drops below the top of the draft tube, as is required for semi-batch operation, the mixing would be adversely effected. The semi-batch reactor was operated at 100°C for all runs.

The operation of the semi-batch reactor consisted of four separate phases and two separate vessels. The four phases were the preheat phase, the filling phase, the batch phase, and the product removal phase. The two vessels were the preheat tank and the semi-batch reactor.

In the preheat phase, the feed to the preheat tank, initially 0.02 M in yttrium nitrate and 0.25 M in urea, was heated to the point where a slight bluish tint was observed. This indicated that nucleation had taken place. The preheat phase was timed so that just at the point when the bluish tint was observed, the filling phase began. In this way, all the nucleation took place during the preheat phase so that only growth took place in the semi-batch reactor.

Runs 9-12 were done in a slightly different manner than the rest of the semi-batch runs. The preheat was done well before the filling phase was to begin. The pre-nucleated feed was cooled to room temperature and then fed to the semi-batch reactor at the appropriate time. This was done because of the significant length of time that the filling phase took under those particular operating conditions. If this measure had

not been taken, then the size of particles entering the semi-batch reactor at the end of the filling phase might have been significantly larger than those particles entering at the beginning of the filling phase.

Analytical Procedures

Particle size distributions

Particle size distributions were obtained by two different methods. One method employed a transmission electron microscope (TEM) to measure the particles directly; the other method used a centrifugal sedigraph made by the Shimadzu Corporation.

For examination by TEM, samples were withdrawn directly from the reactor and immediately placed in an ice bath to quench the urea decomposition reaction. The samples were then filtered through a 0.1 μm Nucleopore filter, washed several times with deionized water, and then dispersed ultrasonically in methanol. A drop of this suspension was placed on a 200 mesh copper grid with a carbon film support and allowed to air dry. The sample grid was placed in a Hitachi Model HU-125 transmission electron microscope and the particles were measured directly on the fluorescent screen of the TEM by looking through an eyepiece graticule. For each sample, the graticule was calibrated against a standard grid (2160 lines/mm.) supplied by Ernest F. Fullam, Inc.

Particles were measured according to guidelines set forth by the American Society of Testing and Materials (81,82). In this standardized procedure, the number of particles measured in the modal size class should not be less than 25 and at least 10 particles should be counted in each size class which has a significant effect on the size distribution. In this research, at least 500 particles were counted for each sample measured.

Figures 18a and 18b, from an early MSMPR reactor run, show what effect, if any, the sampling procedure had on the observed size distribution. For the plot in Figure 18a, 4 ml. of suspension was withdrawn from the center of the annular region of the reactor with a pipet. This suspension was filtered through a .03 μm filter and washed with deionized water. In Figure 18b, the entire contents of the reactor were dumped into a large flask, and the suspension was well shaken. Then, 25 ml of this suspension was filtered through a 0.1 μm filter and washed with deionized water. In both cases the washed particles were resuspended in methanol and prepared for TEM examination in the usual manner. The same tri-modal distribution was observed in both cases. Therefore, it appears that the sampling procedure had little effect on the observed size distribution. It also appears that the size distributions obtained by TEM are reasonably reproducible.

For measuring particle size distributions with the centrifugal sedigraph, approximately 5 ml of suspension was withdrawn from the reactor, cooled in an ice bath, diluted an appropriate amount with mother liquor from the reactor, and placed in the instrument. Data from the centrifugal sedigraph are then converted from a weight percent basis

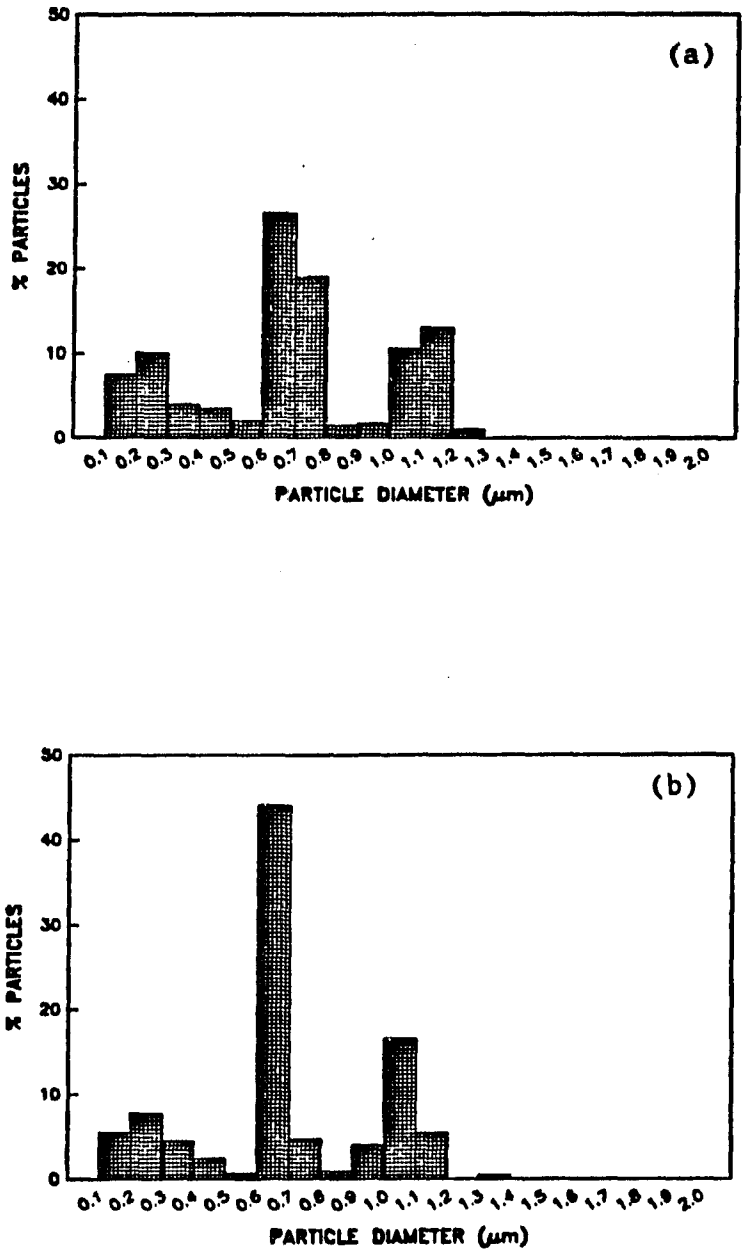

Figure 18. Size distribution data from TEM measurements. Figures 18a and 18b are replicate measurements

to a number percent basis for analysis.

The centrifugal sedigraph, which requires that the density of the particles be known, was calibrated by using highly monodisperse yttrium hydroxycarbonate particles prepared by batch homogeneous precipitation. The size distribution of a sample was first determined by TEM analysis. Then another portion of the sample was measured in the sedimentation analyzer. The particle size distributions obtained by both methods were very similar, and are shown in Figure 19.

Each graph in the results section which was produced with information from the sedigraph is a composite of the data obtained from three replicate measurements. Figure 20 shows three replicate particle size distributions obtained from the sedigraph for run 1 taken at 25 τ and also shows the composite of these three measurements.

Finally, all graphs of MSMPR data have been corrected to account for the fact that particles below 0.2 μm were not measured with the sedigraph and that particles below 0.1 μm were not measured with the TEM. Data from the lower channels of the sedigraph were not used because of the "noise". Particles below 0.1 μm were not counted on the TEM because the suspension had been filtered through a 0.1 μm filter. Since the total area of the histogram produced by these instruments is 100% of the particles measured, a curve representing that result which would be obtained for diffusion-controlled growth was fit to each histogram and the number of particles which should exist in the two lower channels was estimated from the fitted curve. The data in each bar of the histogram were then reduced by multiplying by a fraction, which was 100% divided by the area (> 100%) which would exist if the

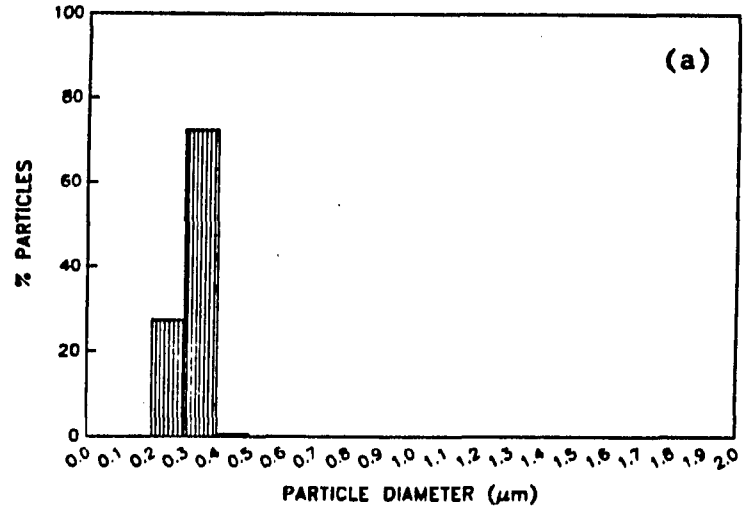

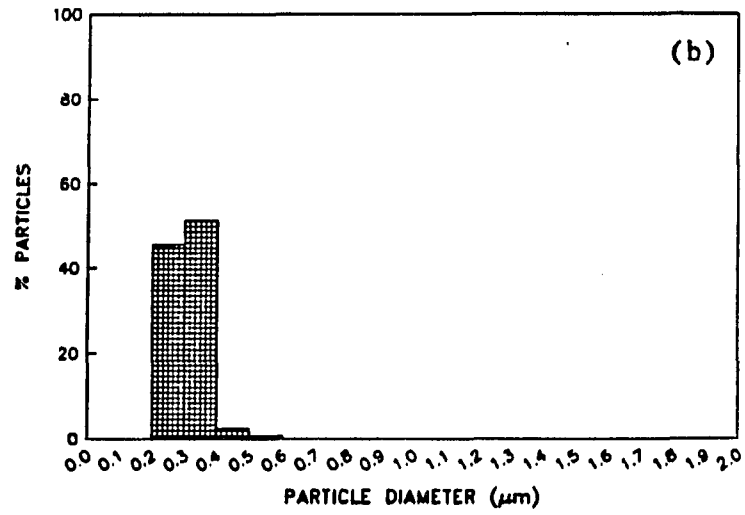

Figure 19. Comparison of size distributions obtained from TEM and sedigraph data. Figure 19a is from TEM data and Figure 19b is from sedigraph data

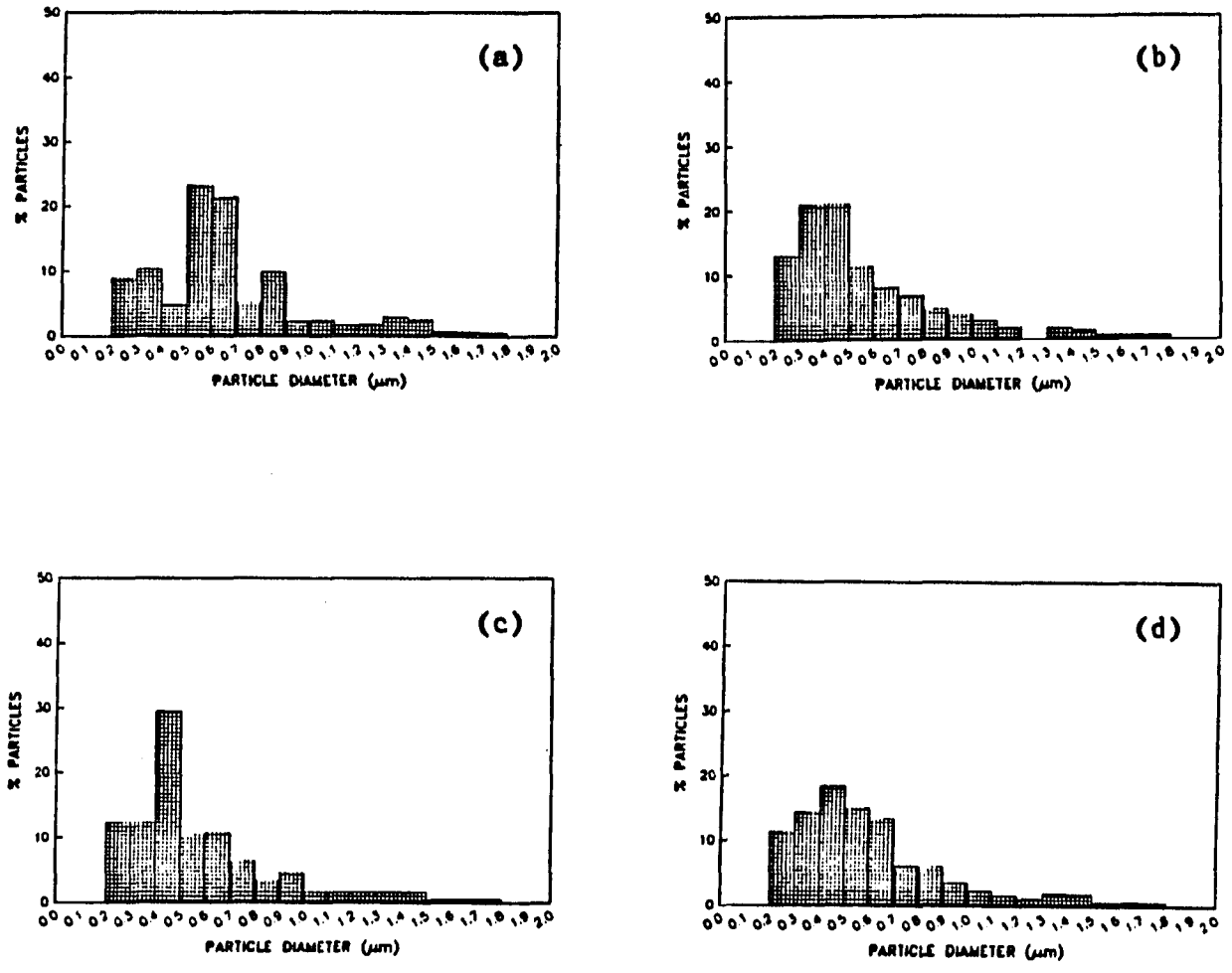

Figure 20. Figures 20a, 20b, and 20c are three replicate size distributions obtained from the sedigraph for run 1 after 25τ. Figure 20d is a composite of Figures 20a, 20b, and 20c

data from the smaller size ranges could have been measured.

Suspension density was measured by taking one liter (hot) of suspension from the reactor at the end of the experimental run, filtering it through a 0.1 μm Nucleopore filter, and drying the solids in an oven at 110° C. The dried solids were then weighed to determine the mass of material per liter of suspension, M_T.

Yttrium ion concentration was determined by ethylenediaminetetraacetate (EDTA) titration (83 ,84), using xylenol orange as an indicator. A sample of the suspension was taken from the reactor and filtered. The filtrate was pH adjusted to a value of 4.5 to 6 with hexamethylenetetramine (HMT). A sample of the pH adjusted filtrate is then titrated with a .005 M EDTA solution from a red to a lemon-yellow color. In this research, this method was found to give results which were accurate to within ± 0.0001 M.

RESULTS AND DISCUSSION

MSMPR Reactor Results

The purpose of the mixed-suspension mixed-product removal (MSMPR) reactor experiments was to obtain information about the formation and growth of the yttria precursor particles, $Y(OH)CO_3 \cdot H_2O$, as well as to determine the importance of various processing variables such as yttrium concentration, urea concentration, operating temperature, residence time, and pH of the feed stream.

Initial experiments were used to determine how many residence times needed to pass before steady-state was achieved. Table 3 shows the yttrium ion concentration as a function of residence time, τ, for runs 1, 2, and 3. For those three runs, the mean residence time was 60 minutes, the yttrium concentration was 0.02 M, the urea concentration was 0.25 M, the temperature of the reactor was 90°C, and the feed pH was 5.5. These conditions will be referred to as the base conditions for the MSMPR reactor. In all the runs to be discussed, the base conditions were used except for the particular variable being studied.

Table 3. Steady-state Y^{+3} concentration (moles/l) vs. residence time, τ. Base conditions

Run #	$[Y^{+3}]_{feed}$	5τ	10τ	15τ	20τ	25τ
1	0.0196	0.0145	0.0146	0.0147	0.0149	0.0144
2	0.0203	0.0151	0.0149	0.0149	0.0152	0.0152
3	0.0201	0.0150	0.0151	0.0149	0.0150	0.0151

Table 3 shows that the yttrium concentration in the reactor reached a steady-state value after five residence times had passed. After that, only minor fluctuations in concentration occured.

Figures 21, 22, and 23 show particle size distributions for runs 1, 2, and 3 measured after 5, 10, 15, 20, and 25 residence times. From these experiments it appears that it takes at least 15 residence times for a steady-state particle size distribution to be established. Therefore, particle size distribution data were collected after at least 15τ for the runs to be discussed later in this section.

At steady-state, the particle size distribution exhibited a maximum in population density at about 0.45 μm. As stated earlier, if diffusion of some species towards the growing particle is the rate controlling step, then the shape of the size distribution curve will be predicted by Equation 22,

$$n = 100\% \left[\frac{L}{k\tau} \exp\left(- \frac{L^2}{2k\tau}\right) \right] \qquad (22)$$

where L is the particle diameter, $k = 4D\bar{v}C$, D is the diffusion coefficient, $\bar{v}$ is the molar volume of the diffusing species in the solid phase, C is the bulk concentration of the diffusing species and τ

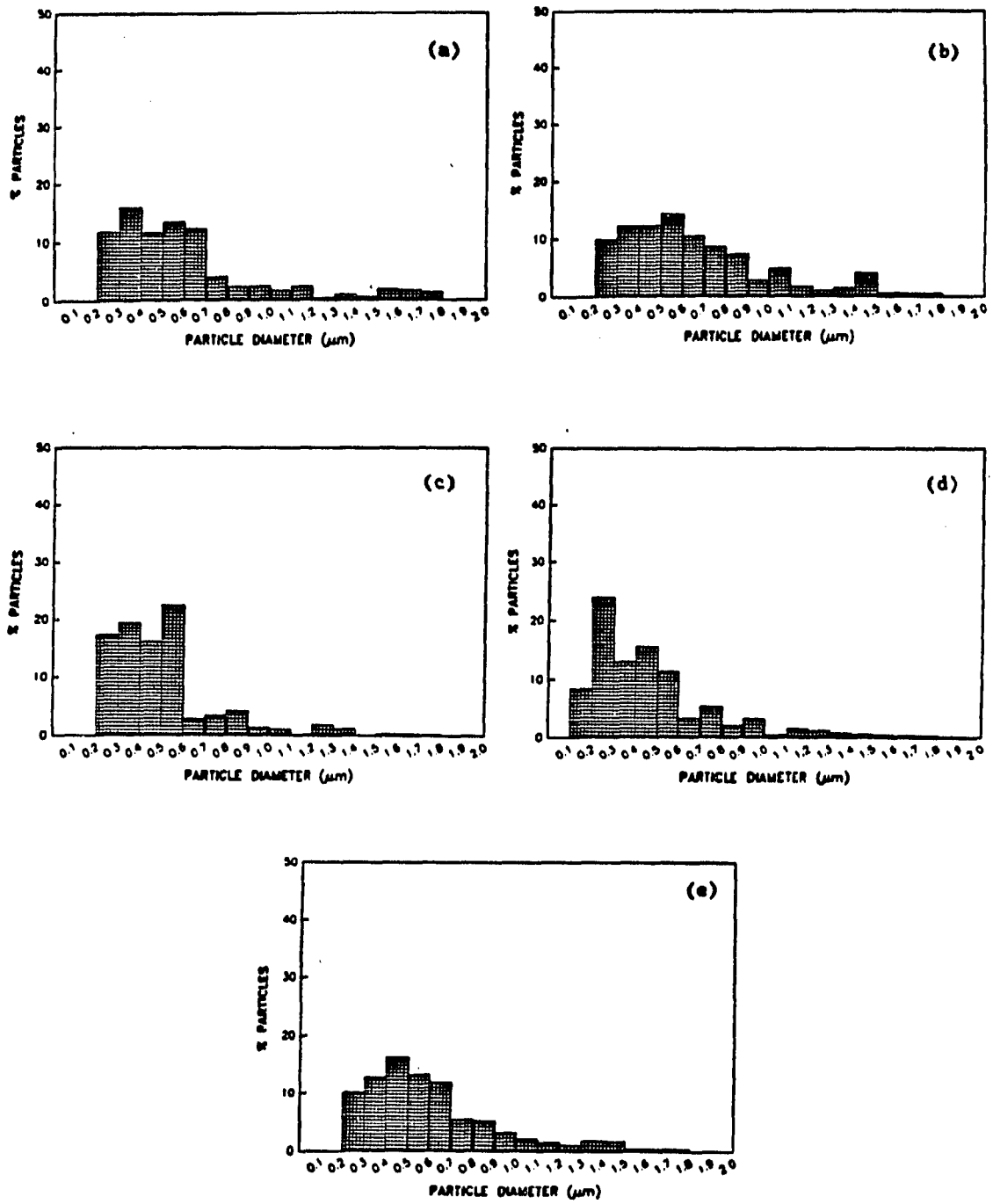

Figure 21. Figures 21a, 21b, 21c, 21d, and 21e show size distribution data for run 1 after 5, 10, 15, 20, and 25τ respectively

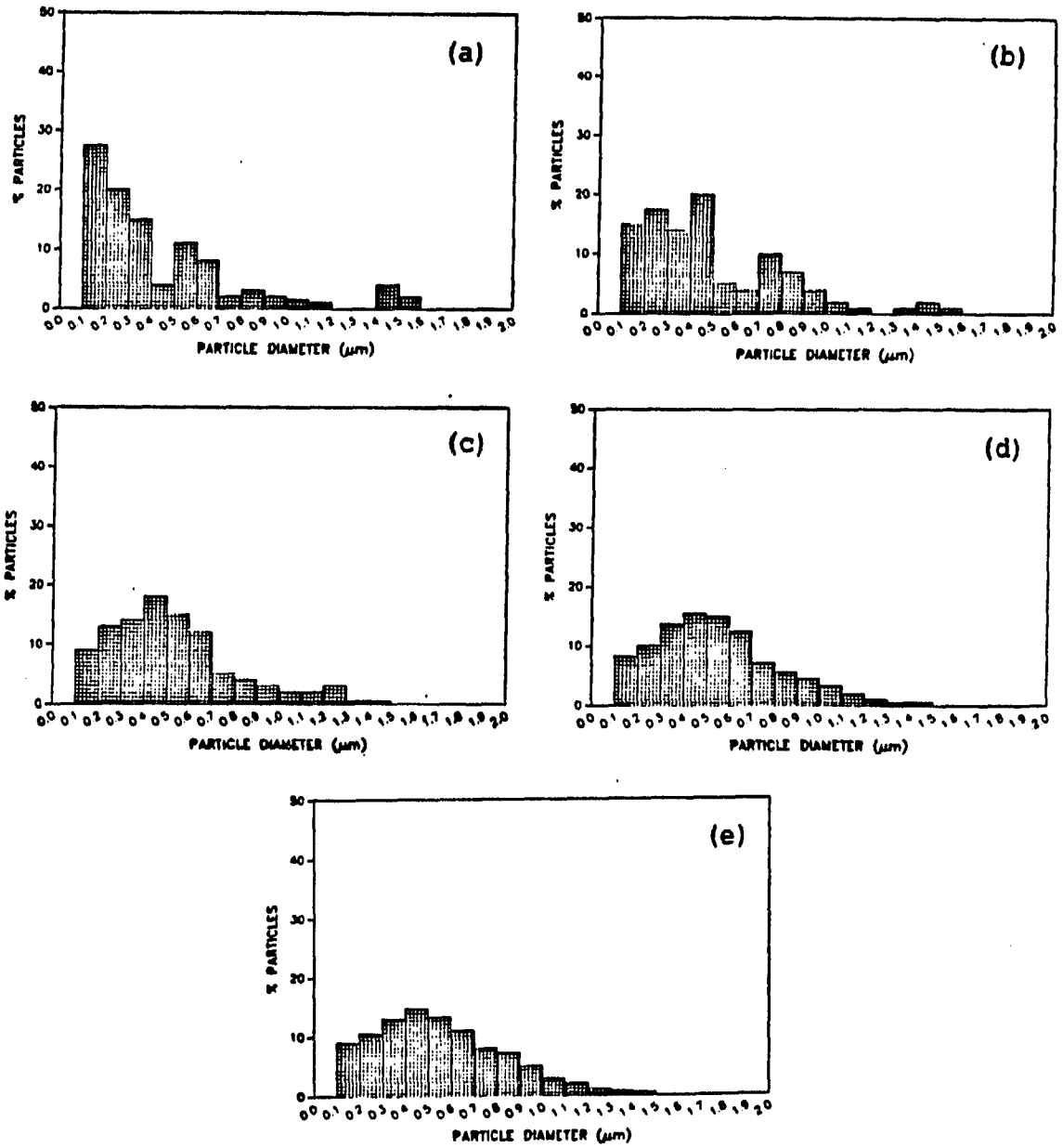

Figure 22. Figures 22a, 22b, 22c, 22d, and 22e show size distribution data for run 2 after 5, 10, 15, 20, and 25τ respectively

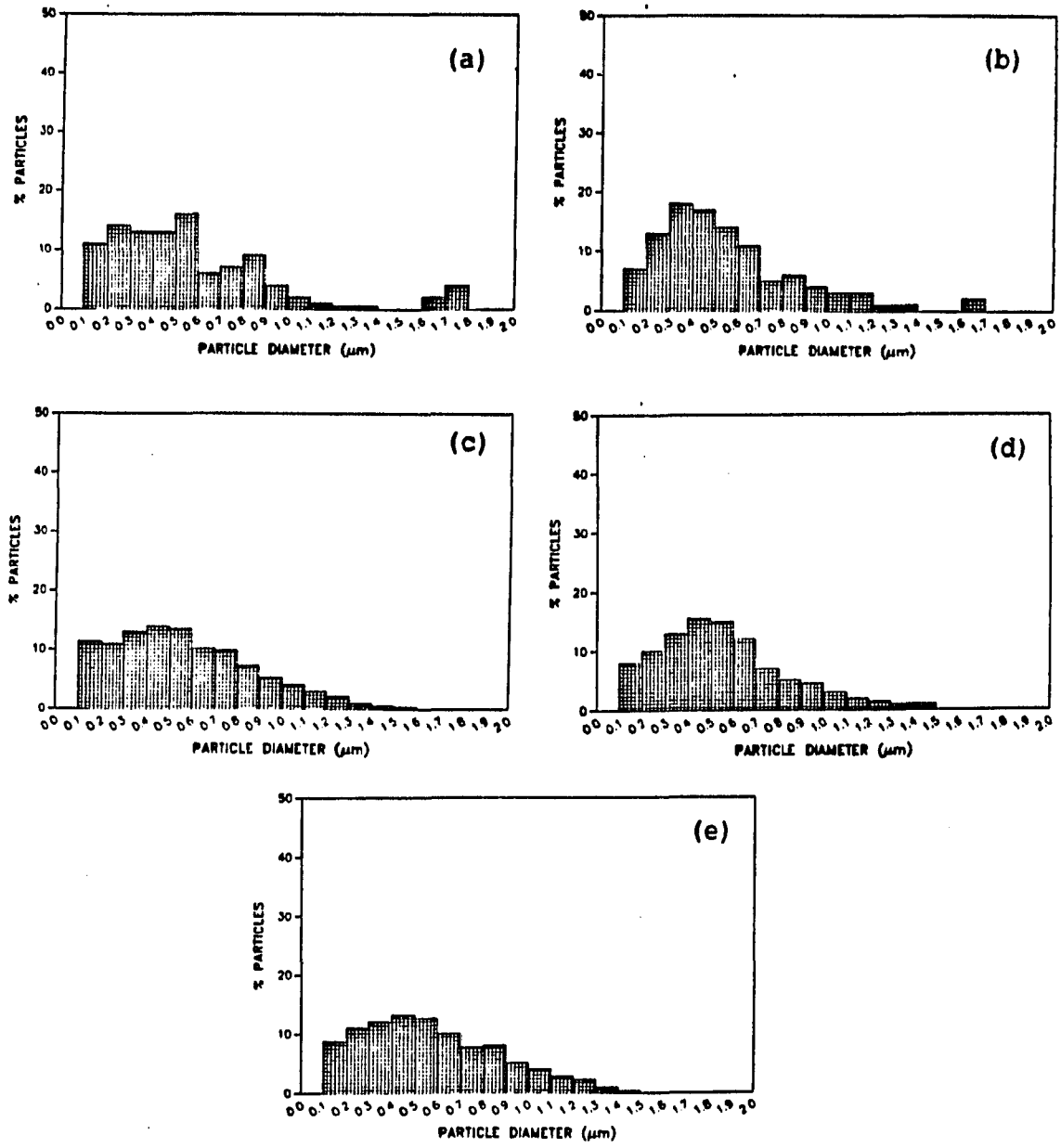

Figure 23. Figures 23a, 23b, 23c, 23d, and 23e show size distribution data for run 3 after 5, 10, 15, 20, and 25τ respectively

is the residence time. Figure 24 shows how well the model fit the experimental data for runs 1, 2, and 3 after 25 residence times had passed. Since Equation 22 is a one-parameter ($k\tau$) model, it was fit to the experimental data by making the modal size of the theoretical curve equal to that indicated by the experimental data. Reasonable fits were obtained, especially when one considers that the theoretical model has only one adjustable parameter ($k\tau$). Figure 7, given earlier, shows that as this parameter is increased the curve broadens and the maximum value shifts to the right. Conversely, when $k\tau$ is decreased, the maximum value decreases and the distribution becomes sharper (all curves must start at zero). However, the coefficient of variation (C.V.), a measure of monodispersivity, does not change.

An important verification of the diffusion-controlled growth model is to compare the concentration of the rate-limiting species, as predicted by the model, to the concentration of species present in the system. If the model is correct, the concentration of one of the species in solution should be of the same order of magnitude as the concentration of the rate-limiting species predicted by the model. The modal particle size, or the particle size at which the populaton density is a maximum, is found by taking the derivative of Equation 22 with respect to L and setting it equal to zero. This yields,

$$L_M = (4D\bar{v}C\tau)^{1/2} = (k\tau)^{1/2} \qquad (27)$$

which can be rearranged to give the concentration of the diffusing species:

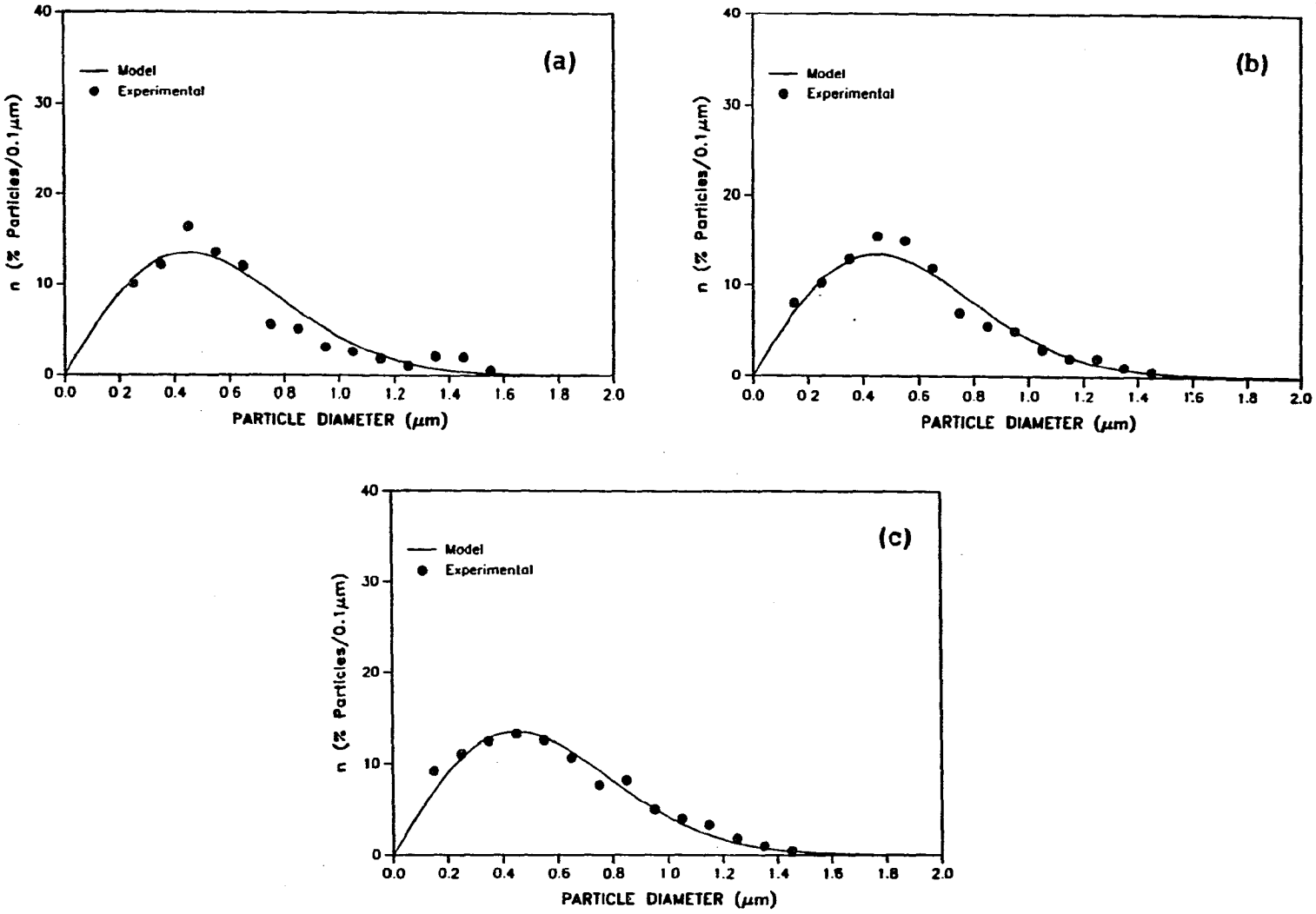

Figure 24. Population density vs particle diameter. Figures 24a, 24b, and 24c show the fit of the model to the experimental data for runs 1, 2, and 3 after 25τ

$$C = (L_M)^2/(4D\bar{v}\tau) \qquad (28)$$

The diffusion coefficient, D, of ions and small molecules in water at 90°C is about 3 x 10^{-5} cm^2/sec. The molar volume, $\bar{v}$, was calculated from density measurements done by Micromeritics with a helium pycnometer. Its value is 65.4 cm^3/mole. The residence time, τ, was 3600 seconds. If L_M is taken to be 4.5 x 10^{-5} cm, then, the theoretical concentration of the rate-limiting diffusant is about 7.2 x 10^{-11} moles/cm^3 or 7.2 x 10^{-8} M. This value rules out the possibility of Y^{+3} being the rate-limiting diffusant. Its concentration in the reactor was about .015 M. This conclusion is also in agreement with the work of Verlinden (38) and Kayima (39) who state that diffusion of Y^{+3} to the particle surface cannot be the rate controlling step.

Since a carbonate is being precipitated, it seems reasonable that carbonate might be the rate-limiting diffusing species. In order to get a rough estimate of the carbonate concentration in solution, it was assumed that the solution was saturated with dissolved CO_2 as a result of the urea decomposition. The amount of CO_2 dissolved in solution was calculated by using Henry's Law

$$[CO_2] = K_H P_{CO2} \qquad (54)$$

where K_H is the Henry's Law constant for CO_2 in water and P_{CO2} is the partial pressure of CO_2 in the airspace above the liquid level of the reactor. The Henry's Law constant was obtained from the data of Butler

(85). The partial pressure of CO_2 in the reactor was calculated by assuming that the air above the liquid consisted of only water vapor and CO_2 at 90°C and 1 atm. The concentration of bicarbonate and carbonate ions, both of which may form when urea decomposes, were calculated from dissociation constant data presented by Butler (85). Table 4 shows the estimated concentration of dissolved CO_2 in solution as well as the estimated concentrations of HCO_3^- and $CO_3^=$ in the reactor at steady-state.

Table 4. Estimation of $[CO_2]$, $[^-HCO_3]$, and $[^=CO_3]$

	$[CO_2]$ M	$[^-HCO_3]$ M	$[^=CO_3]$ M
Estimated	3.5×10^{-3}	1.1×10^{-3}	6.4×10^{-8}

The one species in solution whose concentration is close to that predicted for the rate-limiting diffusant was the carbonate ion, $CO_3^=$, for which the concentration was estimated to be 6.4×10^{-8} M.

Runs 4-7 were done to see what effect changing the yttrium concentration of the feed stream has on the yttrium concentration drop in the reactor as well as the effect it has on the size of particles produced. Table 5 shows the yttrium concentration drop and mean particle size for runs 1-7. These experiments indicate that neither the amount of yttrium precipitated per liter of solution or the mean particle size are significantly affected by the feed concentration of yttrium over the concentration range 0.01-0.03 M. This agrees with the idea that carbonate is the rate-limiting diffusing species.

Table 5. Effect of changing the Y^{+3} concentration (moles/l). Base conditions

Run #	$[Y^{+3}]_{feed}$ (M)	$[Y^{+3}]_{final}$ (M)	ΔY^{+3} (M)	$\bar{L}$ (μm)
1	0.0196	0.0147	0.0049	0.51
2	0.0203	0.0149	0.0054	0.56
3	0.0201	0.0149	0.0052	0.52
4	0.0103	0.0055	0.0048	0.52
5	0.0102	0.0052	0.0050	0.53
6	0.0299	0.0246	0.0053	0.49
7	0.0301	0.0250	0.0051	0.51

At concentrations approaching 0.005 M, the yttrium concentration would limit the rate of precipitation. At yttrium concentrations much larger than 0.03 M, extensive flocculation and agglomeration of particles occur due to the flocculating power of trivalent ions which are about 700 to 1000 times as effective as monovalent ions in flocculating suspended particles (86,87).

In runs 8-11, the initial urea concentration was varied. The results of these runs are shown in Table 6. They are compared with the results from runs 1-3. When the urea concentration was doubled, the yttrium concentration drop approximately doubled. When the urea concentration was decreased by 40%, the yttrium concentration drop decreased by about 40%. This was to be expected since urea decomposition is apparently first-order (88,89,90),

$$dC_u/dt = -k_1 C_u \tag{55}$$

where C_u is the urea concentration and k_1 is the first-order rate constant equal to 0.039 hr^{-1} at 90°C (88,89,90).

Table 6. Effect of changing the urea concentration (moles/l). Base conditions

Run #	$[urea]_{feed}$	ΔY^{+3} (M)	ΔY^{+3} pred. (M)	$\bar{L}$ (μm)
1	0.25	0.0049	0.0063	0.51
2	0.25	0.0054	0.0063	0.56
3	0.25	0.0052	0.0063	0.52
8	0.50	0.0111	0.0125	0.38
9	0.50	0.0115	0.0125	0.35
10	0.15	0.0034	0.0038	0.63
11	0.15	0.0031	0.0038	0.67

For a first-order reaction in a continuous stirred tank reactor, the change in urea concentration in the reactor is given by

$$\Delta C_u = C_{uo}(1 - 1/(k_1\tau+1)) \tag{56}$$

where ΔC_u is the amount of urea decomposed per liter of solution and C_{uo} is the feed concentration of urea. Equation 57 shows that three moles of urea must decompose for every two moles of yttrium that precipitate.

$$2Y^{+3} + 7H_2O + 3NH_2CONH_2 \rightarrow 2YOHCO_3 + 6NH_4^+ + CO_2 \tag{57}$$

Combining Equations 56 and 57 in order to determine the yttrium concentration drop as a function of C_{uo}, k_1, and τ gives

$$\Delta Y^{+3} = 2/3\ C_{uo}(1 - 1/(k_1\tau+1)) \tag{58}$$

Table 6 compares the yttrium concentration drop predicted by Equation 58

with the experimentally observed concentration drop. The observed concentration drop was consistently lower than that predicted by Equation 58. This was probably due to evaporation of water in the reactor at 90°C which resulted in a slightly higher Y^{+3} concentration in the reactor than would have been measured if no water had evaporated.

As the urea concentration increased, the mean particle size decreased. Since more yttrium precipitates at higher urea concentrations, the number of particles per ml of suspension must increase as the urea concentration increases. In other words, the nucleation rate increases with increasing urea concentration. Table 7 shows the average nucleation rate, B^o, for the three different urea concentrations shown in Table 6. The nucleation rate was calculated from a knowledge of the particle size distribution, the mass of material precipitated per liter of suspension, the particle density, and the volumetric flowrate out of the reactor. The number of particles flowing out of the reactor per unit volume per unit time is equal to the number of particles being formed in the reactor per unit volume per unit time which is the nucleation rate, B^o. As will be shown later, the nucleation rate increases exponentially with the rate of urea decomposition. Therefore, as the urea concentration of the feed stream increases, the rate of decomposition of urea increases thus increasing the nucleation rate.

Table 7. Nucleation rate, B^o, and growth rate constant, k, as a function of urea concentration (moles/l). Base conditions

Run #	[urea]	B^o (#/(ml·hr))	k (μm^2/hr)
1-3	0.25	2.3×10^9	0.18
8-9	0.50	1.6×10^{10}	0.085
10-11	0.15	7.8×10^8	0.27

The mean particle size decreased with increasing urea concentration. This means that the particle growth rate constant, k, decreased with an increase in the rate of decomposition of urea. A possible explanation for this is that because of the exponential increase in the number density of particles with increasing urea concentration, the number density of diffusion sinks increases, resulting in the concentration gradient of diffusant that each particle experiences being smaller, even though the rate of decomposition of urea is greater.

Table 8 shows the effect of increasing the temperature in the reactor. Runs 12 and 13 were operated at 95°C and runs 14 and 15 were operated at 100°C. As temperature increased, the yttrium concentration drop increased and the mean particle size decreased. In a manner identical to increasing the urea concentration, the increase in the yttrium concentration drop and the decrease in the mean particle size were a result of the increase in the rate of urea decomposition with increasing temperature.

Table 8. Effect of changing the reactor temperature. Base conditions

Run #	T (°C)	ΔY^{+3} (M)	ΔY^{+3} pred. (M)	$\bar{L}$ (μm)
1	90	0.0049	0.0063	0.51
2	90	0.0054	0.0063	0.56
3	90	0.0052	0.0063	0.52
12	95	0.0080	0.0094	0.41
13	95	0.0077	0.0094	0.42
14	100	0.0117	0.0140	0.27
15	100	0.0113	0.0140	0.29

The rate constant for the first-order decomposition of urea follows an Arrhenius temperature dependence:

$$k_1 = A \exp(-E_a/RT). \tag{59}$$

Sahin and Koseoglu (90) determined that E_a is equal to 22.964 Kcal/mole and that A is equal to 2.74×10^{12} hr^{-1}. Using these values, the rate constants at 90°C, 95°C, and 100°C are 0.039 hr^{-1}, 0.060 hr^{-1}, and 0.092 hr^{-1}, respectively. Again, the measured Y^{+3} concentration drop was slightly lower than that predicted from the urea decomposition kinetics. The largest discrepancy occured for runs 14 and 15 at 100°C. As stated earlier, this discrepancy is probably due to vaporization of water at 90°C-100°C.

Table 9 shows the average nucleation rate and the average growth rate constant for the three different temperatures used in Table 8. As in the case where the urea concentration was varied, as the rate of urea decomposition goes up, the nucleation rate goes up and the growth rate constant, k, goes down.

Table 9. Nucleation rate, B^o, and growth rate constant, k, as a function of temperature. Base conditions

Run #	T(^{o}C)	B^o (#/(ml·hr))	k (μm^2/hr)
1-3	90	2.3×10^9	0.18
12-13	95	7.2×10^9	0.11
14-15	100	3.5×10^{10}	0.050

The results of runs 1-15 strongly suggest that the rate of urea decomposition controls the nucleation and growth rates of the yttria precursor particles. Figure 25 is a plot of the log of the nucleation rate versus the urea decomposition rate, log B^o vs. dC_u/dt. This plot indicates that, within the range of conditions studied here, the rate of urea decomposition is directly proportional to the log of the nucleation rate. This can be expressed mathematically as follows:

$$B^o = C^* \exp(K^* dC_u/dt) \tag{60}$$

where C^* and K^* are determined from the intercept and slope, respectively, of the graph in Figure 25. Equation (60) has the same mathematical form as the fundamental expression for the rate of homogeneous nucleation as proposed by Volmer and Weber (91),

$$B^o = c \exp(-\Delta G^*/\kappa T) \tag{61}$$

where ΔG^* is the free energy of formation of a nucleus, κ is Boltzmann's constant, T is the absolute temperature, and c is a proportionality constant. In comparing Equations (60) and (61), it appears that the

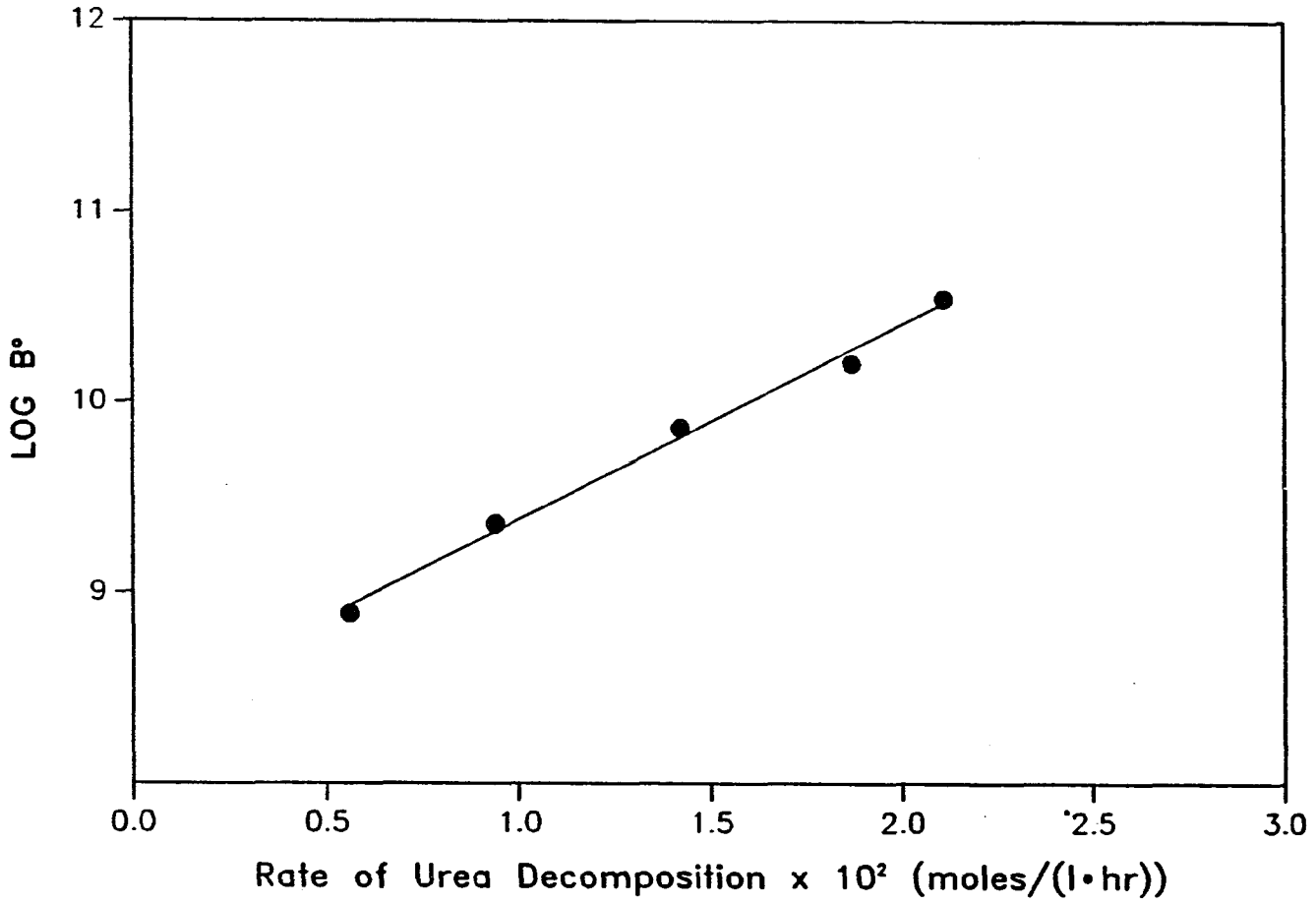

Figure 25. Log of nucleation rate vs. rate of urea decomposition

rate of urea decomposition is related to the free energy of formation of a yttrium hydroxycarbonate nucleus. As the rate of urea decomposition increases, the free energy of formation of a nucleus decreases.

Figure 26 is a plot of growth rate constant versus rate of urea decomposition, k vs. dC_u/dt. This graph shows that the growth rate constant, k, is directly proportional to the negative of the rate of urea decomposition, $-dC_u/dt$, over the range of conditions studied in this work. As stated earlier, this is probably due to the exponential increase in the number density of particles in suspension with increasing rate of urea decomposition. This results in the concentration gradient of diffusant, that each particle experiences, being smaller as the rate of urea decomposition increases.

Runs 16-19 were done at different residence times to see what effect this would have on the mean particle size and the amount of yttrium precipitated per ml of solution. Runs 16 and 17 had a residence time of 45 minutes and runs 18 and 19 had a residence time of 90 minutes. Table 10 shows the observed and predicted yttrium concentration drop and the mean particle size for runs 16-19 as well as runs 1-3.

Table 10. Effect of changing the residence time, τ. Base conditions

Run #	τ (min)	ΔY^{+3} (M)	ΔY^{+3} pred. (M)	$\bar{L}$ (μm)
1	60	0.0049	0.0063	0.51
2	60	0.0054	0.0063	0.56
3	60	0.0052	0.0063	0.52
16	45	0.0040	0.0047	0.47
17	45	0.0041	0.0047	0.46
18	90	0.0082	0.0092	0.61
19	90	0.0085	0.0092	0.67

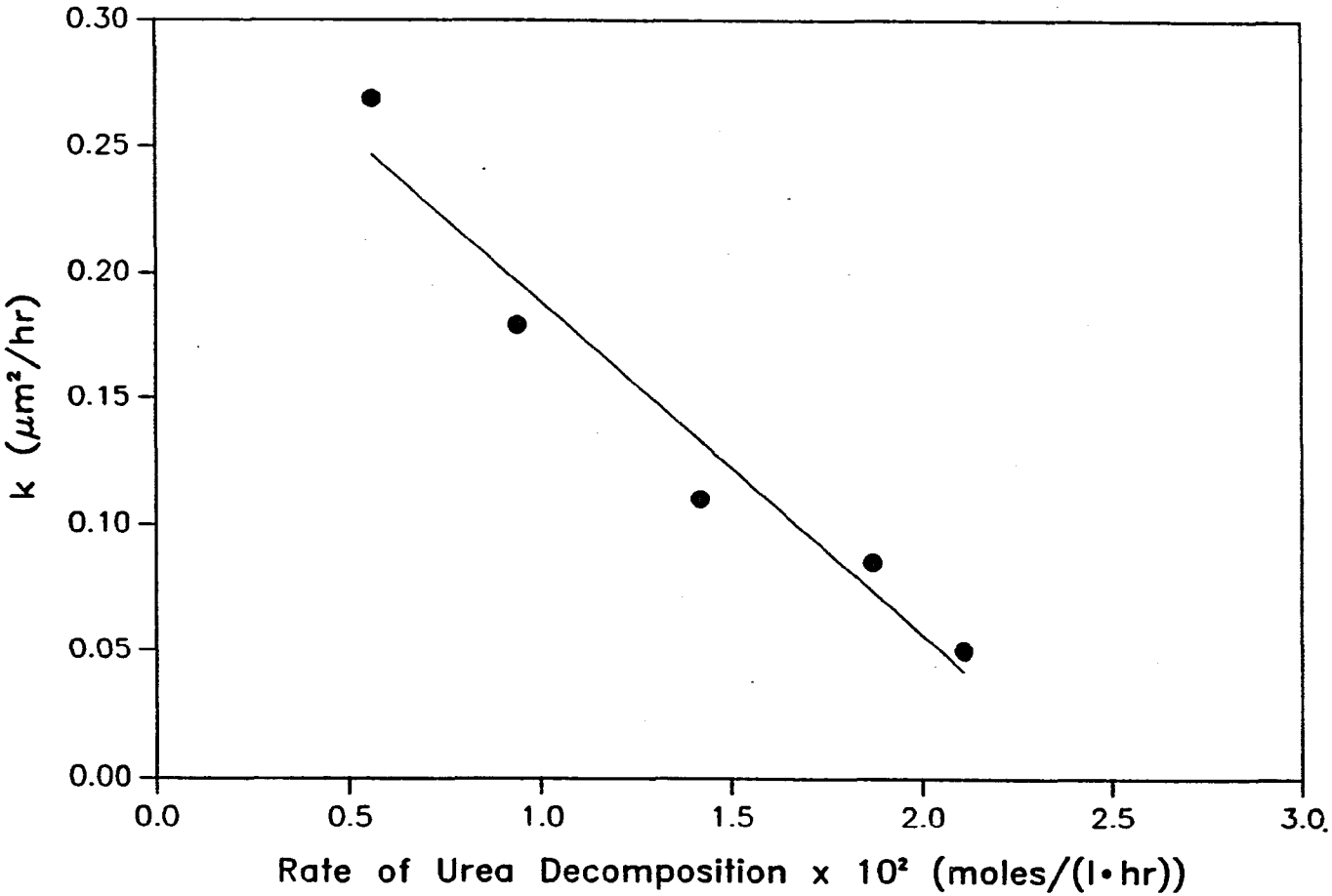

Figure 26. Growth rate constant vs. rate of urea decomposition

As residence time increased, the amount of yttrium precipitated per ml of solution increased. This increase closely tracked that predicted from the decomposition kinetics of urea.

Figure 27 is a plot of the average mean particle size for the three different residence times in Table 10 versus the square root of residence time. The mean particle size increased linearly with the square root of residence time. This is consistent with the diffusion-controlled growth model where the mean particle size is given by Equation 23:

$$\bar{L} = \left(\frac{\pi k \tau}{2}\right)^{1/2}. \qquad (23)$$

The growth rate constant, k, was constant because the rate of decomposition of urea was the same for runs 1-3 and 16-19. The temperature was the same (90°C) for all the runs, and because of the low decomposition rate constant, 0.039 hr^{-1}, the steady-state urea concentration was approximately the same for all the runs. Therefore, the growth rate constant, k, was the same for all the runs and the mean particle size was directly proportional to the square root of the residence time, τ.

Runs 20-22 were done with different pH values for the feed stream, to see what effect, if any, the pH of the feed has on the precipitation. Table 11 shows the results of these experiments. In runs 1-3 the feed pH was 5.5 and the pH measured in the reactor at steady-state was 5.9. In run 20 the feed pH was adjusted to 4.1 with HNO_3. The yttrium concentration drop, mean particle size, and steady-state pH remained

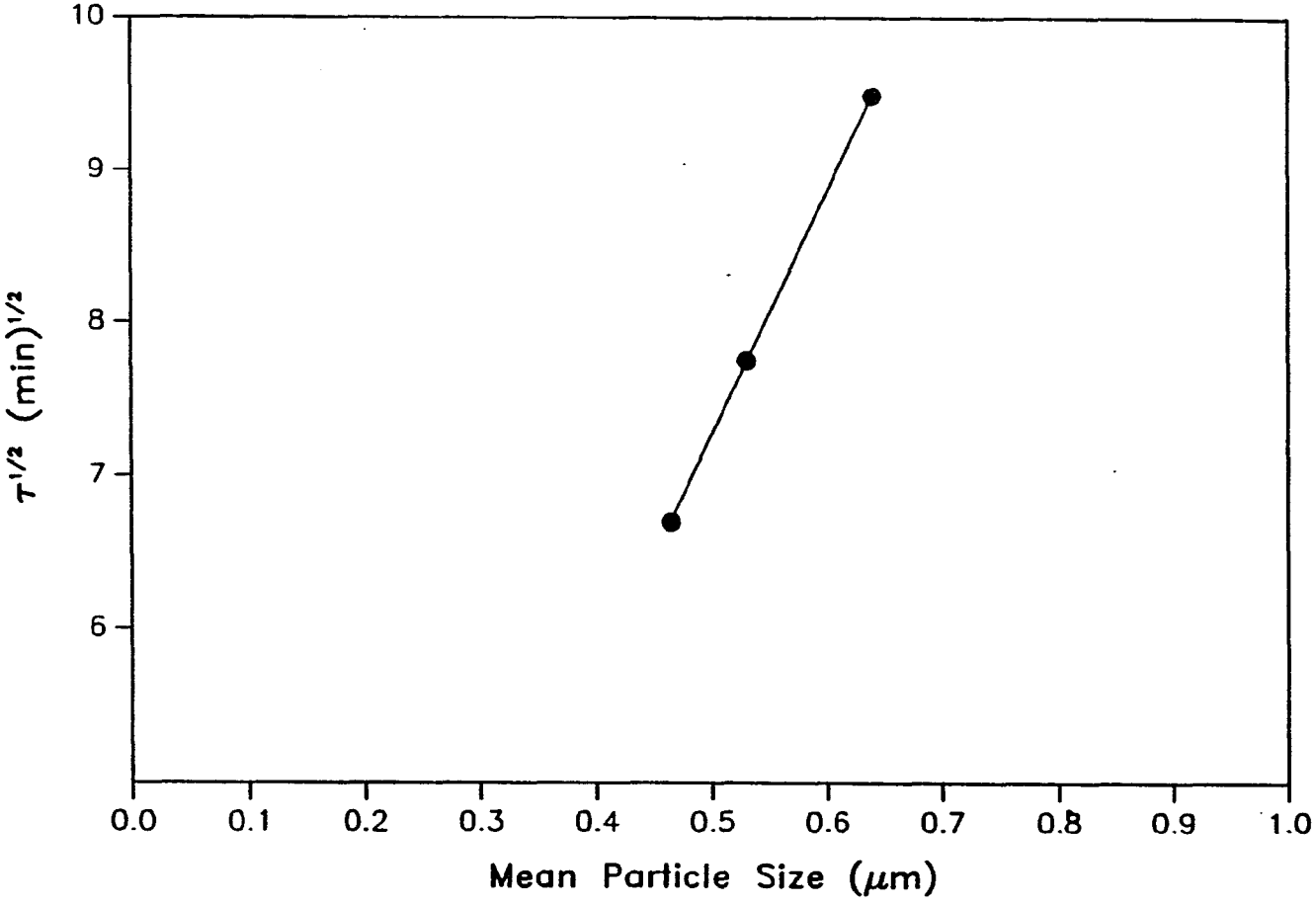

Figure 27. Square root of residence time vs. average mean particle size

unaffected. In run 21 the feed pH was adjusted to 6.9 with sodium hydroxide. Again, the yttrium concentration drop, mean particle size, and steady-state pH remained similar to those values observed in runs 1-3. Finally, in run 22, the pH of the feed was adjusted to 2.2. The steady-state pH was again 5.9 but the Y^{+3} concentration drop was 0.0029 M and the mean particle size increased to 0.74 μm.

Table 11. Effect of changing the pH of the feed stream. Base conditions

Run #	pH(feed)	pH(final)	ΔY^{+3} (M)	ΔY^{+3} pred. (M)	$\bar{L}$(μm)
1	5.5	5.9	0.0049	0.0063	0.51
2	5.5	5.9	0.0054	0.0063	0.56
3	5.5	5.9	0.0052	0.0063	0.52
20	4.1	5.9	0.0050	0.0063	0.55
21	6.9	5.9	0.0049	0.0063	0.50
22	2.2	5.9	0.0029	0.0042	0.74

In runs 20 and 21 the rate of urea decomposition was such that only a small fraction of the decomposing urea was necessary to neutralize the acidity or basicity of the incoming feed stream. The net result being that the same yttrium concentration drop and same mean particle size were observed as in runs 1-3. In run 22, the amount of acid that was needed to be neutralized was of the same order of magnitude as the amount of urea that decomposed per liter of solution. At a pH of 2.2, the H^+ concentration is 0.0063 M. At 90°C, 0.0094 moles of urea decompose per liter of solution in the stirred tank reactor. For every mole of urea that decomposes, two moles of NH_3 are released. Therefore, 0.00315 moles of the decomposing urea are used up neutralizing the acid.

This leaves 0.00625 moles of decomposed urea for the yttrium precipitation. Since two moles of yttrium hydroxycarbonate precipitate for every three moles of urea that decompose, the observed Y^{+3} drop should be 0.0042 M. As in the other runs, the observed Y^{+3} drop is about 0.001 M less than predicted.

The mean particle size was larger than for the other runs in Table 11. This is consistent with the earlier observation that as the yttrium concentration drop goes down, the mean particle size goes up. In this case, the effective rate of decomposition of urea (effective in terms of decomposition resulting in the precipitation of yttrium hydroxycarbonate) is smaller than in runs 1-3, 20, and 21. The lower effective rate of decomposition results in a lower nucleation rate, thus producing fewer, but larger, particles.

In conclusion, for the MSMPR reactor, the shape of the observed size distribution, the size of the particles produced, and the square root dependence of the mean particle size with residence time, are consistent with the model in which the particles grow by diffusion of carbonate ion to the particle surface. The concentration gradient that each particle experiences, hence the growth rate, is controlled by the rate of decomposition of urea. As the rate of urea decomposition increases, the nucleation rate increases exponentially. The increase in the number density of particles, or diffusional sinks, causes the concentration gradient of carbonate that each particle experiences to decrease, even though the rate of urea decomposition is higher.

Semi-batch Reactor Results

The semi-batch reactor was operated at five different sets of volume fraction, V, and batch fraction, σ_B. Figure 28 is a plot of coefficient of variation versus volume fraction for various values of batch fraction. It shows the V and σ_B values for the experimental runs as well as the expected coefficient of variation for each set of conditions. In runs 1-4, the reactor was operated so that it behaved nearly like a batch reactor. At the other extreme, V and σ_B values for runs 16-18 were chosen such that the reactor behaved nearly like a continuous stirred tank reactor, referred to earlier as a MSMPR reactor. For runs 9-12 and 13-15, two different sets of V and σ_B were used but they were chosen so that the coefficient of variation would be the same in both cases, approximately 30%.

Table 12 shows the V and σ_B values for runs 1-18 as well as the length of the total cycle time, t_T, the number of cycle times for each run, the mean residence time, τ, the predicted and observed coefficients of variation, and the mean particle size. The total cycle time was varied for each set of V and σ_B values so as to maintain the same mean residence time for all the semi-batch runs (approximately 60 minutes). The mean residence time for the semi-batch reactor is given by the following equation,

$$\tau = \frac{t_T}{2(1-V)} \{ (1+V)(1-\sigma_B) + 2\sigma_B \} \qquad (62)$$

where $\tau \to \infty$ as $V \to 1$.

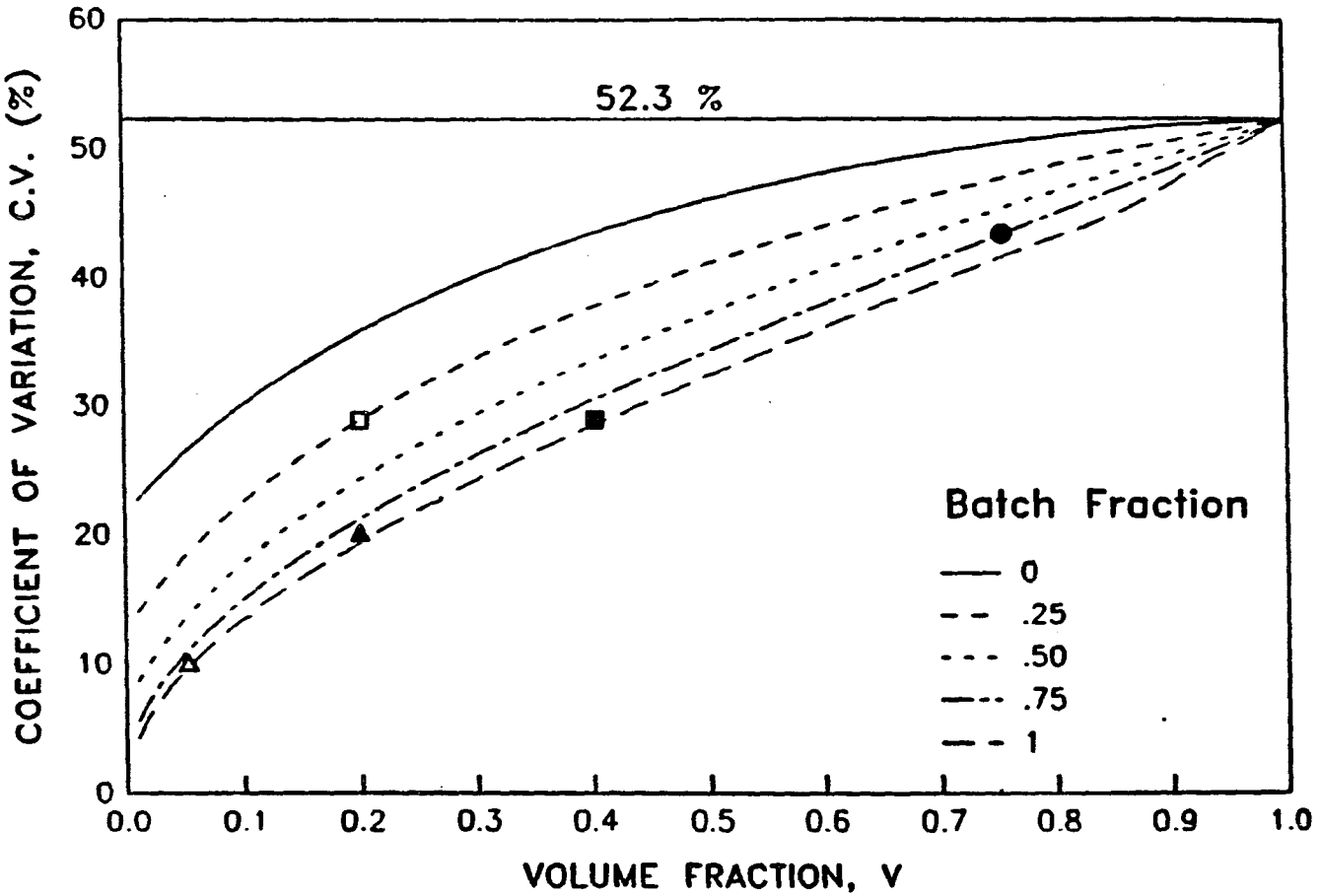

Figure 28. Coefficient of variation vs. volume fraction for various values of batch fraction

Table 12. Summary of semi-batch experiments

Run #	V	σ_B	t_T (min.)	# of t_T	τ (min.)	Predicted C.V.	Exp. obs. C.V.	$\bar{L}$ (μm)
1	0.05	0.95	60	10	61.7	9.5 %	12.6 %	0.55
2	0.05	0.95	60	10	61.7	9.5 %	14.4 %	0.47
3	0.05	0.95	60	10	61.7	9.5 %	12.3 %	0.47
4	0.05	0.95	60	10	61.7	9.5 %	17.1 %	0.50
5	0.2	0.9	50	10	60.0	19.9 %	18.3 %	0.49
6a	0.2	0.9	50	5	60.0	19.9 %	19.5 %	0.43
6b	0.2	0.9	50	15	60.0	19.9 %	21.2 %	0.42
7a	0.2	0.9	50	7	60.0	19.9 %	17.4 %	0.48
7b	0.2	0.9	50	10	60.0	19.9 %	16.6 %	0.48
8	0.2	0.9	50	10	60.0	19.9 %	22.4 %	0.52
9	0.2	0.25	70	10	61.3	28.9 %	28.2 %	0.52
10	0.2	0.25	70	10	61.3	28.9 %	32.7 %	0.51
11	0.2	0.25	70	10	61.3	28.9 %	29.0 %	0.48
12	0.2	0.25	70	10	61.3	28.9 %	26.3 %	0.53
13	0.4	0.9	40	10	64.7	28.9 %	33.1 %	0.48
14a	0.4	0.9	40	5	64.7	28.9 %	36.3 %	0.49
14b	0.4	0.9	40	15	64.7	28.9 %	32.3 %	0.51
15	0.4	0.9	40	10	64.7	28.9 %	28.7 %	0.53
16	0.75	0.75	16	25	62.0	43.1 %	44.8 %	0.44
17a	0.75	0.75	16	15	62.0	43.1 %	42.3 %	0.46
17b	0.75	0.75	16	30	62.0	43.1 %	43.0 %	0.48
18	0.75	0.75	16	20	62.0	43.1 %	43.6 %	0.47

The feed to the semi-batch reactor was nucleated in the preheat tank so that only growth would take place in the reactor (see experimental section). The nuclei particles were about 0.05 μm in diameter. This nucleated feed was then pumped into the semi-batch reactor. The temperature for all the runs was 100°C. The yttrium concentration and the urea concentration of all the feed solutions were 0.02 M and 0.25 M respectively.

The Y^{+3} concentration drop for runs 1-18 are shown in Table 13. For runs 1-15 the Y^{+3} concentration drop was approximately 0.016 M which is slightly higher than the 0.015 M drop predicted from the decomposition kinetics of urea for a batchwise precipitation for an hour at 100°C. This is probably because the ΔY^{+3} measured for the semi-batch reactor is the difference in the Y^{+3} concentration between the product stream and the feed solution before it has been nucleated. If the ΔY^{+3} between the product stream and the nucleated feed stream had been measured instead, the observed ΔY^{+3} would have likely been closer to that predicted for the batch precipitation.

Table 13. Yttrium concentration for the semibatch experiments

Run #	$[Y^{+3}]_{initial}$	$[Y^{+3}]_{final}$	ΔY^{+3}	ΔY^{+3}(ave.) ± std. dev.
1	0.02025 M	0.00355 M	0.01670 M	
2	0.02025 M	0.00402 M	0.01623 M	
3	0.01967 M	0.00377 M	0.01590 M	
4	0.01967 M	0.00352 M	0.01615 M	0.01625 ± 0.00033 M
5	0.02017 M	0.00414 M	0.01603 M	
6a	0.02008 M	0.00399 M	0.01609 M	
6b	0.02008 M	0.00391 M	0.01617 M	
7a	0.02008 M	0.00422 M	0.01586 M	
7b	0.02008 M	0.00416 M	0.01592 M	
8	0.01983 M	0.00328 M	0.01655 M	0.01610 ± 0.00025 M
9	0.01992 M	0.00461 M	0.01531 M	
10	0.01992 M	0.00403 M	0.01589 M	
11	0.02015 M	0.00412 M	0.01603 M	
12	0.02015 M	0.00391 M	0.01624 M	0.01587 ± 0.00040 M
13	0.01961 M	0.00390 M	0.01571 M	
14a	0.01961 M	0.00355 M	0.01606 M	
14b	0.01961 M	0.00376 M	0.01585 M	
15	0.01961 M	0.00412 M	0.01549 M	0.01578 ± 0.00024 M
16	0.01980 M	0.00722 M	0.01258 M	
17a	0.01980 M	0.00800 M	0.01180 M	
17b	0.01980 M	0.00772 M	0.01208 M	
18	0.01980 M	0.00825 M	0.01155 M	0.01200 ± 0.00044 M

Runs 16-18 ($V = 0.75$, $\sigma_B = 0.75$) had a significantly lower Y^{+3} concentration drop than the other semi-batch runs, 0.012 M vs. 0.016 M. In these runs, the semi-batch reactor was operated so that it behaved nearly like a MSMPR reactor. The 0.012 M average concentration drop was almost the same as that for the MSMPR reactor at 100°C, see Table 8.

The number density of particles produced per ml of suspension was calculated from a knowledge of the particle size distribution, the amount of Y^{+3} precipitated out as $Y(OH)CO_3 \cdot H_2O$, and the particle density, 2.8 g/cm^3. The average number densities for the various semi-

batch conditions are shown in Table 14. The table shows that the semi-batch reactor is producing about 1 x 10^{10} particles per cm^3. Kayima estimated that about 3 x 10^{10} particles per cm^3 were produced in his batch precipitations of $Y(OH)CO_3 \cdot H_2O$. In his calculations, he assumed a density of 2.1 g/cm^3, while in this research, using a helium pycnometer, the density was found to be 2.8 g/cm^3. This difference in density would bring Kayima's estimate to about 2 x 10^{10} particles/cm^3. Thus, there was fairly good agreement between Kayima's work and this work on the total number of particles produced per ml. This was to be expected since the particles were all nucleated batchwise before being placed in the semi-batch reactor where only growth took place.

Table 14. Average number densities for the five semi-batch operating conditions

Run #	V	σ_B	# of particles/ml
1-4	0.05	0.95	1.5 x 10^{10}
5-8	0.2	0.9	1.6 x 10^{10}
9-12	0.2	0.25	1.2 x 10^{10}
13-15	0.4	0.9	1.1 x 10^{10}
16-18	0.75	0.75	8.6 x 10^{9}

Table 12 shows the predicted and the observed coefficient's of variation, C.V.'s, for runs 1-18, and Table 15 shows the predicted and the average values of the C.V.'s for the various semi-batch operating conditions, as well as the 95% confidence interval for each average. Except for the case where V = 0.05 and σ_B = 0.95, the C.V. predicted by the model fell within the 95% confidence interval for all the observed C.V.'s. It is not suprising that the average C.V. for runs 1-4 was

significantly higher than that predicted by the model, because runs 1-4 were most nearly like a batch reactor, and the model predicts a C.V. of 0% for a batch reactor. Yttrium hydroxycarbonate particles produced by Verlinden (38) in a batch reactor had C.V.'s that ranged from 3% to 11%. So while the observed C.V.'s for runs 1-4 were higher than predicted, they were not higher than expected.

Table 15. Comparison of predicted and experimental coefficients of variation

Run #	Predicted C.V.	Exp. observed C.V. ± (95% c.i.)	$\bar{L}$ ± (95% c.i.) (μm)
1-4	9.5 %	14.1 % ± 3.5 %	0.50 ± 0.06
5,6b,7b,8	19.9 %	19.6 % ± 4.3 %	0.48 ± 0.06
9-12	28.9 %	29.1 % ± 4.3 %	0.51 ± 0.03
13,14b,15	28.9 %	31.4 % ± 5.7 %	0.51 ± 0.07
16,17b,18	43.1 %	43.8 % ± 2.2 %	0.47 ± 0.05

Figures 29-33 show predicted and observed size distribution data for the semi-batch reactor under the five different operating conditions. Graph (a) in each figure shows the size distribution predicted by the model. Graph (b) shows the predicted size distribution after data from graph (a) had been converted into a bar graph. This is what the observed size distribution would look like if the semi-batch reactor behaved exactly as the model predicted. Graph (c) is a composite of the particle size distribution data of all three or four runs for each set of V and σ_B values. In each case, the growth constant k was varied so as to get the best fit of the model to the data. The k values for Figures 29-33 were 0.11, 0.11, 0.13, 0.12, and 0.10 $\mu m^2/hr$ respectively. This was about twice the average k value for the MSMPR reactor at 100°C

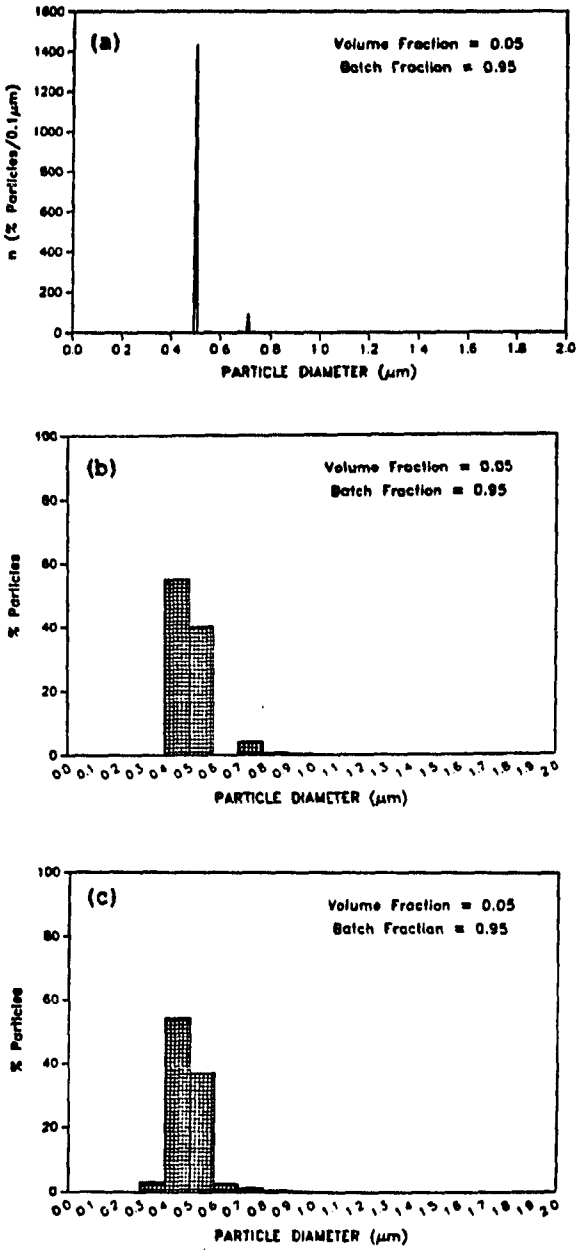

Figure 29. Size distribution data from runs 1-4. Figure 29a is the best fit of the model to the data. Figure 29b is the model expressed as a histogram and Figure 29c is the experimental data

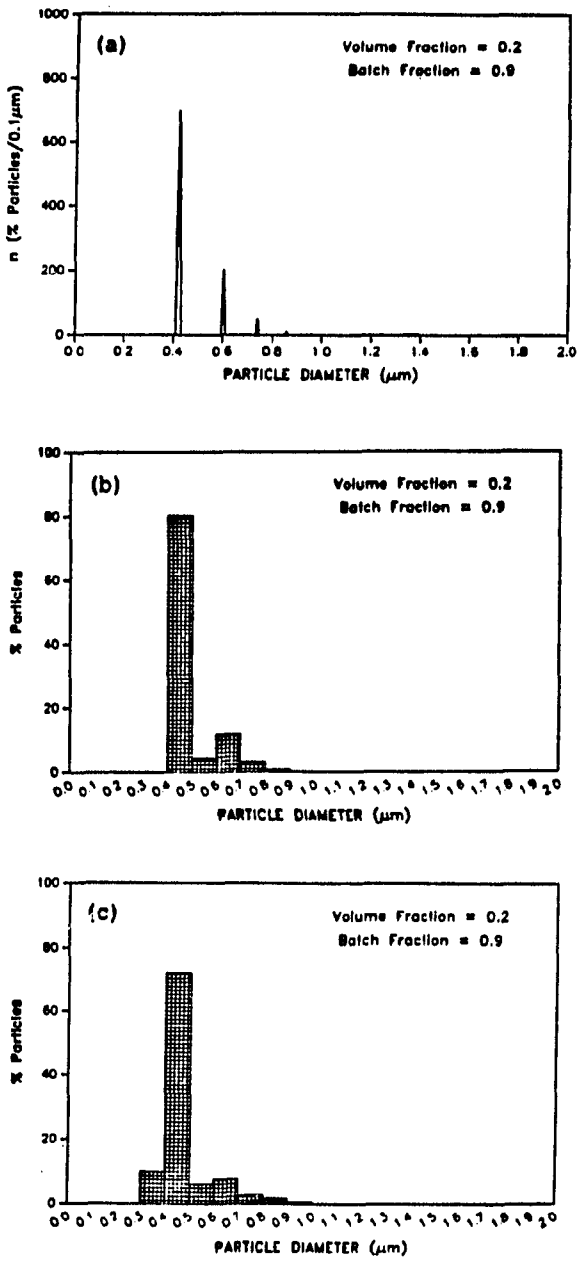

Figure 30. Size distribution data from runs 5-8. Figure 30a is the best fit of the model to the data. Figure 30b is the model expressed as a histogram and Figure 30c is the experimental data

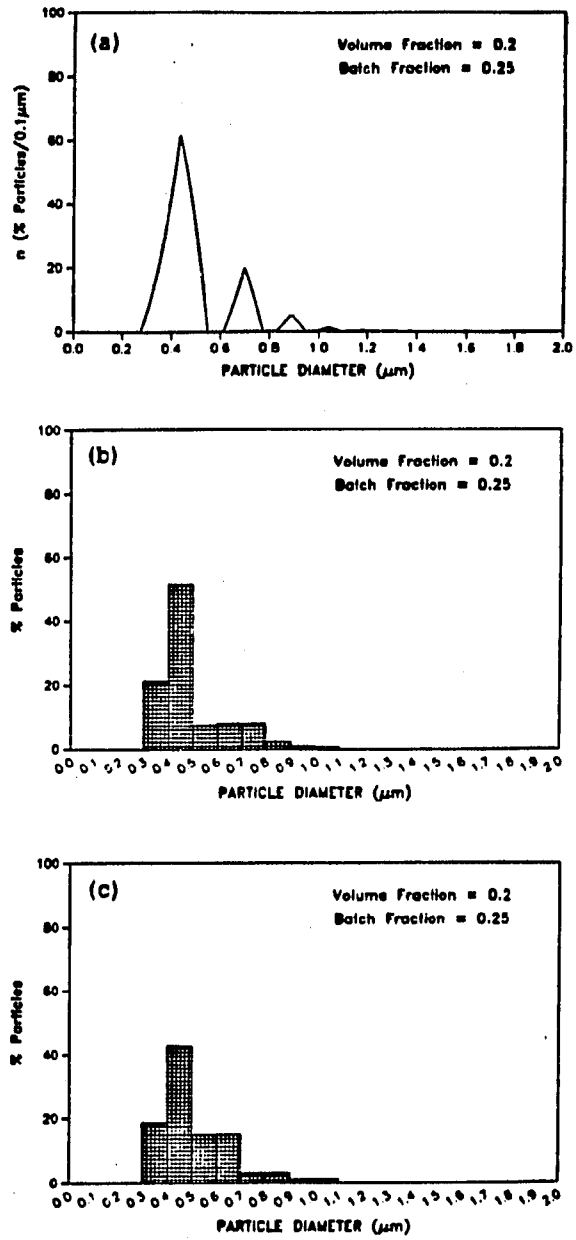

Figure 31. Size distribution data from runs 9-12. Figure 31a is the best fit of the model to the data. Figure 31b is the model expressed as a histogram and Figure 31c is the experimental data

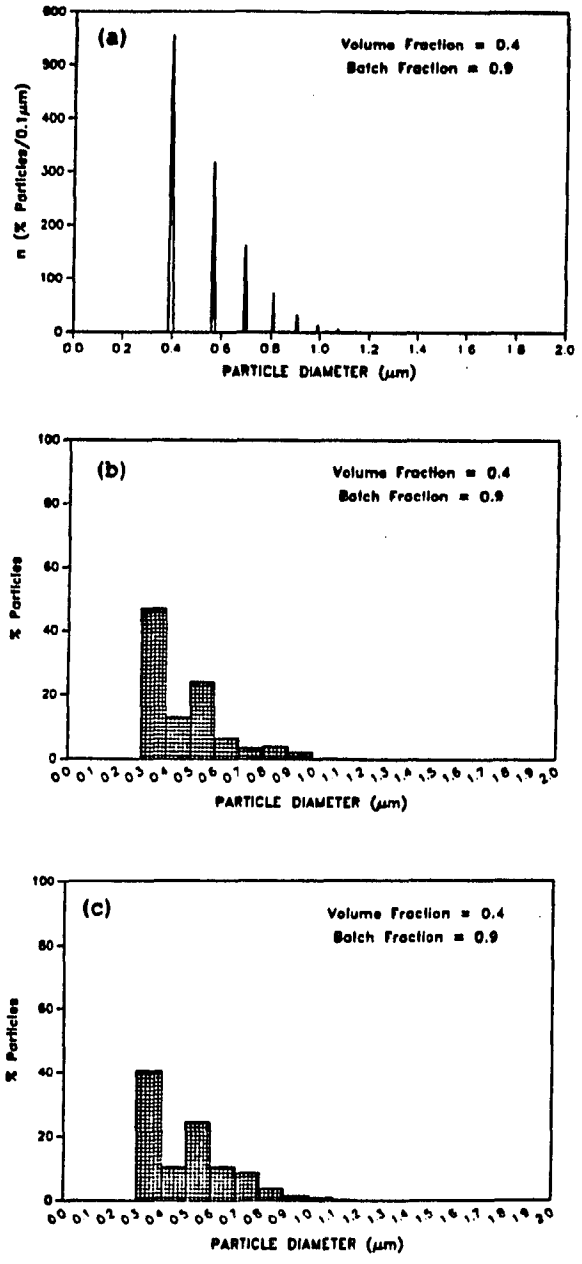

Figure 32. Size distribution data from runs 13-15. Figure 32a is the best fit of the model to the data. Figure 32b is the model expressed as a histogram and Figure 32c is the experimental data

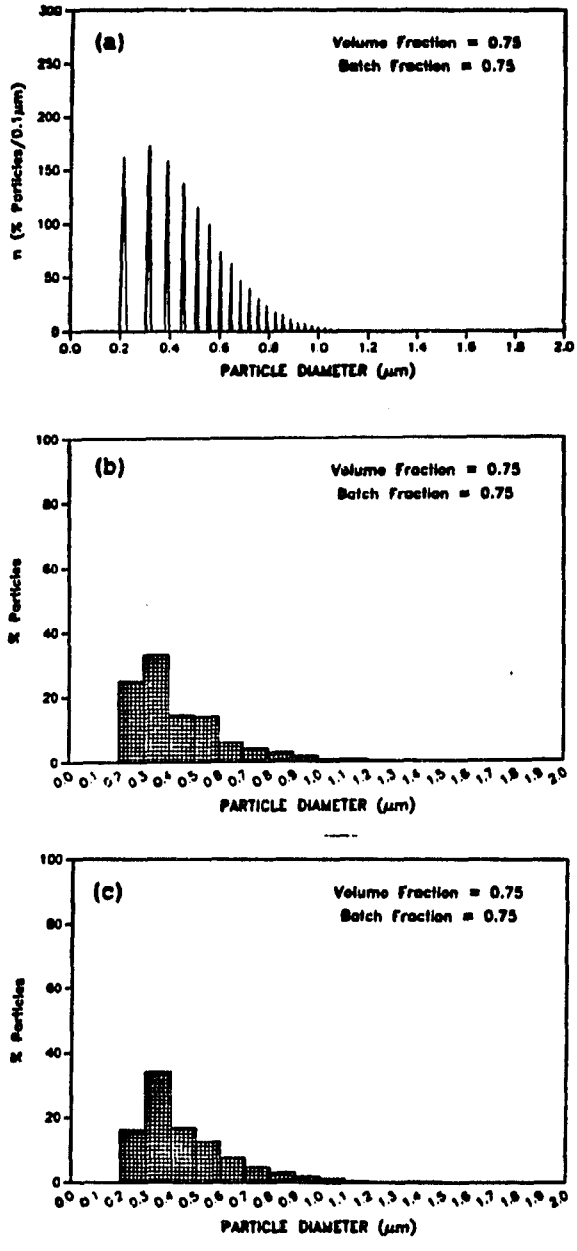

Figure 33. Size distribution data from runs 16-18. Figure 33a is the best fit of the model to the data. Figure 33b is the model expressed as a histogram and Figure 33c is the experimental data

(0.050 $\mu m^2/hr$). This difference is probably related to the fact that no nucleation is taking place. All the decomposition of urea is going towards particle growth in the semi-batch reactor.

Figure 29 shows particle size distribution data from the semi-batch reactor with V = 0.05 and σ_B = 0.95. Under these conditions the reactor is acting nearly like a batch reactor. The average C.V. of 14.1% is slightly larger than the 9.5% predicted by the model, but it seems reasonable compared to the 3-11% observed by Verlinden (38) in his batch studies.

In Figure 30, the volume fraction and batch fraction are 0.2 and 0.9 respectively. This produces a slightly broader distribution with an average C.V. of 19.6% compared with the predicted value of 19.9%.

Figure 31 shows particle size distribution data when V = 0.2 and σ_B = 0.25. This shows an even broader distribution than Figure 30. This is because of the broadening of the residence time distribution curve for the reactor as it behaves increasingly less like a batch reactor and more like a MSMPR reactor.

Figure 32 shows particle size distribution data when V = 0.4 and σ_B = 0.9. The model accurately predicts the two peaks in the observed particle size distribution at 0.35 μm and 0.55 μm. It should be noted that, although runs 9-12 and 13-15 were carried out under two different sets of conditions, it was predicted that the C.V. of the particle size distribution in both cases would be the same. Experimentally, runs 9-12 had a C.V. of 29.1% ± 4.3% and runs 13-15 had a C.V. of 31.4% ± 5.7%.

At this point, an important aspect of particle size distributions needs to be discussed. The reader may have noticed that, although the

mean particle size and C.V. are the same in both Figures 31 and 32, the two particle size distributions look quite a bit different. The reason is that the mean particle size and the C.V. do not, in general, completely specify the particle size distribution. If the distribution is normal or log-normal, for example, then a mean particle size and a C.V. will specify one and only one curve. But, looking at Figure 28, one can see that there can be an infinite number of distributions from the semi-batch reactor that have the same mean and C.V. Therefore, although the C.V. is valuable in assessing the relative widths of different distributions, it does not give information about the shape of the distribution, i.e. whether the distribution is unimodal or multimodal, skewed left or skewed right, etc.

Further information about the shape of the particle size distribution can be obtained by taking higher moments about the mean in order to find the skew and kurtosis of the distribution (66). Qualitatively, positive skewness indicates a distribution skewed to the right and negative skewness indicates a distribution skewed to the left. Kurtosis is a measure of the shape of a distribution curve at the extreme ends, relative to a normal distribution. A distribution with positive kurtosis will have a sharper peak but broader tails than a normal distribution and vice versa for a negative kurtosis.

In Figure 33, with V = 0.75 and σ_B = 0.75, the level of backmixing was such that the semi-batch reactor behaved nearly like a MSMPR reactor. This can be seen by comparing the particle size distribution in Figure 33 with the particle size distribution from a MSMPR reactor as shown in Figures 21e, 22e, and 23e. As in the other semi-batch runs,

there was good agreement between the predictions of the model and the observed particle size distribution.

Packed Bed Reactor

The feed solution for the packed bed reactor was initially 0.02 M in yttrium nitrate and 0.25 M in urea. This feed was nucleated before being pumped into the reactor. The size of the nuclei was approximately 0.05 μm. Nucleated feed was used for two reasons. First, if the feed was not nucleated, nucleation would not occur until the feed was about a third of the way through the column. As a result, a very large particle concentration gradient would be established in the column. This would lead to extensive axial diffusion, resulting in a broad particle size distribution. The second reason was that the packed bed reactor with a nucleated feed should behave as predicted by the tanks-in-series model where nucleation takes place only in the first tank,

$$n_m = 100\% \left[\frac{B^m \, L^{2m-1}}{2^{m-1}(m-1)!}\right] \exp\left(-\frac{BL^2}{2}\right) \qquad (44)$$

where $B = m/k\tau$ and m is the number of stirred tank reactors in series approximated by the packed bed.

Figures 34a and 34b show particle size distribution data from run 1 after five and ten residence times, respectively. The mean residence time for all runs was 60 minutes. From this data, it appears that a steady-state particle size distribution is established after five residence times have passed.

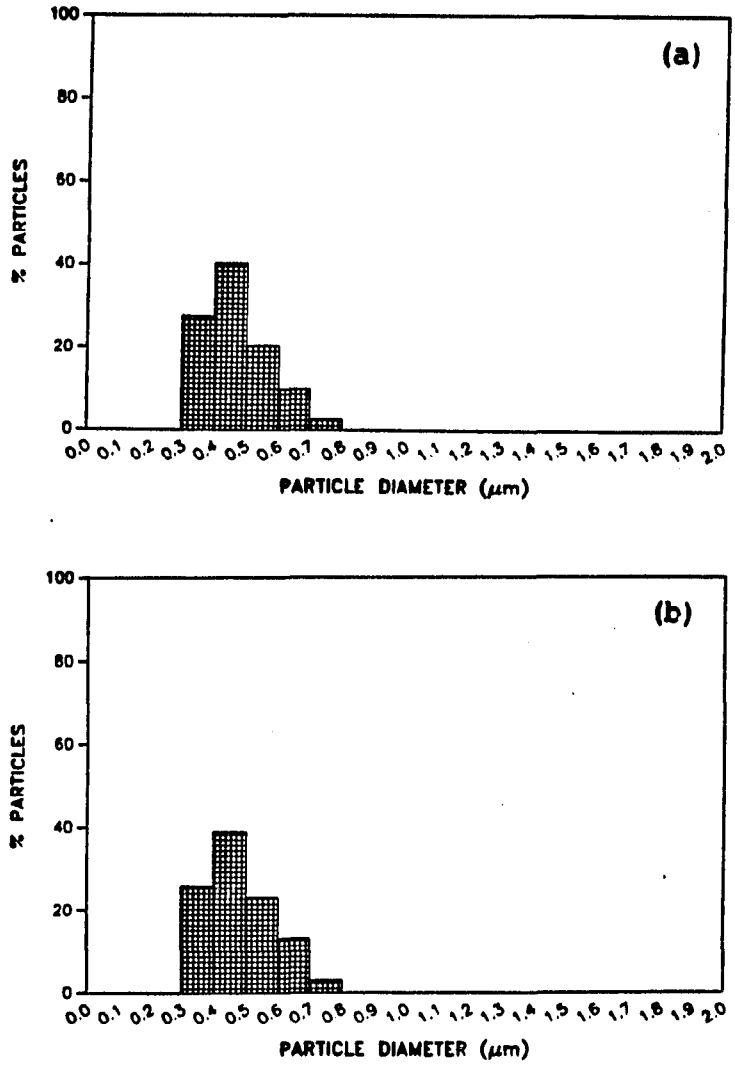

Figure 34. Figures 34a and 34b show size distribution data for run 1 of the packed bed reactor after 5 and 10 residence times, respectively

Table 16 is a summary of the packed bed reactor results. It lists the number of stirred tank reactors approximated by the packed bed, m, the reactor temperature, the yttrium concentration drop, mean particle size, and predicted and observed coefficients of variation.

Table 16. Summary of packed bed reactor results

Run #	Bed Hgt. (mm)	m	T (°C)	ΔY^{+3} (M)	$\bar{L}$ (μm)	Pred. C.V.	Obs. C.V.
1	490	23	98	0.0108	0.47	10.5%	22.1%
1a	490	23	98	0.0110	0.48	10.5%	21.5%
2	490	23	98	0.0105	0.46	10.5%	23.7%
3	250	12	98	0.0106	0.48	14.5%	20.9%
4	250	12	98	0.0109	0.48	14.5%	23.5%
5	490	23	91	0.0047	0.33	10.5%	25.2%
6	490	23	91	0.0048	0.34	10.5%	23.8%

As shown earlier, the number of stirred tank reactors in series, m, that approximates the residence time distribution of the packed bed reactor is given by Equation 43,

$$m = (\varepsilon l)/(4d_p) \tag{43}$$

where ε is the void fraction of the bed, l is the bed height, and d_p is the diameter of the packing beads. The m value for the packed bed reactor can be varied by changing the size of the packing beads or by changing the bed height. Beads ranging in size from 0.1 mm to 3.175 mm were used as packing material, but it was found that the column became plugged after a short period of time if the beads were 1 mm or less. Therefore, to alleviate the plugging problem, the largest beads (3.175 mm) were used and the m value was varied by changing the bed height.

Two different bed heights were used, 490 mm and 250 mm, which gave m values of 23 and 12 respectively. According to the packed bed model, m values of 23 and 12 should produce particle size distributions of 10.5% and 14.5% respectively.

As can be seen in Table 16, the coefficient of variation for all the packed bed runs ranged from 20% - 25% regardless of the m value for the reactor. The distributions were broader than expected and skewed towards larger particle sizes. According to the model, the size distributions should have been symmetrical, see Figure 9. A possible reason for the broadening of the distribution and the skewing towards larger particle sizes is that the time it took for some particles to move through the column was being retarded due to their being in close proximity to either the wall of the reactor or the surface of the packing beads where the fluid velocity is close to zero. Some particles may diffuse to one of these surfaces and remain for awhile before dislodging and continuing onward. The net result being that the particles who have had their trek through the reactor retarded, grow larger than expected because of the increased time in the reactor.

In runs 5 and 6, the temperature of the reactor was decreased to 91^{o}C. The mean particle size decreased from about 0.48 μm for runs 1-4 to about 0.34 μm. This is the opposite of what was observed for the MSMPR reactor where the mean particle size decreased with an increase in temperature. The reason for this is that no nucleation was taking place in the packed bed reactor. As the rate urea decomposition decreased with decreasing temperature, the concentration of diffusant decreased resulting in a lower k value and smaller particles.

CONCLUSIONS AND RECOMMENDATIONS

In this research, spherical particles of the yttria precursor $YOHCO_3 \cdot H_2O$ were continuously produced in three types of reactors: 1. mixed-suspension mixed-product removal (MSMPR), 2. semi-batch , and 3. packed bed. A wide variety of particle size distributions were produced from these reactors. Mathematical models, developed for these reactors, successfully allowed the size and shape of the particle size distributions to be predicted and controlled.

1. Mixed-suspension mixed-product removal (MSMPR) reactor

Particle size distribution data from the MSMPR reactor fit a model in which particle growth was by diffusion of some species to the particle surface. From an analysis of the MSMPR data, the concentration of the diffusing species was found to be of the same order of magnitude as the estimated carbonate concentration, thus suggesting that carbonate is the rate-limiting diffusing species.

The log of the nucleation rate was proportional to the rate of urea decomposition. The growth rate constant decreased linearly with increasing rate of urea decomposition. A possible explanation for this is as follows: as the rate of urea decomposition increases, the number of particles per ml increases exponentially while the amount of carbonate produced increases linearly. Because of the exponential

increase in the number of diffusion sinks per ml, the carbonate concentration gradient for each particle decreases, even though more carbonate is being produced. The carbonate concentration gradient is directly proportional to the growth rate constant, k. Therefore, as the nucleation rate goes up, k goes down and the mean particle size goes down.

Over the range of conditions studied in this research, the yttrium concentration had little effect on the particle size distribution or the amount of precipitate produced. Thus, it appears that the rate of urea decomposition is the controlling factor in the precipitation process. The mechanism of particle growth is by diffusion, but the urea decomposition controls the concentration gradient the particle sees.

2. Semi-batch reactor

The semi-batch reactor was able to produce particle size distributions with different coefficients of variation depending on how the reactor was operated. At one extreme, the reactor produced particle size distributions that were almost like what one would expect from a batch reactor, C.V. = 14.1%. At the other extreme, the reactor produced particle size distributions that were almost like what one would expect from a MSMPR reactor, C.V. = 43.8%. The model for the semi-batch reactor, which assumes that particles grow by a diffusion mechanism, correctly predicted the shape and coefficient of variation of the observed particle size distributions.

3. Packed bed reactor

The packed bed reactor produced particle size distributions that were broader than predicted by the proposed model. The observed particle size distributions were skewed towards larger particle sizes while the model predicted that the size distributions would be symmetrical. This broadening of the distribution and skewing towards larger particle sizes is thought to be caused by the hindered motion of some of the particles as they move through the column. The hindered motion being a result of the close proximity of some particles to either the wall of the reactor or the surface of the packing beads.

Unlike the MSMPR reactor, as the temperature of the packed bed reactor was increased, the mean particle size increased. This was because the feed to the reactor had already been nucleated. Therefore, increasing the rate of urea decomposition, by increasing the temperature, increased the particle growth rate because no nuclei were being produced in the reactor.

Recommendations

The reactors studied in this research produced a wide variety of particle size distributions. These different distributions could be used in sintering studies to determine what characteristics of particle size distributions are important in terms of producing a final sintered product with the desired properties. For example, one could compare two different powder samples having the same coefficient of variation but

different mean particle sizes, or two samples having the same mean particle size but different coefficients of variation, or two samples having the same mean particle size and coefficient of variation but having distributions with different shapes.

Finally, a recycle reactor should be investigated. A recycle reactor is capable of producing levels of backmixing between the two extremes of plugflow and complete backmixing. The advantage a recycle reactor would have over a MSMPR reactor would be that it could produce particle size distributions with different coefficients of variation, depending on how the reactor was operated. Its advantage over the semi-batch and packed bed reactors would be that there is no need to nucleate the feed stream before pumping it into the reactor. Also, since no packing material is needed in a recycle reactor, the problem of particles adhering to surfaces in the reactor would be minimized.

Modelling such a reactor would be complex because particle nucleation and growth would be occuring in the recycle stream as well as in the main reactor. Typically, it is assumed that the portion of the product stream that is recycled to the entrance of the reactor is unchanged from its state when it left the reactor. In this case, however, the tube carrying the recycle stream would behave somewhat like a plug flow reactor. Also, it would have to be taken into account that there would be a distribution of particle sizes in the feed stream and that the number density of particles in the feed stream would be related to the recycle ratio. Thus, not only would the nucleation and growth rates be a fuction of the rate of urea decomposition, but they would

also be a function of the recycle ratio because that would control the population density of particles entering the feed stream.

REFERENCES

1. Barringer, E. A., and H. K. Bowen. 1982. Formation, packing, and sintering of monodisperse TiO_2 powders. J. Am. Ceram. Soc. 65:C199-201.

2. Bowen, H. K. 1980. Basic Research Needs on High Temperature Ceramics for Energy Applications. Mat. Sci. and Eng. 44:1-56.

3. Bowen, H.K. 1984. Ceramics as Engineering Materials: Structure-Property-Processing. Pages 1-11 in Materials Research Society Symposium Proceedings. Vol. 24. Elsevier Publishing Co., New York.

4. Perrin, J. 1909. Mouvement Brownien et Realite Moleculaire. Ann. de Chim. et de Phys. 17:5-114.

5. Einstein, A. 1905. Zur Theorie der Brownschen Bewegung. Ann. der Physik 19:371-381.

6. von Smoluchowski, M. 1906. Zur Kinetischen Theorie der Brownschen Molekularbewegung und der Suspensionen. Ann. der Physik 21:756-780.

7. Zsigmondy, R. and P. A. Thiesseu. 1925. Das kolloide gold. Akad. Verlagsgen Leipzig.

8. Svedberg, G., and H. Rinde. 1924. The Ultra-Centrifuge, A New Instrument for the Determination of Size and Distribution of Size of Particles in Microscopic Colloids. J. Am. Chem. Soc. 46:2677-2681.

9. Overbeek, J. T. G. 1981. Monodisperse colloidal systems. Adv. in Coll. Int. Sci. 15:251-277.

10. LaMer, V. K. and M. D. Barnes. 1946. Monodispersed hydrophobic colloidal dispersions and light scattering properties. I. Preparation and light scattering properties of monodispersed colloidal sulphur. J. Coll. Int. Sci. 1:71-77.

11. Mie, G. 1908. Beitrage zur Optik Truber Medien, Speziell Kolloidaler Metallosungen. Ann. der Physik 25:377-445.

12. LaMer, V. K., and R. H. Dinegar. 1950. Theory, production, and mechanism of formation of monodispersed hydrosols. J. Am. Chem. Soc. 72:4847-4854.

13. Reiss, H., and F. K. LaMer. 1950. Diffusional boundary value problems involving moving boundaries, connected with the growth of colloid particles. J. Chem. Phys. 18(1):1-12.

14. Zaiser, E. M. and V. K. LaMer. 1947. The kinetics of the formation and growth of monodispersed sulphur hydrosols. J. Coll. Int. Sci. 2:257-273.

15. Bradford, E. B., J. W. Vanderhoff, and T. Alfrey, Jr. 1956. The Use of Monodisperse Latexes in an Electron Microscope Investigation of the Mechanism of Emulsion Polymerization. J. Coll. Sci. 11:135-149

16. Rubens, L. C., and R. F. Bayer. The Polymerization of Styrene. Pages 274-286 in R. H. Boundy and R. F. Boyer, eds. Styrene Its Polymers, Copolymers and Derivatives. Reinhold, New York.

17. Demchak, R. and E. Matijevic. 1969. Preparation and particle size analysis of chromium hydroxide hydrosols of narrow size distributions. J. Coll. Int. Sci. 31:257-262.

18. Matijevic, E. 1976. Preparation and characterization of monodispersed metal hydrous oxide sols. Progress in Colloid and Polymer Sci. 61:24-35.

19. Matijevic, E. 1981. Monodispersed metal hydrous oxides - A fascinating field of colloid science. Acc. Chem. Res. 14:22-29.

20. Matijevic, E., A. D. Lindsay, S. Kratohvid, M. E. Jones, R. A. Larson, and N. W. Cayey. 1971. Characterization and stability of chromium hydroxide sols of narrow size distributions. J. Coll. Interface Sci. 36(2):273-281.

21. Matijevic, E. 1978. Preparation and properties of monodispersed colloidal metal hydrous oxides. Pure and Appl. Chem. 50:1193-1210.

22. Matijevic, E., M. Budnik, and L. Meites. 1977. Preparation and mechanisms of formation of titanium dioxide hydrosols of narrow size distributions. J. Coll. Int. Sci. 61:302-311.

23. Matijevic, E., R. S. Sapieszko, and J. B. Melville. 1975. Ferric Hydrous Oxide Sols I. J. Coll. Int. Sci. 50(3):567-581.

24. Scott, W. B. and E. Matijevic. 1978. Aluminum hydrous oxide sols. III. Preparation of uniform particles by hydrolysis of aluminum chloride and perchlorate salts. J. Coll. Int. Sci. 66:447-454.

25. Brace, R. and E. Matijevic. 1973. Aluminum hydrous oxide sols. I. Spherical particles of narrow size distributions. J. Coll. Sci. 35:3691-3705.

26. McFadyen, P., and E. Matijevic. 1973. Copper Hydrous Oxide Sols of Uniform Particle Shape and Size. J. Coll. and Int. Sci. 44(1):95-106.

27. Matijevic, E. 1986. Monodispersed Colloids: Art and Science. Langmuir 2:12-20.

28. Catone, D. L., and E. Matijevic. 1974. Aluminum hydrous oxide sols. II. Preparation of uniform spherical particles by hydrolysis of Al sec-butoxide. J. Coll. Sci. 48:291-301.

29. Fegley, B., Jr., and E. A. Barringer. 1984. Synthesis, characterization, and processing of monosized ceramic powders. Pages 187-197 in C. J. Brinker, D. E. Clark and D. R. Ulrich, eds. Better ceramics through chemistry. North Holland, New York.

30. Pickles, D. G. and E. Lilley. 1985. Ultramicrotoming of Ceramic Powders for Electron Microscopy. J. Am. Ceram. Soc. 68(9):C222-223.

31. Heistand, R. H. and Y. Chia. 1986. Synthesis of Submicron, Narrow Size Distribution Spherical Zincite. Mat. Res. Soc. Symp. Proc. 73:93-98.

32. Stober, W., A. Fink and E. Bohn. 1968. Controlled growth of monodispersed silica spheres in the micron size range. J. Coll. Sci. 26:62-69.

33. Willard, N. H., and N. K. Tang. 1937. A study of the precipitation of aluminum basic sulfate by urea. J. Am. Ceram. Soc. 59:1190-1196.

34. Willard, H. S. and L. Gordon. 1953. Preparation of Basic Stannic Sulfate from Homogeneous Solution. Anal. Chem. 25:170-172.

35. Gordon, L., M. L. Salutsky, and H. S. Willard. 1959. Precipitation from homogeneous solution. John Wiley and Sons, Inc., New York.

36. Williams, R., P. N. Yocom, and F. S. Stofko. 1985. Preparation and properties of spherical zinc sulfide particles. J. Coll. Int. Sci. 106:388-398.

37. Haruta, M., J. Lemaitre, F. Delamney, and B. Delmon. 1984. Preparation and properties of colloidal spherical particles of molybdenum and cobalt sulfides. J. Coll. Int. Sci. 101:59-71.

38. Verlinden, M. C. 1987. Preparation of monodispersed yttrium hydroxycarbonate spheres by homogeneous precipitation. M. S. thesis. Iowa State University, Ames, Iowa.

39. Kayima, P. M., and R. S. Hansen. 1987. Monodispersed spherical colloid particles of yttrium hydroxy-carbonate:(II) Nucleation and Growth. Ames lab document library. Iowa State University, Ames, Iowa.

40. Gobet, J., and E. Matijevic. 1984. Preparation of uniform colloidal cadmium and lead selenide particles. J. Coll. Sci. 100:555-560.

41. Cornilsen, B. C., and J. S. Reed. 1979. Homogeneous precipitation of basic aluminum salts as precursors for alumina. Am. Ceram. Soc. Bull. 58:1199.

42. Blendell, J. E., H. K. Bowen, and R. L. Coble. 1984. High purity alumina by controlled precipitation from aluminum sulfate solutions. Am. Ceram. Soc. Bull. 63:797-801.

43. Alfrey, T., Jr., E. B. Bradford, J. W. Vanderhoff, and G. Oster. 1954. Optical Properties of Uniform Particle-Size Latexes. J. Optical Soc. Am. 44:603-609.

44. Gerould, C. H. 1950. Comments on the Use of Latex Spheres as Size Standards in Electron Microscopy. J. Appl. Phys. 21:183-184.

45. Luck, W., M. Klier, and H. Wesslau. 1963. Kristallisation Ubermolekularer Bausteine. Naturwissenschaften 50:485-494.

46. Kreiger, I. M., and P. A. Hiltner. 1971. Order and Disorder in Monodisperse Latexes. Pages 63-72 in R. M. Fitch, ed. Polymer Colloids. Plenum Press, New York.

47. Hachisu, S., Y. Kobayashi, and A. Rose. 1973. Phase Separation in Monodisperse Latexes. J. Coll. Interface Sci. 42:342-348.

48. Vanderhoff, J. W., H. J. van den Hul, R. J. M. Tansk, J. T. G. Overbeek. 1970. The Preparation of Monodisperse Latexes with Well-Characterized Surfaces. Pages 15-44 in G. Goldfinger, ed. Clean Surfaces: Their Preparation and Characterization for Interfacial Studies. Marcel Dekker, New York.

49. Ise, N., T. Okubo, K. Ito, and S. Dasho. 1985. Visible Evidence for Interparticle Attraction in Polymer Latex Dispersions. Langmuir 1:176.

50. Kirkwood, J. G. 1939. Molecular Distribution in Liquids. J. Chem. Phys. 7:919-925.

51. Aksay, I., and C. H. Schilling. 1986. Colloidal Filtration Route to Uniform Microstructures. Pages 439-447 in L. L. Hench and D. R. Ulrich, eds. Science of Ceramic Chemical Processing. Wiley, New York.

52. Hurd, A. J., S. Fraden, and R. B. Meyer. 1986. AC Field-Induced Order in Dense Colloidal Systems. Pages 555-560 in L. L. Hench and D. R. Ulrich, eds. Science of Ceramic Chemical Processing. Wiley, New York.

53. Russel, W. B. 1987. Personal Communication. Dow Chemical Company, Midland, Michigan.

54. Iler, R. K. 1986. Inorganic Colloids for Forming Ultrastuctures. Pages 1-20 in L. L. Hench and D. R. Ulrich, eds. Science of Ceramic Chemical Processing. Wiley, New York.

55. Ciftcioglu, M. and L. E. Burkhart. 1988. Sintering of Ordered Cakes of Yttria Prepared by Homogeneous Precipitation of Yttrium Hydroxycarbonate from Aqueous Solution (to be submitted to Bull. Am. Ceram. Soc.).

56. Kallay, N., I. Fischer, and E. Matijevic. 1985. A method for the preparation of uniform colloidal hematite particles. Colloids and Surfaces 13:145-149.

57. Ring, T. A. 1984. Continuous precipitation and monosized particles with a packed bed crystallizer. Chem. Eng. Sci. 39(12):1731-1734.

58. Jean, H. J., D. M. Goy, and T. A. Ring. 1987. Continuous Production of Narrow-Sized and Unagglomerated TiO_2 Powders. Am. Ceram. Soc. Bull. 66(10):1517-20.

59. Haggerty, J. S. 1984. Growth of Precisely Controlled Powders from Laser Heated Gases. Pages 353-366 in L. L. Hench and D. R. Ulrich, eds. Ultrastucture Processing of Ceramics, Glasses, and Composites. Wiley, New York.

60. Kerker, M., P. Scheiner, D. D. Cooke, and J. P. Kratohvil. 1979. Absorption Index and Color of Colloidal Hematite. J. Coll. Interface Sci. 71:176-187.

61. Bischoff, K. B. 1961. A study of dispersion intensity as a function of Reynolds number for packed bed flow. Ph.D. thesis. Illinois Institute of Technology.

62. Levenspiel, O. 1971. Chemical reaction engineering. John Wiley and Sons, Inc., New York.

63. Abegg, C. F. and N. S. Balakrishnan. 1971. The tanks-in-series concept as a model for imperfectly mixed crystallizers. Chem. Eng. Prog. Symp. Series 67:88-96.

64. Watson, A. G. 1967. The formation and properties of precipitates. Interscience Publishers, New York.

65. Mullin, J. 1972. Crystallization. Butterworths, London.

66. Randolph, A. D., and M. A. Larson. 1971. Theory of particulate processes. Academic Press, New York.

67. Garside, J. 1985. Industrial crystallization from solution. Chemical Engineering Science 40(1):3-26.

68. Nielsen, A. E. 1964. Kinetics of precipitation. The Macmillan Company, New York.

69. Walton, A. G. 1967. The Formation and Properties of Precipitates. Interscience Publishers, New York.

70. Frossling, N. 1938. Gerlands Beitr. Geophys. 52:170.

71. Miller, D. N. 1971. Scale-up of agitated vessels. Ind. Eng. Chem. Process Des. Develop., 10(3):365-375.

72. Volmer, M., and A. Weber. 1926. Nucleus formation in supersaturated systems. Zeitschrift fur Physikalische Chemie 119:277.

73. Frank, F. C. 1950. Radially symmetric phase growth controlled by diffusion. Proc. Roy. Soc. 201:586-599.

74. Nielsen, A. E. 1961. Diffusion-controlled growth of a moving sphere. The kinetics of crystal growth in potassium perchlorate precipitation. J. Phys. Chem. 65:46-59.

75. Ham, F. S. 1958. Theory of diffusion-limited precipitation. J. Phys. Chem. Solids 6:335-351.

76. Walpole, R. E. and R. H. Myers. 1978. Probability and statistics for engineers and scientists. Macmillan Publishing Co., Inc., New York.

77. Smith, J. M. 1981. Chemical engineering kinetics. McGraw-Hill, New York.

78. Froment, G. F. and K. B. Bischoff. 1979. Chemical reactor analysis and design. John Wiley and Sons, New York.

79. Roth, D. D., V. Basaran, and R. C. Seagrave. 1979. Mixing Effects in Variable-Volume Chemical Reactors. I. and E. C. Fundamentals 18:376-383.

80. Davitt, J. P. 1972. Crystallizer withdrawal behavior. M. S. thesis. Iowa State University, Ames, Iowa.

81. Yamate, G. and J. D. Stockham. 1978. Sizing particles using the microscope. Pages 23-33 in J. D. Stockham and E. G. Fochtman, eds. Particle Size Analysis. Ann Arbor Science Publishers, Inc., Ann Arbor, MI.

82. American Society for Testing and Materials. 1973. Recommended practice for the analyses by microscopical methods. Parts 23 and 30. ASTM, Philadelphia, PA.

83. Korbl, J. and R. Pribil. 1956. Xylenol Orange: New Indicator for the EDTA Titration. Chemist-Analyst 45(4):102-103.

84. Kinnunen, J. and B. Wennerstrand. 1957. Some further applications of Xylenol Orange as an indicator in the EDTA titration. Chemist-Analyst 46(4):92-93.

85. Butler, J. N. 1982. Carbon Dioxide Equilibria and Their Applications. Addison-Wesley Publishing Co., Inc., Reading, Massachusetts.

86. Vold, R. D., and M. J. Vold. 1983. Colloid and Interface Chemistry. Addison-Wesley Publishing Co., Inc., Reading, Massashusetts.

87. Shaw, D. J. 1970. Introduction to Colloid and Surface Chemistry. 2nd ed. Butterworths, London.

88. Shaw, W. H. R., and J. J. Bordeaux. 1955. The Decomposition of Urea in Aqueous Media. J. Am. Chem. Soc. 77:4729-4733.

89. Warner, R. C. 1941. The Kinetics of the Hydrolysis of Urea and of Arginine. J. Biol. Chem. 142:705-723.

90. Sahin, M., and A. Koseoglu. 1984. The Decomposition of Urea in Water. Chimica Acta Turcica 12:106-112.

91. Volmer, M., and A. Weber. 1926. Nucleus Formation in Supersaturated Systems. Zeitschrift fur Physikalische Chemie. 119:227.

92. CRC Handbook of Chemistry and Physics. 1980. R. C. Weast, ed. CRC Press, Inc., Boca Raton, Florida.

ACKNOWLEDGEMENTS

The author would like to thank Dr. L. E. Burkhart, my major professor and friend, for his advice and encouragement during the course of this work. His untimely death left all who knew him with a deep sense of loss. Dr. Burkhart's boundless energy, enthusiastic curiosity, and commitment to education will long be remembered.

Special thanks go to Dr. A. E. Cahill for his invaluable chemistry advice and expertise, and to Harlan Baker for his help in operating the transmission electron microscope. More important than their technical help was our friendship during my time at Iowa State.

Finally, I would like to thank my parents, Mr. and Mrs. Harold Jouett, for their constant support and encouragement throughout my entire academic career.

APPENDIX A

Mathematical Model for a Stirred Tank Reactor with Diffusion-Controlled Growth

The population density, n(L), is a continuous variable which is used to represent the distribution of the particle population about a particle-size coordinate, L. It is defined such that

$$\Delta N = \int_{L_1}^{L_2} n dL \tag{A.1}$$

where ΔN is the number of particles in the size range L_1 to L_2 (66). For spherical particles the coordinate, L, is taken to be the particle diameter. Alternately, n can be defined as

$$\lim_{\Delta L \to 0} \left(\frac{\Delta N}{\Delta L}\right) = \frac{dN}{dL} = n \tag{A.2}$$

Consider a well-mixed vessel which is continuously fed a solution of constant composition. A well-mixed slurry with unclassified product is removed continuously; no particle attrition occurs in the reaction vessel.

A steady-state population balance for an arbitrary size range L_1 to L_2 for an arbitrary time interval Δt in terms of the particle population is

$$\text{INPUT} = \text{OUTPUT} \tag{A.3}$$

$$VG_1n_1\Delta t + Q\bar{n}_i\Delta L\Delta t = VG_2n_2\Delta t + Q\bar{n}\Delta L\Delta t \tag{A.4}$$

# of particles growing into the size range over the time interval.	# of particles in the size range coming into the reactor over the time interval.	# of particles growing out of the size range over the time interval.	# of particles in the size range removed from the reactor over the time interval.

where G_j = growth rate of particles of size L_j, [cm/s].

V = reactor volume, [cm^3].

Q = total feed flow rate, [cm^3/s].

$\bar{n}_i$ = average population density in the size interval of the feed stream, [$\#/(cm^3 \cdot cm)$].

$\bar{n}$ = average population density in the size interval of the output stream, [$\#/(cm^3 \cdot cm)$].

n_j = population density of particles of size L_j, [$\#/(cm^3 \cdot cm)$].

No particle formation term appears in Equation A.4 since particles are assumed to grow from nuclei of zero size. Also, the function n(L) has been abbreviated to n for brevity; the functionality still exists. Rearranging Equation A.4 and dividing by ($\Delta L\Delta t$) gives

$$\frac{V(G_2n_2 - G_1n_1)}{\Delta L} + Q\bar{n} = Q\bar{n}_i \tag{A.5}$$

In the limit as $L \to 0$

$$\frac{d(Gn)}{dL} + \frac{n}{\tau} = \frac{n_i}{\tau} \tag{A.6}$$

where $\tau = \frac{V}{Q}$ = the average residence time of the reactor.

If particle growth is diffusion-limited, then Fick's law can be used to relate the molar flux J to the concentration gradient dC/dx,

$$J = D\left(\frac{dC}{dx}\right) \tag{A.7}$$

where x is the length of the diffusion path, C is the concentration of the diffusing species and D is the diffusion coefficient. The rate of material diffusing to a spherical surface, a distance r from the center is given by

$$\frac{dm}{dt} = 4\pi r^2 D\frac{dC}{dr} \tag{A.8}$$

where m is moles of diffusant.

If a steady state concentration gradient is set up relatively faster than the particle grows, then dm/dt may be considered to be constant and Equation A.8 can be integrated to give

$$4\pi D\int_{C_1}^{C_2} dc = \frac{dm}{dt}\int_{r_1}^{r_2} \frac{dr}{r^2} \tag{A.9}$$

or,

$$\frac{dm}{dt} = \frac{4\pi D(C_2 - C_1)}{\frac{1}{r_1} - \frac{1}{r_2}} \tag{A.10}$$

If $C_1 = C_e$ (equilibrium concentration) at $r_1 = r$ (the surface of the sphere) and $C_2 = C$ (the bulk liquid concentration) at $r_2 = \infty$, then

$$\frac{dm}{dt} = 4\pi r D(C-C_e) \tag{A.11}$$

The growth rate can be found by multiplying both sides of Equation A.11 by the molar volume $\bar{v}$ and dividing by the particle surface area, $4\pi r^2$ to yield

$$\frac{dr}{dt} = \frac{D\bar{v}(C - C_e)}{r} \tag{A.12}$$

Equation A.12 can be modified to express the rate of change in particle diameter, L, as follows:

$$G = \frac{dL}{dt} = \frac{4D\bar{v}(C - C_e)}{L} = \frac{k}{L} \tag{A.13}$$

where k is a constant for a stirred tank reactor operating at steady state.

Substituting Equation A.13 into Equation A.6 and assuming that no particles enter in the feed stream, ($\bar{n}_i = 0$), gives,

$$\frac{kd(\frac{n}{L})}{dL} + \frac{n}{\tau} = 0 \tag{A.14}$$

$$\frac{-nk}{L^2} + \frac{kdn}{LdL} + \frac{n}{\tau} = 0 \tag{A.15}$$

$$\frac{dn}{dL} = (\frac{1}{L} - \frac{L}{k\tau})n \tag{A.16}$$

Equation A.16 is a linear ordinary differential equation. If n^o is defined as the population density of nuclei of size L_o, then Equation A.16 can be integrated,

$$\int_{n_o}^{n} \frac{dn}{n} = \int_{L_o}^{L} \left(\frac{1}{L} - \frac{L}{k\tau}\right) dL \tag{A.17}$$

which gives

$$n = \frac{n^o}{L_o} \exp\left(\frac{L_o^2}{2k\tau}\right) L \exp\left(-\frac{L^2}{2k\tau}\right) \tag{A.18}$$

or,

$$n = cL \exp\left(-\frac{L^2}{2k\tau}\right) \tag{A.19}$$

where c is a constant.

Modal Particle Size

The modal particle size, L_M, is found by taking the derivative of Equation A.19 with respect to L and setting it equal to zero.

$$\frac{dn}{dL} = \frac{d\left[cL \exp\left(-\frac{L^2}{2k\tau}\right)\right]}{dL} = 0 \tag{A.20}$$

$$(1 - \frac{L^2}{k\tau}) \exp(- \frac{L^2}{2k\tau}) = 0 \qquad (A.21)$$

$$L = L_M = (k\tau)^{1/2} \qquad (A.22)$$

Mean Particle Size

The mean particle size, $\bar{L}$, is calculated by dividing the total particle length, L_T, (the sum of the characteristic lengths of all the particles in the distribution) by the total number of particles in the distribution, N_T.

$$\bar{L} = \frac{\int_0^\infty LndL}{\int_0^\infty ndL} = \frac{L_T}{N_T} \qquad (A.23)$$

$$N_T = \int_0^\infty cL \exp(- \frac{L^2}{2k\tau}) dL \qquad (A.24)$$

From integral tables (92), Equation A.24 becomes

$$N_T = ck\tau \qquad (A.25)$$

$$L_T = \int_0^\infty cL^2 \exp(- \frac{L^2}{2k\tau}) dL \qquad (A.26)$$

From integral tables (92), Equation A.26 becomes

$$L_T = c(\frac{\pi}{2})^{1/2} (k\tau)^{3/2} \qquad (A.27)$$

Substituting Equations A.24 and A.27 into Equation A.23 we get

$$\bar{L} = \frac{L_T}{N_T} = \left(\frac{\pi k\tau}{2}\right)^{1/2} \tag{A.28}$$

Variance

The variance, σ^2, of a distribution is the mean of the squared deviations about the mean. It is useful in characterizing the width of the size distribution. The positive square root of the variance is the standard deviation, σ.

$$\sigma^2 = \frac{\int_0^\infty (L - \bar{L})^2 ndL}{\int_0^\infty ndL} \tag{A.29}$$

$$\sigma^2 = \frac{\int_0^\infty L^2 ndL}{\int_0^\infty ndL} - (\bar{L})^2 \tag{A.30}$$

$$\int_0^\infty L^2 ndL = \int_0^\infty cL^3 \exp\left(-\frac{L^2}{2k\tau}\right) dL \tag{A.31}$$

From integral tables (92), Equation A.31 becomes

$$\int_0^\infty L^2 ndL = 2c(k\tau)^2 \tag{A.32}$$

Substituting Equations A.25 and A.32 into Equation A.30 gives

$$\frac{\int_0^\infty L^2 n dL}{\int_0^\infty n dL} = 2k\tau \qquad (A.33)$$

Combining Equations A.28, A.30, and A.33 yields

$$\sigma^2 = \frac{k\tau}{2}(4 - \pi) \qquad (A.34)$$

Coefficient of Variation

The variance or standard deviation is often inadequate for comparing the dispersions of different sets of data, either because the values for different sets are larger than for other sets, or because they are expressed in different units. The coefficient of variation, C.V., avoids these difficulties by expressing the standard deviation as a percent of the mean:

$$C.V. = \frac{\sigma}{\bar{L}} \times 100\% \qquad (A.35)$$

$$C.V. = \frac{(4 - \pi)^{1/2}}{(\pi)^{1/2}} \times 100\% = 52.3\% \qquad (A.36)$$

APPENDIX B

Mathematical Model for a Laminar Flow Reactor with Diffusion-Controlled Growth.

The velocity profile in the axial direction for laminar flow in a tube is parabolic, and may be described by the equation

$$u(\rho) = \frac{2Q}{\pi\rho_o^2}\left[1 - \left(\frac{\rho}{\rho_o}\right)^2\right] \qquad (B.1)$$

where $u(\rho)$ = fluid velocity as a function of radial position

Q = flow rate

ρ_o = tube radius

ρ = radial position measured from the center of the tube.

Since u is a function of ρ, residence time also varies with ρ. If the reactor length is l, then the residence time, t_R, as a function of radial position at any ρ is

$$t_R = \frac{L}{u} = \frac{\pi\rho_o^2 l}{2Q[1 - (\rho/\rho_o)^2]} \qquad (B.2)$$

where,

$$l\pi r_o^2 = V = \text{volume of tube} \qquad (B.3)$$

therefore,

$$t_R = \frac{V/Q}{2[1 - (\rho/\rho_o)^2]} = \frac{\tau}{2[1 - (\rho/\rho_o)^2]} \tag{B.4}$$

where τ is the mean residence time.

The fraction of effluent, F, flowing between radial positions ρ and $\rho + d\rho$ is

$$F(\rho) = \frac{u(2\pi\rho\, d\rho)}{Q} \tag{B.5}$$

The fraction $F(\rho)$ will have residence times between t_R and $t_R + dt_R$. Therefore, $F(\rho) = F(t_R)$. Substituting Equation B.1 for u and simplifying gives

$$F(t_R) = \frac{4}{\rho_o^2}[1 - (\rho/\rho_o)^2]\rho\, d\rho \tag{B.6}$$

To replace ρ with t_R in Equation B.6, differentiate Equation B.4 and solve for $\rho\, d\rho$.

$$t_R = \frac{\tau}{2[1 - (\rho/\rho_o)^2]} \tag{B.4}$$

$$\frac{2t_R}{\tau} = [1 - (\rho/\rho_o)^2]^{-1} \tag{B.7}$$

$$\frac{2dt_R}{\tau} = -[1 - (\rho/\rho_o)^2]^{-2}[-(2/\rho_o^2)\rho\, d\rho] \tag{B.8}$$

Combine Equations B.7 and B.8 to get

$$\frac{2dt_R}{\tau} = \left[\frac{4t_R^2}{\tau^2}\right]\left[\frac{2}{\rho_o^2}\rho d\rho\right] \tag{B.9}$$

or,

$$\rho d\rho = \frac{\rho_o^2 \tau}{4t_R^2} dt_R \tag{B.10}$$

Substituting Equations B.10 and B.7 into Equation B.6 gives

$$F(t_R) = \frac{4}{\rho_o^2}\left[\frac{\tau}{2t_R}\right]\left[\frac{\rho_o^2\tau}{4t_R^2} dt_R\right] = \frac{\tau^2}{2t_R^3} dt_R \tag{B.11}$$

$F(t_R)$ is the fraction of effluent with residence times between t_R and $t_R + dt_R$. It also represents the fraction, dN, of the total number of particles leaving the tubular reactor at radial position ρ. At this position in the tube, assuming that nucleation takes place only at the entrance to the reactor, the particles will have grown from zero size to size L in time t_R, at a growth rate of k/L. Thus,

$$\frac{dL}{dt} = \frac{k}{L} \tag{B.12}$$

so,

$$dt_R = \frac{LdL}{k} \tag{B.13}$$

and

$$\int_0^{t_R} dt = \frac{1}{k} \int_0^{L} L dL \tag{B.14}$$

or,

$$t_R = \frac{L^2}{2k} \tag{B.15}$$

Substituting this information into Equation B.11 gives

$$dN = F(t_R) = \frac{\tau^2}{2} \left(\frac{8k^3}{L^6}\right) \left(\frac{L dL}{k}\right) \tag{B.16}$$

and

$$dN = \frac{4(k\tau)^2}{L^5} dL \tag{B.17}$$

and the population density is

$$\frac{dN}{dL} = n = \frac{4(k\tau)^2}{L^5} \tag{B.18}$$

The minimum residence time in the laminar flow reactor occurs for the material at the center of the tube, where the velocity of flow is a maximum.

$$(t_R)_{min} = \tau/2 \tag{B.19}$$

The minimum particle size is found using Equations B.12 and B.19

$$\int_0^{L_{min}} L dL = k\int_0^{(t_R)_{min}} dt_R \tag{B.20}$$

$$\frac{L_{min}^2}{2} = k(t_R)_{min} \tag{B.21}$$

$$\frac{L_{min}^2}{2} = \frac{k\tau}{2} \tag{B.22}$$

$$L_{min} = (k\tau)^{1/2} \tag{B.23}$$

The maximum population density occurs at the minimum particle size.

Therefore,

$$n_{max} = \frac{4(k\tau)^2}{(k\tau)^{5/2}} = \frac{4}{(k\tau)^{1/2}} \tag{B.24}$$

Mean Particle Size

$$\bar{L} = \frac{\int_{L_{min}}^{\infty} LndL}{\int_{L_{min}}^{\infty} ndL} = \frac{L_T}{N_T} \tag{B.25}$$

$$N_T = \int_{L_{min}}^{\infty} \frac{4(k\tau)^2}{L^5} dL \tag{B.26}$$

$$N_T = 4(k\tau)^2 \left[\frac{-1}{4L^4}\right]\Big|_{(k\tau)^{1/2}}^{\infty} \tag{B.27}$$

$$N_T = 1 \tag{B.28}$$

Therefore,

$$L_T = \bar{L} = \int_{L_{min}}^{\infty} \frac{4(k\tau)^2}{L^4}\, dL \tag{B.29}$$

$$= 4(k\tau)^2 \left[\frac{-1}{3L^3}\right]\Big|_{(k\tau)^{1/2}}^{\infty} \tag{B.30}$$

$$\bar{L} = \frac{4}{3}(k\tau)^{1/2} \tag{B.31}$$

Variance

$$\sigma^2 = \frac{\int_{L_{min}}^{\infty} L^2 n dL}{\int_{L_{min}}^{\infty} n dL} - (\bar{L})^2 \tag{B.32}$$

$$= \int_{(k\tau)^{1/2}}^{\infty} L^2 n dL - (\bar{L})^2 \tag{B.33}$$

$$\int_{(k\tau)^{1/2}}^{\infty} \frac{4(k\tau)^2}{L^3}\, dL = \int_{(k\tau)^{1/2}}^{\infty} L^2 n dL \tag{B.34}$$

$$= 4(k\tau)^2 \left[\frac{-1}{2L^2}\right]\Big|_{(k\tau)^{1/2}}^{\infty} \tag{B.35}$$

$$= 2k\tau \tag{B.36}$$

Therefore,

$$\sigma^2 = 2k\tau - \left(\frac{4(k\tau)^{1/2}}{3}\right)^2 \qquad (B.37)$$

or,

$$\sigma^2 = \frac{2k\tau}{9} \qquad (B.38)$$

Coefficient of Variation

$$C.V. = \frac{\sigma}{\bar{L}} \times 100\% \qquad (B.39)$$

$$= \frac{(2k\tau/9)^{1/2}}{\frac{4(k\tau)^{1/2}}{3}} \times 100\% = \frac{(2/9)^{1/2}}{(4/3)} \times 100\% = 35.4\% \qquad (B.40)$$

APPENDIX C

Mathematical Model for m Stirred Tank Reactors in Series with Diffusion-Controlled Growth.

As shown in Appendix A, the population balance for a stirred tank reactor at steady state is

$$\frac{d(Gn)}{dL} + \frac{n}{\tau} - \frac{n_i}{\tau} = 0 \qquad (C.1)$$

where n_i is the population density of particles entering the feed stream. If the growth rate, G , is equal to k/L as is the case for diffusion-controlled growth, then Equation C.1 becomes

$$\frac{dn}{dL} = \frac{L(n_i - n)}{k\tau} + \frac{n}{L} \qquad (C.2)$$

If no particles enter the feed stream, then Equation C.2 becomes

$$\frac{dn}{dL} = n\left(\frac{1}{L} - \frac{L}{k\tau}\right) \qquad (C.3)$$

For m stirred tank reactors in series with equal residence times and no particles in the inlet feed stream, the following set of simultaneous differential equations are obtained,

$$\frac{dn_1}{dL} = n_1\left(\frac{1}{L} - \frac{mL}{k\tau}\right) \tag{C.4.1}$$

$$\frac{dn_2}{dL} = n_2\left(\frac{1}{L} - \frac{mL}{k\tau}\right) + \frac{mLn_1}{k\tau} \tag{C.4.2}$$

$$\vdots \qquad \vdots \qquad \vdots$$

$$\frac{dn_m}{dL} = n_m\left(\frac{1}{L} - \frac{mL}{k\tau}\right) + \frac{mLn_{m-1}}{k\tau} \tag{C.4.m}$$

where τ is the total mean residence time of the tanks in series and τ/m is the mean residence time of one tank.

These m simultaneous differential equations, with appropriate boundary conditions, can be solved to give the population density distribution of the particles leaving the m^{th} stirred tank reactor. For convenience, let

$$m/(k\tau) = B \tag{C.5}$$

Solve Equations C.4.1 through C.4.m in succession to find a pattern,

$$\frac{dn_1}{n_1} = \left(\frac{1}{L} - BL\right)dL \tag{C.6}$$

If n^o is defined as the population density of nuclei of size L_o, then Equation C.6 can be integrated,

$$\int_{n_1^o}^{n_1} \frac{dn_1}{n_1} = \int_{L_o}^{L} (1/L - BL)\,dL \tag{C.7}$$

which gives

$$n_1 = \frac{n^o}{L_o} \exp\left(\frac{L_o^2}{2k\tau}\right) L \exp\left(-\frac{L^2}{2k\tau}\right) \tag{C.8}$$

or,

$$n_1 = c_1 L \exp\left(-\frac{BL^2}{2}\right) \tag{C.9}$$

Next,

$$\frac{dn_2}{dL} = \left(\frac{1}{L} - BL\right) n_2 + BLn_1 \tag{C.10}$$

Substitute Equation C.9 into Equation C.10 for n_1 gives,

$$\frac{dn_2}{dL} = \left(\frac{1}{L} - BL\right) n_2 + Bc_1 L^2 \exp\left(-\frac{BL^2}{2}\right) \tag{C.11}$$

$$\frac{dn_2}{dL} + \left(BL - \frac{1}{L}\right) n_2 = Bc_1 L^2 \exp\left(-\frac{BL^2}{2}\right) \tag{C.12}$$

Find an integrating factor, I, for Equation C.12.

$$I = \exp\left[\int \left(BL - \frac{1}{L}\right) dL\right] \tag{C.13}$$

$$= \exp\left[\int BL\,dL - \int \frac{dL}{L}\right] \tag{C.14}$$

$$= \exp\left[\frac{BL^2}{2} - \ln L\right] \tag{C.15}$$

$$I = \frac{1}{L} \exp(\frac{BL^2}{2}) \tag{C.16}$$

Multiplying both sides of Equation C.12 by the integrating factor I, yeilds,

$$I[\frac{dn_2}{dL} + (BL - \frac{1}{L})n_2] = I[Bc_1L^2\exp(-\frac{BL^2}{2})] \tag{C.17}$$

$$\frac{d[n_2I]}{dL} = Bc_1L \tag{C.18}$$

$$d[n_2I] = Bc_1LdL \tag{C.19}$$

$$n_2 = \frac{\frac{1}{2}Bc_1L^2}{I} + \frac{c_2}{I} \tag{C.20}$$

And for n_2, the solution is,

$$n_2 = (\frac{Bc_1L^3}{2} + c_2L) \exp(-\frac{BL^2}{2}) \tag{C.21}$$

In a similar fashion,

$$\frac{dn_3}{dL} + (BL - \frac{1}{L})n_3 = BLn_2 \tag{C.22}$$

$$= [\frac{B^2c_1L^4}{2} + Bc_2L^2] \exp(-\frac{BL^2}{2}) \tag{C.23}$$

Multiply both sides of Equation C.23 by I,

$$\frac{d[n_3I]}{dL} = \frac{B^2c_1L^3}{2} + Bc_2L \tag{C.24}$$

$$n_3 I = \frac{B^2 c_1 L^4}{8} + \frac{B c_2 L^2}{2} + c_3 \tag{C.25}$$

$$n_3 = [\frac{B^2 c_1 L^5}{8} + \frac{B c_2 L^3}{2} + c_3 L] \exp(-\frac{BL^2}{2}) \tag{C.26}$$

Next, follow the same procedure to find n_4,

$$\frac{dn_4}{dL} + (BL - \frac{1}{L}) n_4 = BLn_3 \tag{C.27}$$

Multiply both sides of Equation C.27 by I.

$$\frac{d[In_4]}{dL} = IBLn_3 \tag{C.28}$$

$$= \frac{B^3 c_1 L^5}{8} + \frac{B^2 c_2 L^3}{2} + B c_3 L \tag{C.29}$$

$$In_4 = \frac{B^3 c_1 L^6}{48} + \frac{B^2 c_2 L^4}{8} + \frac{B c_3 L^2}{2} + c_4 \tag{C.30}$$

$$n_4 = [\frac{B^3 c_1 L^7}{48} + \frac{B^2 c_2 L^5}{8} + \frac{B c_3 L^3}{2} + c_4 L] \exp(-\frac{BL^2}{2}) \tag{C.31}$$

From Equations C.31, C.26, C.21, and C.9 a pattern emerges from which one can write the population density distribution of particles coming from the m^{th} tank by inspection as,

$$n_m = \sum_{a=0}^{m-1} \frac{B^a c_{m-a} L^{2a+1}}{2^a a!} \exp(-\frac{BL^2}{2}) \tag{C.32}$$

The constants c_{m-a} are determined by the nucleation rate in each tank. There are two limiting cases, both of which will be discussed. They are,

1. Nucleation only in the first tank.
2. Equal nucleation rates in all tanks.

Nucleation Only in the First Tank

For nucleation only in the first tank, the nuclei population density is n^o in tank one and is zero for all other tanks. For these conditions, the integration constants are

$$\left.\begin{aligned} c_1 &= c \\ c_{j\neq 1} &= 0 \end{aligned}\right\} \tag{C.33}$$

In this case all the c_{m-a}'s are zero except for c_1 which we will call c. Equation C.32 then becomes

$$n_m = c\left[\frac{B^{m-1}L^{2m-1}}{2^{m-1}(m-1)!}\right] \exp\left(-\frac{BL^2}{2}\right) \tag{C.34}$$

Mean Particle Size

$$\bar{L} = \frac{\int_0^\infty L n_m dL}{\int_0^\infty n_m dL} = \frac{L_T}{N_T} \tag{C.35}$$

$$N_T = \int_0^\infty c\left[\frac{B^{m-1} L^{2m-1}}{2^{m-1}(m-1)!}\right] \exp\left(-\frac{BL^2}{2}\right) dL \tag{C.36}$$

$$= \frac{cB^{m-1}}{2^{m-1}(m-1)!} \int_0^\infty L^{2m-1} \exp\left(-\frac{BL^2}{2}\right) dL \tag{C.37}$$

From the integral tables (92), Equation C.37 becomes

$$N_T = \frac{cB^{m-1}}{2^{m-1}(m-1)!} \left[\frac{2^{m-1}\Gamma(m)}{B^m}\right] \tag{C.38}$$

$$N_T = \frac{c\Gamma(m)}{B(m-1)!} \tag{C.39}$$

$$L_T = \frac{cB^{m-1}}{2^{m-1}(m-1)!} \int_0^\infty L^{2m} \exp\left(-\frac{BL^2}{2}\right) dL \tag{C.40}$$

From integral tables (92), Equation C.40 becomes

$$L_T = \frac{cB^{m-1}}{2^{m-1}(m-1)!} \left[\frac{1 \cdot 3 \cdot 5 \cdots (2m-1)}{2^{m+1}(B/2)^m} \cdot \left(\frac{2\pi}{B}\right)^{1/2}\right] \tag{C.41}$$

$$L_T = \frac{c(2m-1)!!}{2^m B(m-1)!} \cdot \left(\frac{2\pi}{B}\right)^{1/2} \tag{C.42}$$

$$\bar{L} = \frac{L_T}{N_T} = \frac{(2m-1)!!}{2^m(m-1)!} \cdot \left(\frac{2\pi}{B}\right)^{1/2} \tag{C.43}$$

Variance

$$\sigma^2 = \frac{\int_0^\infty L^2 n_m dL}{\int_0^\infty n_m dL} - (\bar{L})^2 \tag{C.44}$$

$$\int_0^\infty L^2 n_m dL = \frac{cB^{m-1}}{2^{m-1}(m-1)!} \int_0^\infty L^{2m+1} \exp\left(-\frac{BL^2}{2}\right) dL \tag{C.45}$$

From integral tables (92), Equation C.45 becomes

$$\int_0^\infty L^2 n_m dL = \frac{cB^{m-1}}{2^{m-1}(m-1)!} \left[\frac{m!}{2(B/2)^{m+1}}\right] \tag{C.46}$$

$$= \frac{2cm}{B^2} \tag{C.47}$$

Combining Equations C.39, C.43, and C.47 one gets

$$\sigma^2 = \frac{\frac{2cm}{B^2}}{\frac{c\Gamma(m)}{B(m-1)!}} - \left[\left[\frac{(2m-1)!!}{2^m\Gamma(m)}\right]^2 \cdot \left(\frac{2\pi}{B}\right)^{1/2}\right]^2 \tag{C.48}$$

$$= \frac{2(m!)}{B\Gamma(m)} - \left[\left[\frac{(2m-1)!!}{\Gamma(m)}\right]^2 \cdot \left(\frac{2\pi}{B}\right)^{1/2}\right]^2 \tag{C.49}$$

or,

$$\sigma^2 = \frac{2}{B}\left[m - \left(\frac{(2m-1)!!}{2^m(m-1)!}\right)^2 \cdot \pi\right] \tag{C.50}$$

Coefficient of Variation

$$C.V. = \frac{\sigma}{\bar{L}} \times 100\% \tag{C.51}$$

$$C.V. = \frac{\{\frac{2}{B}\,[m-(\frac{(2m-1)!!}{2^m(m-1)!})^2 \cdot \pi]\}^{1/2}}{\frac{(2m-1)!!}{2^m(m-1)!} \cdot (\frac{2\pi}{B})^{1/2}} \times 100\% \tag{C.52}$$

$$C.V. = \frac{2^m(m-1)!\,[m-(\frac{(2m-1)!!}{2^m(m-1)!})^2 \cdot \pi]^{1/2}}{(2m-1)!! \cdot \pi^{1/2}} \times 100\% \tag{C.53}$$

Equal Nucleation Rates in All Tanks

For equal nucleation rates in all tanks, all the c_{m-a}'s are equal to c.

$$c_1 = c_2 = c_3 = \cdots = c \tag{C.54}$$

Equation C.32 then becomes

$$n_m = c\sum_{a=0}^{m-1} \frac{B^a L^{2a+1}}{2^a a!} \exp(-\frac{BL^2}{2}) \tag{C.55}$$

Mean Particle Size

$$\bar{L} = \frac{\int_0^\infty L n_m dL}{\int_0^\infty n_m dL} = \frac{L_T}{N_T} \tag{C.35}$$

$$N_T = c\int_0^\infty \sum_{a=0}^{m-1} \frac{B^a L^{2a+1}}{2^a a!} \exp(-\frac{BL^2}{2})\ dL \tag{C.56}$$

$$= c\sum_{a=0}^{m-1} \frac{B^a}{2^a a!} \int_0^\infty L^{2a+1} \exp(-\frac{BL^2}{2})\ dL \tag{C.57}$$

From integral tables (92), Equation C.57 becomes

$$N_T = c\sum_{a=0}^{m-1} \frac{B^a}{2^a a!} \cdot \frac{a!2^a}{B^{a+1}} = \frac{mc}{B} \tag{C.58}$$

$$L_T = c\int_0^\infty \sum_{a=0}^{m-1} \frac{B^a L^{2a+2}}{2^a a!} \exp(-\frac{BL^2}{2})\ dL \tag{C.59}$$

$$= c\sum_{a=0}^{m-1} \frac{B^a}{2^a a!} \int_0^\infty L^{2a+2} \exp(-\frac{BL^2}{2})\ dL \tag{C.60}$$

From integral tables (92), Equation C.60 becomes

$$L_T = c\sum_{a=0}^{m-1} \frac{B^a}{2^a a!} \cdot \frac{2^{a+1/2}\Gamma(a + 3/2)}{B^{a+3/2}} \tag{C.61}$$

$$L_T = 2^{1/2} c \sum_{a=0}^{m-1} \frac{\Gamma(a + 3/2)}{a!B^{3/2}} \tag{C.62}$$

$$\bar{L} = \frac{L_T}{N_T} \tag{C.35}$$

$$L = \frac{2^{1/2} c \sum_{a=0}^{m-1} \frac{\Gamma(a + 3/2)}{a! B^{3/2}}}{mc/B} \tag{C.63}$$

$$\bar{L} = \frac{2^{1/2}}{mB^{1/2}} \sum_{a=0}^{m-1} \frac{\Gamma(a + 3/2)}{a!} \tag{C.64}$$

Variance

$$\sigma^2 = \frac{\int_0^\infty L^2 n_m dL}{\int_0^\infty n_m dL} - (\bar{L})^2 \tag{C.44}$$

$$\int_0^\infty L^2 n_m dL = c \int_0^\infty \sum_{a=0}^{m-1} \frac{B^a L^{2a+3}}{2^a a!} \exp(-\frac{BL^2}{2}) \, dL \tag{C.65}$$

$$= c \sum_{a=0}^{m-1} \frac{B^a}{2^a a!} \int_0^\infty L^{2a+3} \exp(-\frac{BL^2}{2}) \, dL \tag{C.66}$$

From integral tables (92), Equation C.66 becomes

$$\int_0^\infty L^2 n_m dL = c \sum_{a=0}^{m-1} \frac{B^a}{2^a a!} \cdot \frac{2^{a+1} \Gamma(a+2)}{B^{a+2}} \tag{C.67}$$

$$= \frac{2c}{B^2} \sum_{a=0}^{m-1} \frac{\Gamma(a + 2)}{a!} \tag{C.68}$$

Therefore,

$$\frac{\int_0^\infty L^2 n_m dL}{\int_0^\infty n_m dL} = \frac{2c/B^2 \sum_{a=0}^{m-1} \frac{\Gamma(a+2)}{a!}}{mc/B} = \frac{2}{mB} \sum_{a=0}^{m-1} \frac{\Gamma(a+2)}{a!} \qquad (C.69)$$

Substituting Equations C.64 and C.69 into Equation C.47 yields

$$\sigma^2 = \frac{2}{m^2 B} \left\{ m \sum_{a=0}^{m-1} \frac{\Gamma(a+2)}{a!} - \left[\sum_{a=0}^{m-1} \frac{\Gamma(a+3/2)}{a!} \right]^2 \right\} \qquad (C.70)$$

Coefficient of Variation

$$C.V. = \frac{\sigma}{\bar{L}} \times 100\% \qquad (C.51)$$

$$C.V. = \frac{\left\{ m \sum_{a=0}^{m-1} \frac{\Gamma(a+2)}{a!} - \left[\sum_{a=0}^{m-1} \frac{\Gamma(a+3/2)}{a!} \right]^2 \right\}^{1/2}}{\sum_{a=0}^{m-1} \frac{\Gamma(a+3/2)}{a!}} \times 100\% \qquad (C.71)$$

APPENDIX D

Mathematical Model for a Semi-Batch Reactor with Diffusion-Controlled Growth

Roth et al. (79) have shown that, after an infinite number of cycles, the residence time distribution for a semi-batch reactor can be expressed as

$$f(\theta) = \sum_{z=0}^{\infty} (V)^z \frac{(\theta-\theta_B-z\theta_T)}{\theta_F} [U(\theta-\theta_B-z\theta_T) - U(\theta-\theta_B-\theta_E-z\theta_T)]$$
$$+ \sum_{z=0}^{\infty} (V)^z [1- \frac{(\theta-\theta_B-\theta_E-z\theta_T)}{\theta_F}] [U(\theta-\theta_B-\theta_E-z\theta_T) - U(\theta-(z+1)\theta_T)] \quad (D.1)$$

where

$$U(x)=1 \quad (x\geq 0)$$
$$=0 \quad (x<0) \quad (D.2)$$

and

dimensionless time, $\theta = Q_S t/V_m$
volume fraction, $V = V_Q/V_m$
Q_S = flow rate during filling mode
t = time
V_m = maximum reactor volume
V_Q = minimum reactor volume
θ_B, θ_E, θ_F, and θ_T are the dimensionless batch, emptying, filling, and total cycle time, respectively.

If the residence time distribution and also an expression for particle growth rate are known for a particular reactor, then the residence time distribution can be transformed into a population density distribution.

Let $f(\theta)$ be defined such that

$$\int_0^\infty f(\theta)\ d\theta = 1 \qquad (D.3)$$

therefore, the fraction of particles with residence time between θ and $\theta+d\theta$ is $f(\theta)\ d\theta$.

We now need to transform $f(\theta)\ d\theta$ to real time.

$$\theta = Q_S t/V_m \qquad (D.4)$$

and

$$d\theta = Q_S/V_m\ dt \qquad (D.5)$$

substituting Equations D.4 and D.5 into Equation D.1 gives

$$f(\theta)\ d\theta = Q_S/V_m\ f(t)\ dt \tag{D.6}$$

We now need to transform f(t) dt to a length basis.

$$dL/dt = k/L \quad \text{(diffusion-controlled growth)} \tag{D.7}$$

$$L/k\ dL = dt \tag{D.8}$$

$$t = L^2/2k \tag{D.9}$$

substituting Equations D.8 and D.9 into Equation D.6 gives

$$Q_S/V_m\ f(t)\ dt = (Q_S/V_m)\,(L/k)\ g(L)\ dL \tag{D.10}$$

= fraction of particles with a size between L and L+dL

= dN

$$dN/dL = n = (Q_S/V_m)\,(L/k)\ g(L) = \text{population density distribution} \tag{D.11}$$

$$n = \left(\frac{Q_S}{V_m}\right)\left(\frac{L}{k}\right)\left\{\sum_{z=0}^{\infty} V^z\ \frac{\left(\frac{L^2}{2k} - t_B - zt_T\right)}{t_F}\left[U\left(\frac{L^2}{2k} - t_B - zt_T\right) - U\left(\frac{L^2}{2k} - t_B - t_E - zt_T\right)\right]\right.$$

$$\left. + \sum_{z=0}^{\infty} V^z \left[1 - \frac{\left(\frac{L^2}{2k} - t_B - t_E - zt_T\right)}{t_F}\right]\left[U\left(\frac{L^2}{2k} - t_B - t_E - zt_T\right) - U\left(\frac{L^2}{2k} - (n+1)\,t_T\right)\right]\right\} \tag{D.12}$$

where t_B, t_E, and t_F are the duration of the batch, emptying, and filling modes, respectively and t_T is the total cycle time.

Using the following relations,

$$Q_S = (V_m - V_o)/t_F \tag{D.13}$$

$$V = V_o/V_m = \text{volume fraction} \tag{D.14}$$

$$t_F = t_E = (t_T - t_B)/2 \tag{D.15}$$

$$\sigma_B = t_B/t_T = \text{batch fraction} \tag{D.16}$$

Equation D.12 can be written in terms of volume fraction, batch fraction, total cycle time, k, and L.

$$n = \frac{4L(1-V)}{k[(1-\sigma_B)t_T]^2}\{\sum_{z=0}^{\infty} V^z(\frac{L^2}{2k} - (\sigma_B+z)t_T)[U(\frac{L^2}{2k} - (\sigma_B+z)t_T)$$

$$- U(\frac{L^2}{2k} - \frac{1}{2}(\sigma_B+2z+1)t_T)] + \sum_{z=0}^{\infty} V^z[\frac{t_T(1-\sigma_B)}{2} - \frac{L^2}{2k} - \frac{1}{2}(\sigma_B+2z+1)t_T]$$

$$[U(\frac{L^2}{2k} - \frac{1}{2}(\sigma_B+2z+1)t_T) - U(\frac{L^2}{2k} - (z+1)t_T)]\} \tag{D.17}$$

Mean Particle Size

$$\bar{L} = \frac{\int_0^{\infty} LndL}{\int_0^{\infty} ndL} = \frac{L_T}{N_T} = \frac{\int_0^{\infty} LndL}{1} \tag{D.18}$$

The first term of Equation D.17 is nonzero only for the following values of L

$$(2kt_T(\sigma_B+z))^{1/2} < L < (kt_T(\sigma_B+2z+1))^{1/2} \qquad (D.19a)$$

or,

$$L_2 < L < L_1 \qquad (D.19b)$$

The second term of Equation D.17 is nonzero only for the following values of L

$$(kt_T(\sigma_B+2z+1))^{1/2} < L < (2k(z+1)t_T)^{1/2} \qquad (D.20a)$$

or,

$$L_1 < L < L_3 \qquad (D.20b)$$

Using Equations D.19 and D.20 as the limits of integration for Equation D.18 gives

$$\bar{L} = \frac{4(1-V)}{k[(1-\sigma_B)t_T]^2} \left\{ \sum_{z=0}^{\infty} V^z \left[\frac{1}{10k} (L_1^5 - L_2^5) - \frac{1}{3} (L_1^3 - L_2^3)(\sigma_B+z)t_T \right] \right.$$

$$\left. + \sum_{z=0}^{\infty} V^z \left[\frac{1}{3} (L_3^3 - L_1^3)(z+1)t_T - \frac{1}{10k} (L_3^5 - L_1^5) \right] \right\} \qquad (D.21)$$

Rearranging gives

$$\bar{L} = \frac{4(1-V)(kt_T)^{1/2}}{(1-\sigma_B)^2} \left\{ \sum_{z=0}^{\infty} V^z \left[\frac{1}{10} (T_1^5 - T_2^5) - \frac{1}{3} (T_1^3 - T_2^3)(\sigma_B + z) \right] \right.$$

$$\left. + \sum_{z=0}^{\infty} V^z \left[\frac{1}{3} (T_3^3 - T_1^3)(z+1) - \frac{1}{10} (T_3^5 - T_1^5) \right] \right\} \qquad (D.22)$$

where

$$T_1 = (\sigma_B + 2z + 1)^{1/2} \tag{D.23}$$

$$T_2 = (2\sigma_B + 2z)^{1/2} \tag{D.24}$$

$$T_3 = (2z + 2)^{1/2} \tag{D.25}$$

Later, it will be convenient to express Equation D.22 in the more compact form,

$$\bar{L} = \frac{4(1-V)(kt_T)^{1/2}}{(1-\sigma_B)^2} \{ \Phi \} \tag{D.26}$$

where Φ is equal to the sum of the terms in the braces in Equation D.22.

Variance

$$\sigma^2 = \frac{\int_0^\infty L^2 n dL}{\int_0^\infty n dL} - (\bar{L})^2 \tag{D.27}$$

Substituting Equations D.17 and D.26 into Equation D.27 and using Equations D.19 and D.20 as the limits of integration gives

$$\sigma^2 = \frac{4(1-V)}{k[(1-\sigma_B)t_T]^2} \left\{ \sum_{z=0}^{\infty} V^z \left[\frac{1}{12k} (L_1^6 - L_2^6) - \frac{1}{4} (L_1^4 - L_2^4)(\sigma_B + z)t_T \right] \right.$$

$$\left. + \sum_{z=0}^{\infty} V^z \left[\frac{1}{4} (L_3^4 - L_1^4)(z+1)t_T - \frac{1}{12k} (L_3^6 - L_1^6) \right] \right\} - (\bar{L})^2 \qquad (D.28)$$

rearranging gives

$$\sigma^2 = \frac{4(1-V)kt_T}{(1-\sigma_B)^2} \left\{ \sum_{z=0}^{\infty} V^z \left[\frac{1}{12} (T_1^6 - T_2^6) - \frac{1}{4} (T_1^4 - T_1^4)(\sigma_B + z) \right] \right.$$

$$\left. + \sum_{z=0}^{\infty} V^z \left[\frac{1}{4} (T_3^4 - T_1^4)(z+1) - \frac{1}{12} (T_3^6 - T_1^6) \right] \right\} - (\bar{L})^2 \qquad (D.29)$$

Equation D.29 can be written in the more compact form,

$$\sigma^2 = \frac{4(1-V)kt_T}{(1-\sigma_B)^2} \{ \Psi \} - (\bar{L})^2 \qquad (D.30)$$

where Ψ is equal to the sum of the terms in the braces in Equation D.29.

Coefficient of Variation

The coefficient of variation is a dimensionless measure of the width of a distribution. It is

$$C.V. = \sigma/\bar{L} \times 100\% \tag{D.31}$$

Substituting Equations D.26 and D.30 into Equation D.31 gives,

$$C.V. = \frac{\left[\frac{4(1-V)kt_T}{(1-\sigma_B)^2} \{ \Psi \} - \frac{16(1-V)^2 kt_T}{(1-\sigma_B)^4} \{ \Phi \}^2 \right]^{1/2}}{\frac{4(1-V)(kt_T)^{1/2}}{(1-\sigma_B)^2} \{ \Phi \}} \times 100\% \tag{D.32}$$

or,

$$C.V. = \frac{(1-\sigma_B)\left[\{ \Psi \} - \frac{4(1-V)}{(1-\sigma_B)^2} \{ \Phi \}^2 \right]^{1/2}}{2(1-V)^{1/2} \{ \Phi \}} \times 100\% \tag{D.33}$$

The coefficient of variation is most easily calculated numerically. Figure 14 shows the coefficient of variation for various values of volume fraction, V, and batch fraction, σ_B.